TIME DEPENDENT AND EQUILIBRIUM STRESS-STRAIN BEHAVIOR OF RUBBERS IN MODERATELY LARGE DEFORMATIONS.

by

Cigdem Gurer

In Partial Fulfillment of the Requirements

for the Degree of

Doctor of Philosophy

California Institute of Technology

Pasadena, CA. 91125

1984

(Submitted December 16, 1983)

to Omar

ACKNOWLEDGEMENTS

I would like to acknowledge the moral, and at times financial, support of my family. The contribution of my husband Omar Newland to this thesis, both in terms of moral support and in terms of help with the figures, is greatly appreciated.

I would like to thank all my friends and collegues at Cal Tech for their numerous suggestions and recommendations at times. Among those, I would especially like to mention Bill Moonan for his technical help. The guidance of my advisor, Dr. N. W. Tschoegl is greatly appreciated.

I would like to extend my sincere thanks to the people of the Chemical Engineering Machine Shop, especially George Griffith, for their technical advise. Miss Linda Liu's help with experiments and data reduction is appreciated.

I also would like to acknowledge the financial support of the Department of Energy, which made this work possible.

ABSTRACT

In this work, time dependent and equilibrium stress-strain properties of elastomeric networks are investigated for moderately large deformation. A two network potential is proposed, which constitutively describes stress-strain behavior at elastic equilibrium. The potential is applied to time dependent deformations thorough a molecular model.

TABLE OF CONTENTS

INTRODUCTION

This work addresses some questions relating to nonlinear deformations of crosslinked polymers. In Chapter I, the phenomenological theory of hyperelastic materials is presented in its most general form. The theory is then specialized to moderately large deformations of polymer networks through the introduction of a strain energy density function, W, of the form

$$W = \frac{G_X}{2}(\lambda_1^2 + \lambda_2^2 + \lambda_3^2 - 3) + \frac{2G_N}{m^2}(\lambda_1^m + \lambda_2^m + \lambda_3^m - 3) \qquad (1)$$

where G_X is the modulus associated with the chemical crosslinks of the network, and G_N is the modulus contribution arising from the presence of topological constraints. The moduli are linked by the relation $G_X+G_N=G$, where G is the shear modulus. The parameter m can be taken as 0.34.

The constitutiveness of this two network potential is demonstrated on published data in general biaxial deformation of natural rubber. Some of our own data on natural and styrene-butadiene rubber crosslinked to different degrees are also discussed. The nature of G_N has been studied on published data on several swollen networks.

In Chapter II, it is shown that, in moderately large deformations, G_N is proportional to G_N^0, the plateau modulus of a high-molecular-weight uncrosslinked sample of the same polymer. Since the sum of G_N and G_X, the equilibrium modulus, G, can be obtained from stress relaxation measurements on the crosslinked material in the linear region, it is possible to predict non-linear stress-strain behavior in large deformations from linear behavior in small (theoretically infinitesimal) deformations.

In Chapter III a molecular theory is proposed which is capable of describing the nonlinear, time dependent properties of polymer networks. The model is

derived for a uniaxial deformation applied as a step function of time. It is then generalized to other strain histories via the Boltzmann superposition integral. Although a full tensorial form for the constitutive equation is obtained through the molecular model, the resulting strain function can be determined analytically only for a uniaxial deformation. To avoid the necessity of numerical integrations, an approximation is proposed and its range of applicability is discussed.

This thesis was written as a collection of three independent papers. Chapters I and II will be submitted to Macromolecules for publication. Chapter III together with Appendix III will be submitted to the Journal of Polymer Science. For that reason, each chapter is complete in itself. Thus, the equations, the figures and the references are numbered starting from 1 in each chapter.

I. PROPERTIES OF ELASTOMER NETWORKS AT ELASTIC EQUILIBRIUM

Introduction

The basic laws of motion, conservation of mass, balance of momenta, conservation of energy, and principle of entropy, valid for all types of continuum, do not form a complete set of equations to describe the response of a material to a mechanical excitation. It is necessary to complement the set with constitutive equations that characterize the material response.

Though largely arbitrary in form, constitutive equations are subject to the restrictions of the constitutive theory.[1] To formulate a constitutive equation valid for all types of material is a useless task because, due to the generality of such an equation, it would have to contain too many experimentally determined parameters. It is more expedient to group materials into various classes and find a constitutive equation for each class.

Because of their novel characteristics and easy processibility, polymeric materials are being used in increasing amounts instead of conventional materials. For design purposes it is necessary to be able to predict the deformation properties of these materials under given conditions. The theories of linear elasticity and linear viscoelasticity are exact theories that describe the equilibrium and time dependent properties of polymeric materials when they undergo infinitesimal deformations. In applications, however, the deformations are not infinitesimal, and it is therefore necessary to be able to predict their behavior in finite deformations.

Most crosslinked polymers in the rubbery state are capable of large deformations vastly exceeding those of other elastic materials. Elongations of 300-400% are not uncommon with rubber networks. Due to this characteristic, they have been termed *hyperelastic* materials.

To describe the equilibrium stress-strain behavior of hyperelastic materials, two paths are available for the formulation of an elastic potential valid for large deformations. Either the small-scale response of the polymer chains to a given macroscopic excitation is assumed to be known, and one then describes the material response using the methods of statistical mechanics; or one proposes a potential consistent with the axioms of constitutive theory and the available experimental data, and then tries to interpret the molecular nature of the phenomenological coefficients. This is needed to understand the region of validity of the equation and to enable one, eventually, to design a material for a given application.

A potential is commonly called constitutive when it does not violate any of the principles of continuum mechanics. Many potentials which are constitutive in this sense, are restricted to certain types of deformation. We call a potential constitutive in the narrower sense when it appears to describe the mechanical properties of the network with the same material parameters in any deformation. This will be discussed separately further below.

Molecular Theories of Rubber Elasticity

One of the earliest theories to describe the isothermal equilibrium stress-strain behavior of polymeric materials in finite deformation has been formulated by modelling a polymer network as a network of freely jointed chains. The displacement length (end-to-end distance) of a chain is considered to be Gaussian in the undeformed state. The chains are allowed to pass through each other without hindrance, constituting what is commonly known as a phantom network. The stress resulting from a given elongation then is a result of a decrease in entropy of the hypothetical network. Imperfections in the network structure, such as dangling chain ends, loops, and entanglements, are neglected. The

equilibrium stress resulting from an elongation is then given by

$$\bar{\sigma} = RTF(\lambda^2 - 1/\lambda) \tag{1}$$

where $\bar{\sigma}$ is the Cauchy stress based on the deformed cross-sectional area, F is the structure factor, λ is the stretch ratio in the direction of the pull, R is the gas constant, and T is the absolute temperature. The derivation and the thermodynamic implications of eq 1 have been discussed in detail by Flory.[2]

The structure factor is determined by the specific assumptions made about the microscopic movement of the junction points. James and Guth[3] assumed that the displacements of the mean position of the junction points are affine in the macroscopic strain and that the fluctuations about the junction points are independent of the strain. These assumptions lead to a structure factor that can be expressed as

$$F = \nu_X(1-2/\psi) \tag{2}$$

where ν_X is the number of chains between crosslink points per unit volume, and ψ is the functionality of the junction points. Flory[2] made the assumption that the junction points are firmly imbedded in the polymer matrix and therefore do not fluctuate. Their displacements, not the mean positions of the junctions, are affine in the macroscopic strain. Flory's assumption led to a structure factor given simply by

$$F = \nu_X \tag{3}$$

Stress resulting from a given strain in a crosslinked rubber follows Flory's predictions in small deformations, but is consistently overestimated in even moderately large deformations. In simple tension we consider a deformation to be moderately large if the principal stretch ratio remains below the inflection point in a plot of the nominal stress vs the ratio. Our discussion will be confined to moderately large deformations. We will give a more general description

further below.

More recently, Flory[4], and Flory and Erman[5] proposed a new statistical mechanical theory which is based on the idea that topological constraints affect the fluctuations of the junction points. According to this theory, in small deformations topological constraints restrict the fluctuations about the junction points to a large extent so that their displacements are still affine in the macroscopic strain. In large deformations, however, the chains are further apart; therefore, only the mean positions of the junction points are affine in the macroscopic strain. The fluctuations about the junction points are independent of the strain in this region. To be able to make the transition between the two limiting cases Flory expresses the stress resulting from a given strain as the sum of two additive terms. The first arises from modelling the displacement of the mean positions of the junction points and has the form given by eq 1 with eq 2. The second term accounts for the severity of the constraints. The form of the equation is too lengthy to be reported here, but it is important to point out that the second term is evaluated using statistical mechanical methods and contains one adjustable parameter to characterize the severity of topological constraints. We will refer to this theory as the *Flory-Erman theory*.

Phenomenological Equations in Terms of the Invariants of the Deformation Tensor

One can formulate a constitutive equation phenomenologically for large equilibrium deformations of hyperelastic materials by postulating the existence of a strain energy density function (reversible work of deformation), W , from which the stress is derivable. The most general constitutive equation for equilibrium deformations of an initially isotropic, homogeneous, incompressible material has been derived by Rivlin [6] and also by Ariano.[7]. It contains no

assumptions other than the ones stated above. The Rivlin-Ariano equation has the form

$$\bar{\sigma}_{kl} = -P\delta_{kl} + 2\frac{\partial W}{\partial I_1}B_{kl} - 2\frac{\partial W}{\partial I_2}(B^{-1})_{kl} \tag{4}$$

in indicial notation,where $\bar{\sigma}_{kl}$ is the Cauchy stress tensor, B_{kl} is the Finger deformation tensor, $(B^{-1})_{kl}$ is its inverse, and P is an arbitrary hydrostatic pressure required by the assumption of incompressiblity. I_1 is the first, and I_2 is the second invariant of the deformation tensor. Thus, if W is known, one can describe the equilibrium deformations of rubberlike materials using the Rivlin-Ariano equation. W is most commonly expressed in terms of the invariants of the deformation tensor for a material that is homogeneous, initially isotropic, and incompressible. The assumption of incompressibility requires that the third invariant be unity. If W is now expanded around the undeformed state of the material in a Taylor series, one obtains

$$W = \sum_{i,j=0}^{\infty} C_{ij}\,(I_1-3)^i\,(I_2-3)^j \tag{5}$$

where C_{ij} are the phenomenological coefficients. The two invariants of the deformation tensor are given by

$$I_1 = \lambda_1^2 + \lambda_2^2 + \lambda_3^2 \tag{6}$$

$$I_2 = 1/\lambda_1^2 + 1/\lambda_2^2 + \lambda_3^2 \tag{7}$$

in terms of the stretch ratios. The fact that W must be zero for an undeformed material imposes the restriction that $C_{00} = 0$. Once a form for W is known, the stress resulting from a given deformation characterized by the three principal stretch ratios λ_1, λ_2, λ_3 (i.e., the positive square roots of the eigenvalues of the deformation tensor) can be obtained as

$$\bar{\sigma}_i = \lambda_i \frac{\partial W}{\partial \lambda_i} - P \qquad i=1,2,3 \tag{8}$$

where $\bar{\sigma}_i$ is the Cauchy stress in the ith principal direction. The assumption of incompressibility further relates the three stretch ratios by the equation

$$\lambda_1\lambda_2\lambda_3 = 1 \tag{9}$$

Thus only two of the three stretch ratios can be specified independently. Note that eq 8 is identical with eq 4.

If one keeps only the first term of eq 5, then eqs 6, 7, 8, and 9 would yield

$$\bar{\sigma}_1 - \bar{\sigma}_2 = 2C_{10}\,(\lambda_1^2 - 1/\lambda_1) \tag{10}$$

for simple tension, where λ_1 is the stretch ratio in the direction of the pull, $\bar{\sigma}_1$ is the corresponding Cauchy stress, and $\bar{\sigma}_2$ is zero since the boundary normal to the direction of the pull is a free boundary. It is apparent that $2C_{10} = G$, the shear modulus, because of the requirement that the results of linear elasticity should be reproduced as $\lambda_1 \to 1$. It can be seen that eq 10 is identical with eq 1 letting $2C_{10} = RTF$.

Equation 10 models the behavior of a polymer network constitutively in deformations when the stretch ratio is not much larger than about 1.2. Mooney[8] proposed an extension of eq 10 by postulating that a plot of $\bar{\sigma}/(\lambda^2 - \lambda^{-1})$ vs. $1/\lambda$ is linear in simple tension, and Hooke's law is obeyed in simple shear. Mooney's equation, which is commonly referred to as the Mooney-Rivlin equation, has the form

$$\bar{\sigma}_1 - \bar{\sigma}_2 = 2C_1\,(\lambda_1^2 - 1/\lambda_1) + 2C_2\,(\lambda_1 - 1/\lambda_1^2) \tag{11}$$

for simple tension, where C_1 and C_2 are the phenomenological coefficients. It is required that $2C_1 + 2C_2 = G$. Equation 11 can be derived with $C_1 = C_{10}$ and $C_2 = C_{01}$, by retaining the first two terms of eq 5. It shows good agreement with experimental data in simple tension, but it does not do so constitutively. In

other words, if one estimates the values of C_1 and C_2 from simple tension data, and predicts the results for a different mode of deformation, the predictions do not fit the data.

Phenomenological Equations in Terms of the Stretch Ratios

Later workers in the field abandoned the idea that W is most easily formulated in terms of the invariants of the Finger deformation tensor, and expressed it in terms of the stretch ratios.

Carmichael and Holdaway[9], Mooney[10],and Valanis and Landel[11] concluded, on the basis of certain symmetry arguments that W should be the same function of the three stretch ratios. Thus W should have the form

$$W = w(\lambda_1) + w(\lambda_2) + w(\lambda_3) \tag{12}$$

for a homogeneous, initially isotropic, incompressible rubber. Valanis and Landel[11], and Kawabata et al.[12], have confirmed eq 12 experimentally.

Most of the well-known nonlinear strain measures can be subsumed in a strain energy density function of the form

$$W = \frac{2G}{n^2}\left(\lambda_1^n + \lambda_2^n + \lambda_3^n - 3\right) \tag{13}$$

where n is allowed to take on any integer value between - 2 and 2. With n=2, eq 13 reduces to the so-called neohookean potential from which eq 10 follows at once. Eq 13 with integer values was first proposed by Seth.[13] It was later generalized by allowing n to be a material parameter,[14] which can take non-integral values. Ogden[15] used three terms of this same form to describe the behavior of rubbers in large tensile deformations, up to break. By allowing n to be a material parameter, none of the axioms of the constitutive theory are violated.[16] Hence from the point of view of continuum mechanics, eq 13 is a valid constitutive equation. Equation 13 has been shown by Blatz, Sharda, and Tschoegl,[14] to

be constitutive in the narrower sense for a styrene-butadiene rubber (SBR), and for natural rubber (NR), below the upswing region. Henceforth we shall call eq 13 the BST potential for convenience.

The 2NW Potential

Although the BST potential is a valid constitutive equation, the parameter n appears to be difficult to interpret molecularly. Tschoegl[17] proposed a related elastic potential which is based on the assumptions that:

(1) A crosslinked polymer can be modelled as consisting of two networks: the phantom, and the constraint network.

(2) The contribution of the two networks to W is additive.

(3) The stress-strain behavior of the phantom and the constraint networks can be described by the neohookean and the BST potentials, respectively.

The first network characterizes the effect of the change in the mean positions of the chemically crosslinked junction points. This network is called the phantom network. The chains in the phantom network can freely pass through each other and have no physical characteristics such as volume. Junction points can fluctuate freely about their mean positions. The modulus associated with the phantom network is denoted as G_X.Its stress-strain behavior is neohookean.

The second network will be called the constraint network. It models the effects of the physical nature of the polymer chains, which causes the fluctuations of the junction points to be different from their phantom counterparts. The constraint network can be modelled as if it were held together by equivalent crosslinks and may be considered to have a modulus G_N associated with it.

On the basis of these assumptions the most general form for the strain energy density function W can be written as

$$W = \frac{G_X}{2}(\lambda_1^2 + \lambda_2^2 + \lambda_3^2 - 3) + \frac{2G_N}{m^2}(\lambda_1^m + \lambda_2^m + \lambda_3^m - 3) \qquad (14)$$

where the λ's are the three principal stretch ratios, and m is the nonlinear strain parameter of the BST potential. We use m=0.34 because it closely approximates the strain function we obtain from a molecular theory which we will discuss elsewhere[16]. This reduces the unknown parameters to two, and they occur linearly in the model. This is convenient when treating experimental data. We will name the potential represented by eq 14 the 2NW (or two-network) potential. To investigate the validity of the above assumptions, we will show that eq 14 predicts the stress-strain behavior of rubber networks constitutively, in the narrower sense, and is able to predict the swelling behavior correctly. The problem of constitutiveness will be addressed first.

Constitutiveness in the Narrower Sense

In continuum mechanics, any equation that does not violate the axioms of constitutive theory[1] is a valid constitutive equation. In a stricter sense, a constitutive equation must represent material response to any mode of deformation with the same set of phenomenological coefficients. The Flory-Erman theory as well as the BST and the 2NW potentials discussed earlier appear to meet this requirement. The 2NW potential is attractive, because it has only two linear material parameters.

It can be shown[16] that, for an initially isotropic, homogeneous, and incompressible material, all possible deformations lie in the wedge-shaped region of the I_1,I_2 plane shown in Figure 1. Uniaxial tension and equibiaxial tension form the boundaries of this region, pure shear being the straight line with unit slope. Deformations outside of this wedge-shaped region are not admissible. (For a mathematical definition of admissible deformations, see Appendix 1). The whole region inside the wedge can be covered experimentally by biaxial tension

experiments in which two dimensions of a rectangular piece of material are changed independently, leaving the third dimension stress-free. Therefore, it is possible to cover all deformations that an incompressible material can undergo by performing biaxial tension measurements covering the whole range from simple tension to equibiaxial tension. If a proposed equation can describe such experiments with a single set of material parameters, the equation will very likely be constitutive. We emphasize that it is not possible to prove constitutiveness in the narrower sense; it is only possible to disprove it. One can, however, gather sufficient evidence from biaxial tension measurements to support the constitutiveness of an equation in the narrower sense.

When eq 14 is used in the Rivlin-Ariano equation, one obtains the true normal stress difference as

$$\bar{\sigma}_\alpha - \bar{\sigma}_\beta = G_\chi(\lambda_\alpha^2 - \lambda_\beta^2) + \frac{2G_N}{m}(\lambda_\alpha^m - \lambda_\beta^m) \tag{15}$$

Kawabata et al. have performed [19] general biaxial tension measurements on natural rubber crosslinked with dicumyl peroxide. Their data are plotted in Figure 2. The axes were chosen so that the theoretical predictions, as indicated by eq 15, would lie on the straight line with unit slope. The two moduli, G_χ and G_N, were obtained from simple tension data. As can be seen from the figure, agreement between experiment and theory is excellent. Some of the general biaxial tension data were left out of the figure for clarity, but the agreement for those is just as good.

Using eqs 14 and 4, one obtains

$$2\frac{\partial W}{\partial I_1} = \frac{1}{\lambda_\alpha^2 - \lambda_\gamma^2}\left[\frac{\lambda_\alpha^2(\bar{\sigma}_\alpha - \bar{\sigma}_\beta)}{\lambda_\alpha^2 - \lambda_\beta^2} - \frac{\lambda_\gamma^2(\bar{\sigma}_\gamma - \bar{\sigma}_\beta)}{\lambda_\gamma^2 - \lambda_\beta^2}\right] \quad \alpha,\beta,\gamma = 1,2,3 \tag{16}$$

$$2\frac{\partial W}{\partial I_2} = \frac{1}{\lambda_\gamma^2 - \lambda_\alpha^2}\left[\frac{\bar{\sigma}_\alpha - \bar{\sigma}_\beta}{\lambda_\alpha^2 - \lambda_\beta^2} - \frac{\bar{\sigma}_\gamma - \bar{\sigma}_\beta}{\lambda_\gamma^2 - \lambda_\beta^2}\right] \quad \alpha,\beta,\gamma = 1,2,3 \tag{17}$$

where the stress differences are given by eq 15. Figures 3-6 show the contour plots of $\partial W/\partial I_1$, and $\partial W/\partial I_2$ vs I_1 and I_2. The general shapes of the curves at large I_1 and I_2 are in agreement with those shown by Kawabata[20] et. al. They observe rather complex behavior for these contours at infinitesimal deformations which are not reproduced by our theory. We would like to point out that $\partial W/\partial I_1$ and $\partial W/\partial I_2$ have meaning only in large deformation theory. Values corresponding to infinitesimal deformations must be obtained from extrapolation of large deformation data, and are critically dependent on experimental accuracy in small extensions. Unfortunately, data in that region are subject to the largest experimental error. Therefore, the discrepancy between the contours given by our theory and Kawabata's experimental contours is not critical.

Figure 3 shows plots of $\partial W/\partial I_1$ vs I_1 for various constant values of I_2 for representative values of $\bar{\nu}_N$. Here $\bar{\nu}_N$ is the ratio G_N/G. The various values of this parameter represent different materials, $\bar{\nu}_N$=0 corresponding to a material whose stress-strain behavior is neohookean, and $\bar{\nu}_N$=1 corresponding to an uncrosslinked rubber. In most phenomenological theories, it is assumed that $\partial W/\partial I_1$ is constant with I_1 independent of I_2. As can be seen from the figure, $\partial W/\partial I_1$ as given by the 2NW potential varies linearly with I_1 but it is not independent of I_2. The variation with I_2 is small but it is nonzero for $\bar{\nu}_N$=0. The dependence of $\partial W/\partial I_1$ on I_2 is shown in Figure 4.

Figure 5 shows the variation of $\partial W/\partial I_2$ with I_1 for various constant values of I_2. It is usually assumed that this quantity is independent of I_1 and is constant with I_2. It is apparent from the figure that the predicted behavior of $\partial W/\partial I_2$ is very complex with respect to the invariants. Clearly, if the 2NW potential describes observed behavior, the Mooney Rivlin equation can not be a valid

constitutive equation. Figure 6 shows the variation of $\partial W/\partial I_2$ with I_2 for various constant values of I_1.

Crosslink Density

Figure 2 strongly supports the constitutiveness, in the narrower sense, of the 2NW potential. We now proceed to probe the nature of the phenomenological parameters. For that purpose natural rubber networks were prepared by crosslinking them to various degrees with dicumyl peroxide. (The composition of the networks and the conditions of crosslinking can be found in Appendix 2.) The crosslinking conditions were chosen on the basis of the work of Lorenz and Parks[21]. The networks were tested in simple tension using a floor model Instron Tensile Tester. The specimens prepared from the networks were end-bonded to copper U-tabs to minimize problems with clamping. A large aspect ratio was used to minimize end effects.

Applied to simple tension, eq 15 yields

$$\sigma_M = G_X + G_N \varphi_m(\lambda) \tag{18}$$

where σ_M is the Mooney stress given by

$$\sigma_M = \frac{\bar{\sigma}_1 - \bar{\sigma}_2}{\lambda_1^2 - \lambda_1^{-1}} \tag{19}$$

and $\varphi_m(\lambda)$ is given by

$$\varphi_m(\lambda) = \frac{2(\lambda_1^m - \lambda_1^{-m/2})}{m(\lambda_1^2 - \lambda_1^{-2})} \tag{20}$$

These equations follow from eq 15 with $\bar{\sigma}_2=0$, $\lambda_1=\lambda$, and $\lambda_2=\lambda_3=\lambda^{-1/2}$. Figure 7 shows of the experimental data plotted according to eq 18. The straight lines are the lines of best fit. A value of $m=0.34$ was used as mentioned earlier. The lines for these samples are almost parallel to each other indicating that G_N is closely the same for these networks.

Similar results are shown in figure 8 for SBR networks crosslinked to various extents with dicumyl peroxide. For composition of the networks, see Appendix 1. Once again the lines of best fit to the data, for the three crosslinked samples, are parallel to each other indicating that G_N is again the same for all of the networks. This point will be discussed in detail later.

We have produced evidence in support of the constitutiveness of the 2NW potential in the narrower sense. It is capable of explaining the data on networks crosslinked to various extent. The second term of the potential appears to be independent of the degree of crosslinking. This supports the assumption of additivity of the moduli as a plausible one.

Swelling of Elastomeric Networks

Swelling has been used for a long time to study the structure of polymeric networks. The stress-strain behavior of swollen networks in a uniaxial deformation is frequently analysed using the Mooney-Rivlin equation. The most important observation then concerns the Mooney constant, $2C_2$. This decreases with increasing swelling ratio, eventually becoming zero. Therefore,it has commonly been held that the values of the phantom modulus, $2C_1$, obtained from extrapolation of swollen stress-strain data are closer to the modulus calculated from the chemical constitution of these networks than $2C_1$ obtained on the dry networks.

In this section we interpret the stress-strain behavior of swollen networks using the 2NW potential. We discuss in detail the importance of the study of swollen networks, and their topological environment. We demonstrate that the parameters of the 2NW potential required to describe the behavior of dry networks serve equally to describe the behavior of swollen networks. This implies that the effect of an inert solvent is merely a dilution effect and the nature of

the topological constraints are not altered in swelling. In conclusion, we discuss these implications.

The strain energy density function, W, for unit volume of unswollen rubber is given by eq 14. Equation 14 applies to swollen networks as well as dry networks. However, to describe the stress-strain behavior of swollen networks, one needs to alter the reference state from the unswollen, undeformed state to the swollen, undeformed state. To that end, let v_2 denote the volume fraction of the polymer in the swollen state, and W_{sw} denote the strain energy density function per unit volume of swollen rubber. Then,

$$W_{sw} = v_2 W \tag{21}$$

and

$$\alpha_i = v_2^{1/3} \lambda_i \qquad i=1,2,3 \tag{22}$$

Equation 14 then becomes

$$W_{sw} = \frac{G_X}{2} v_2^{1/3} (\alpha_1^2+\alpha_2^2+\alpha_3^2-3) + \frac{2G_N}{m^2} v_2^{-(m-3)/3} (\alpha_1^m+\alpha_2^m+\alpha_3^m-3) \tag{23}$$

the α 's being the stretch ratios referred to the swollen, undeformed lengths. Using the Rivlin-Ariano equation, and the condition of incompressibility, one obtains

$$\bar{\sigma} = G_X v_2^{1/3} (\alpha_1^2-\alpha_1^{-1}) + \frac{2G_N}{m} v_2^{-(m-3)/3} (\alpha_1^m-\alpha_1^{-m/2}) \tag{24}$$

for the true stress $\bar{\sigma}$ in simple tension. The symbol $\bar{\sigma}$ has been used to denote the quantity $\bar{\sigma}_1 - \bar{\sigma}_2$, since in simple tension, $\bar{\sigma}_2$ is zero. It is customary to report the nominal Mooney stress f^* when relating the results of stress-strain measurements. One can obtain the appropriate expression for f^* from eq 5 by converting the swollen to the unswollen area, and dividing by the factor $\alpha^2-\alpha^{-1}$. Thus

$$f^* = \frac{(f/A)\, v_2^{1/3}}{\alpha - \alpha^{-2}} = G_X + G_N\, v_2^{(-m+2)/3}\, \varphi_m(\alpha) \qquad (25)$$

where A is the unswollen, undeformed cross-sectional area, and f is the force acting on it. Both eqs 24 and 25 describe the behavior of swollen networks in a uniaxial deformation, if the solvent is inert, i.e., it does not interact with the polymer chains to change their configuration, but acts merely as a diluent.

Figure 9 shows the data of Allen[22] et al. on natural rubber (NR) networks swollen in n-decane. The solid lines show the predictions of eq 25. The parameters of the two-network potential, G_X and G_N, were obtained from stress-strain measurements on the dry network as G_X=0.107 MPa and G_N=0.144 MPa. The value of m=0.34 was used for all predictions. As can be seen from the figure, the predictions of the theory are excellent for the first three volume fractions, v_2=1.00, 0.79, and 0.61. For v_2=0.42 and v_2=0.36, the predictions are fair but not very good. The discrepancy between the theory and the experiments is attributed to the solvent interacting strongly with the polymer at those swelling ratios. Such a behavior would be expected from a strong concentration dependence of the Flory-Huggins χ_1 factor. For v_2=0.24 the agreement becomes very good again. If the above inconsistency is due to a concentration effect, it is not observed at this volume fraction, because the data lie on a curve that is relatively flat.

Figure 10 shows the data of Flory and Tatara[23] on poly(dimethyl siloxane) (PDMS) networks swollen in benzene. It is apparent from the figure that the polymer-solvent interactions play a dominant role in this system. Here the χ_1 factor is highly concentration dependent, implying a marked difference in polymer configuration as the concentration is changed. Part of the difficulty arises from the fact that the experiments were performed at constant solvent activity rather than constant composition. Again the two parameters of the potential

were obtained from experiments on the dry network, and a value of m=0.34 was used. The value of the moduli were G_X=0.056 MPa and G_N=0.149 MPa.

Figure 11 shows the effect of polymer solvent interaction more clearly. In the figure Mooney plots are shown for a PDMS network swollen in three different diluents to the same volume fraction. The points in Figure 11 were calculated using the values of $2C_1$ and $2C_2$ reported by Mark[24]. At v_2=0.80 the data points for all three diluents lie on the same curve indicating the absence of polymer-solvent interactions. At v_2=0.60, differences between the three diluents are apparent.

Figure 12 shows the data of Erman and Flory [25] on poly(ethyl acrylate) (PEA) networks swollen in bis(2-ethoxy ethyl) ether at 25^0C. The experiments were made on networks crosslinked to different degrees which were then swollen to equilibrium. The open circles are the experimental points for dry networks, and the closed circles are the experimental points for the swollen networks. The solid lines show the predictions of eq 24 with m=0.34, and the two moduli obtained from the dry network stress-strain data. As can be seen, the agreement is very good.

One point is worth mentioning here. Flory and Erman[26] have examined the same data sets using their two-network theory. The value of the phantom modulus they obtain from their analysis is always larger than our G_X. Although the two quantities are supposed to represent the phantom network contribution to stress, there apparently is a difference. The reason for this difference and the resulting implications is unknown.

Conclusions

We have demonstrated the constitutiveness, in the narrower sense, of the 2NW potential. Further, we have shown that it represents data on varying

crosslink densities adequately, with a G_N that is sensibly independent of crosslink density.

We have also examined the stress-strain properties of swollen networks. When the diluent does not interact with the polymer strongly (changing the configuration of the chains in space), parameters obtained from the dry network are adequate to describe the stress-strain behavior of swollen networks. This implies that, when a network is swollen, the topological environment around the network chains is not altered significantly. The effect of the neighboring chains on a given network chain is diminished due to dilution only and is not altered significantly in character. This observation casts doubt on the existence of trapped entanglements because once swollen, their nature as well as their concentration would change.

References

1. A.C. Eringen, *Mechanics of Continuous Media*, John Wiley and Sons Inc; New York, NY (1967), 142
2. P.J. Flory, *Principles of Polymer Chemistry*, Cornell University Press, Ithaca, NY (1953)
3. H.M. James, E.J. Guth, *J. Chem Phys.*, **11** (1943), 455
4. P.J. Flory, *J. Chem. Phys.*, **66** (1977), 5720
5. P.J. Flory, B. Erman, *Macromolecules*, **15** (1982), 800
6. R.S. Rivlin, *Phil. Trans. Roy. Soc. London (A)*, **240** (1948), 459
7. R. Ariano, *Rend. Ist. Lombardo Sci. (2)*, **63** (1930), 740
8. M. Mooney, *J. App. Phys.*, **10** (1940), 485
9. A.J. Carmichael, H.W. Holdaway, *J. App. Phys.*, **32** (1961), 159
10. M. Mooney, *J. App. Phys.*, **11** (1940),582
11. K.C. Valanis, R.F. Landel, *J. App. Phys.*, **38** (1967), 2997
12. S. Kawabata, H. Kawai, *Adv. Polym. Sci.*, Springer Verlag, Berlin, **24** (1977), 89
13. Seth, in *Second Order Effects in Elasticity, Plasticity, and Fluid Dynamics*, Reiner and Abir, eds., Mc Millan, New York, NY (1973), 162
14. P. Blatz, S. Sharda, N.W. Tschoegl, *Trans. Soc. Rheol.*, **18** (1974), 145
15. R.W. Ogden, *Proc. Roy. Soc.*, **A326** (1975), 485
16. R.S. Rivlin, K.N. Sawyers, *Trans. Soc. Rheol.*, **20** (1976), 545
17. N.W. Tschoegl, *Polymer*, **20** (1979), 1365
18. Chapter III of this thesis

19. S. Kawabata, M. Matsuda, K. Tei, H. Kawai, *Macromolecules*, **14** (1981), 154

20. Y. Obata, S. Kawabata, H. Kawai, *J. Polym. Sci A-2*, **8** (1970), 903

21. O. Lorenz and C.R. Parks, *J. Polym. Sci.*, **50** (1961), 299

22. G. Allen, M.J. Kirkham, J. Padget, C. Price, *Trans. Faraday Soc.*, **67** (1971), 1278

23. P.J. Flory, Y.J. Tatara, *J. Polym. Sci. Polym. Phys. ed.*, **13** (1975), 683

24. C.U. Yu, J.E. Mark, *Macromolecules*, **7** (1974), 229

25. B. Erman, P.J. Flory, *Macromolecules* **15** (1982), 806

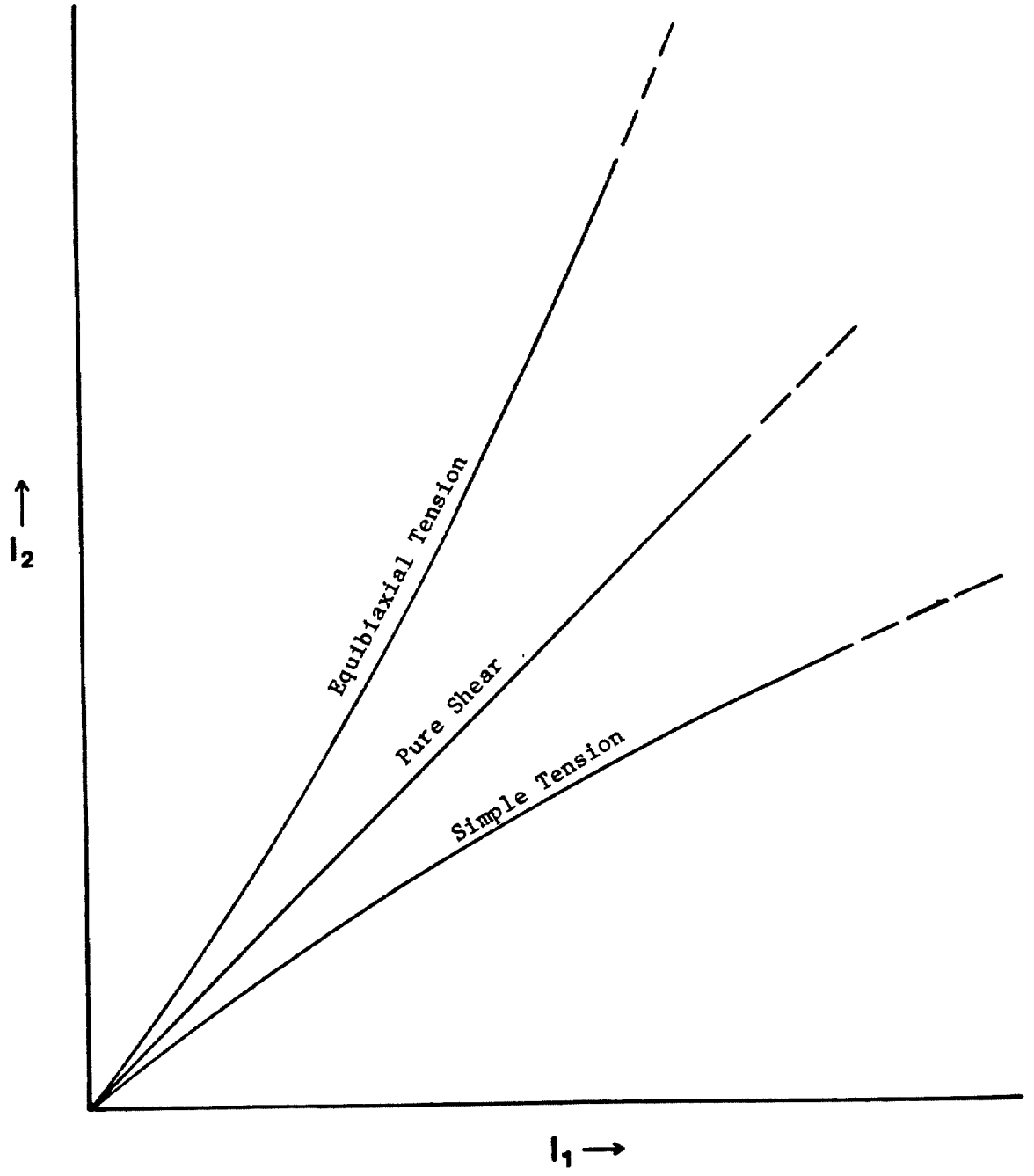

Figure 1: Region of admissible deformations for an incompressible material.

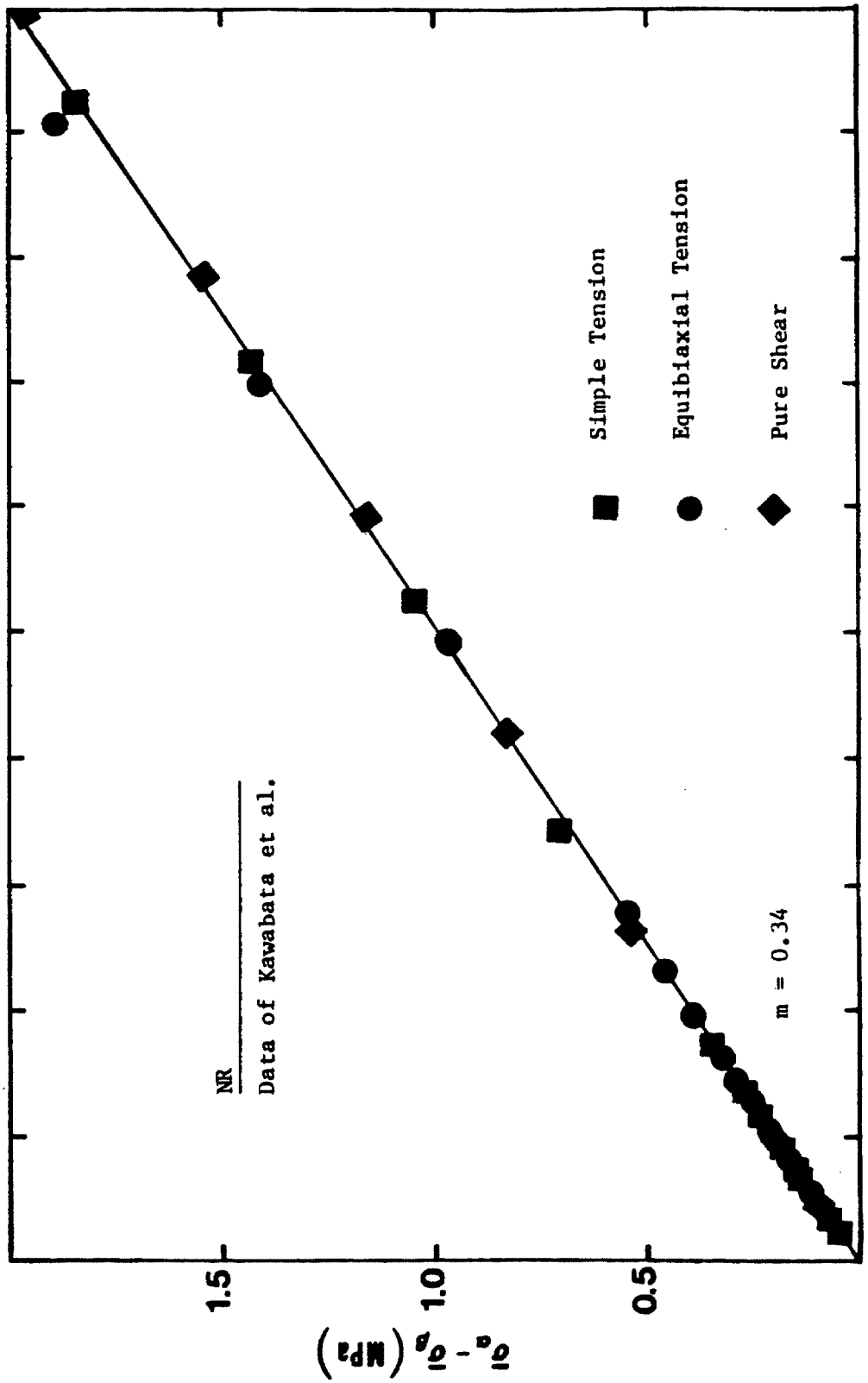

Figure 2: Data on NR compared with the predictions of the 2NW potential.

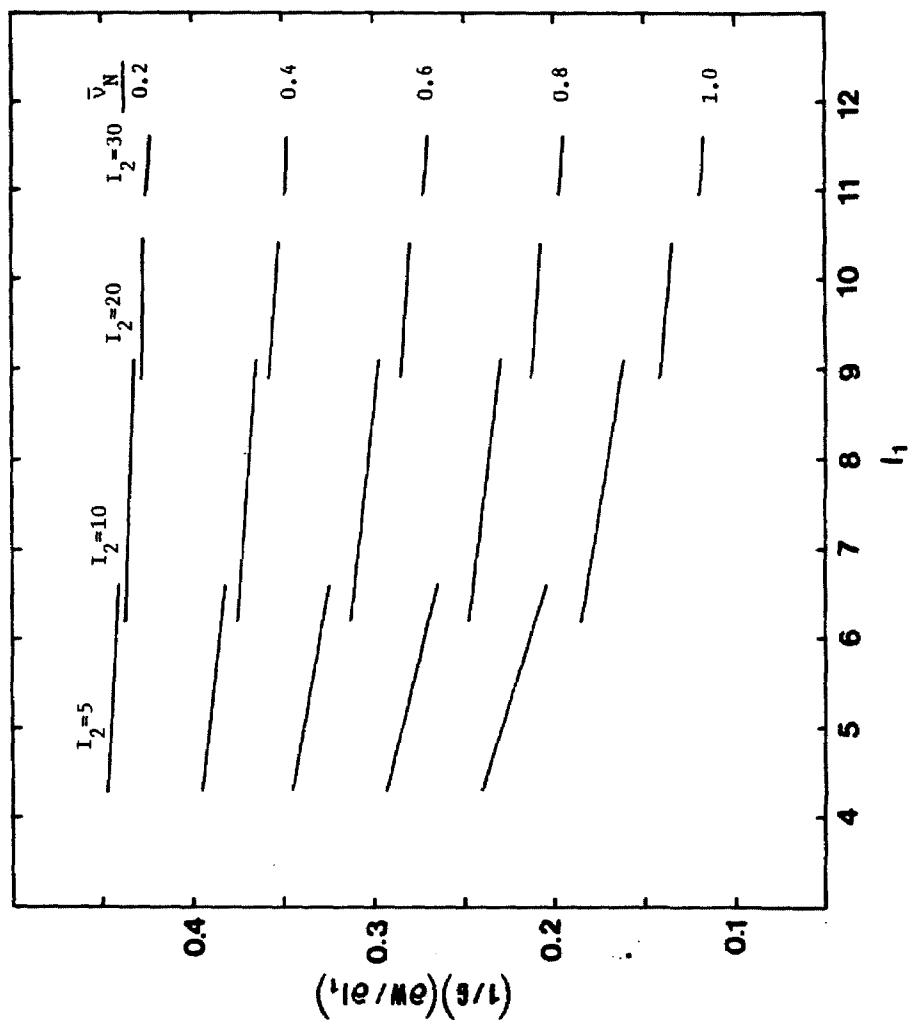

Figure 3: Predicted behavior of the derivative of the strain energy density function, W.

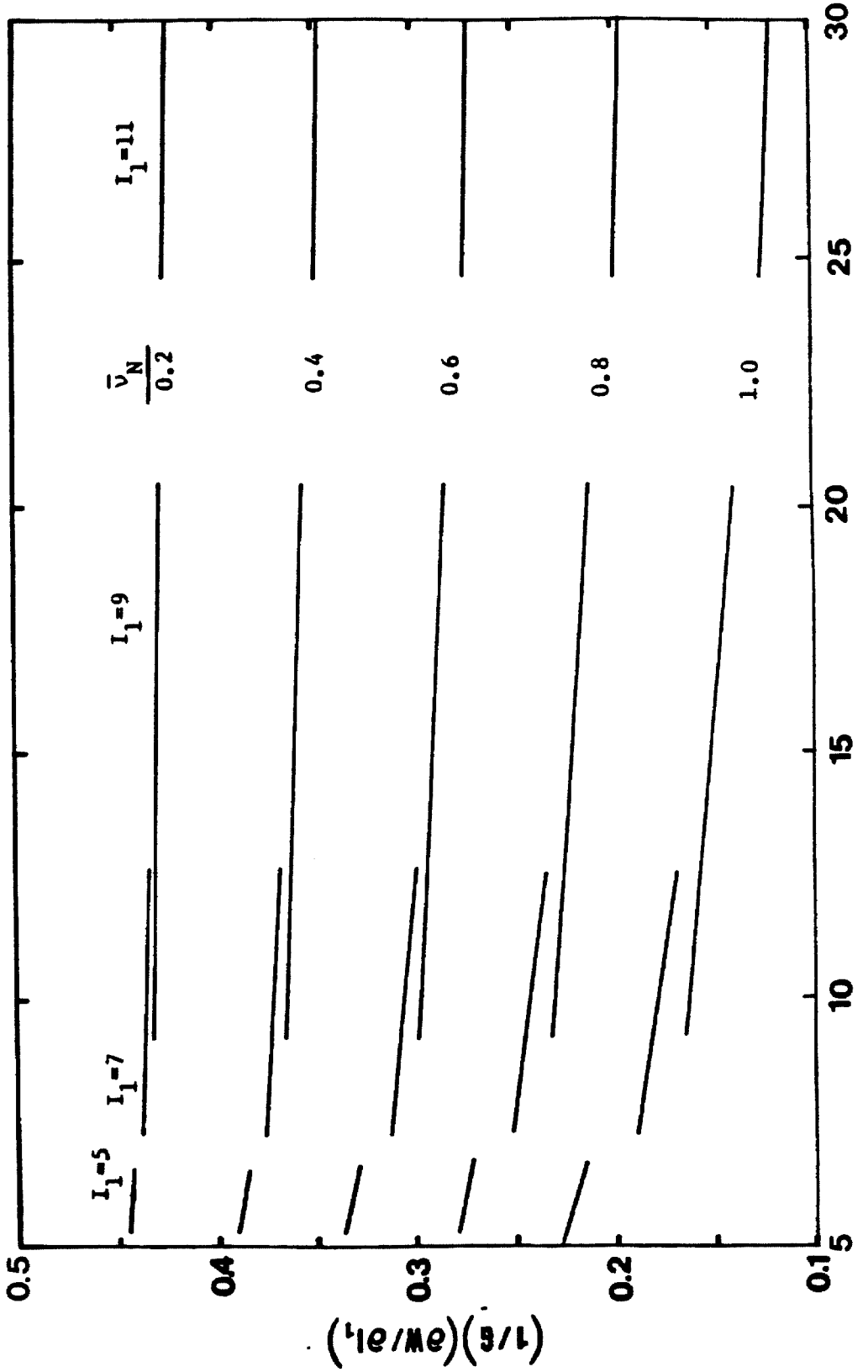

Figure 4: Predicted behavior of the derivative of the strain energy density function, W.

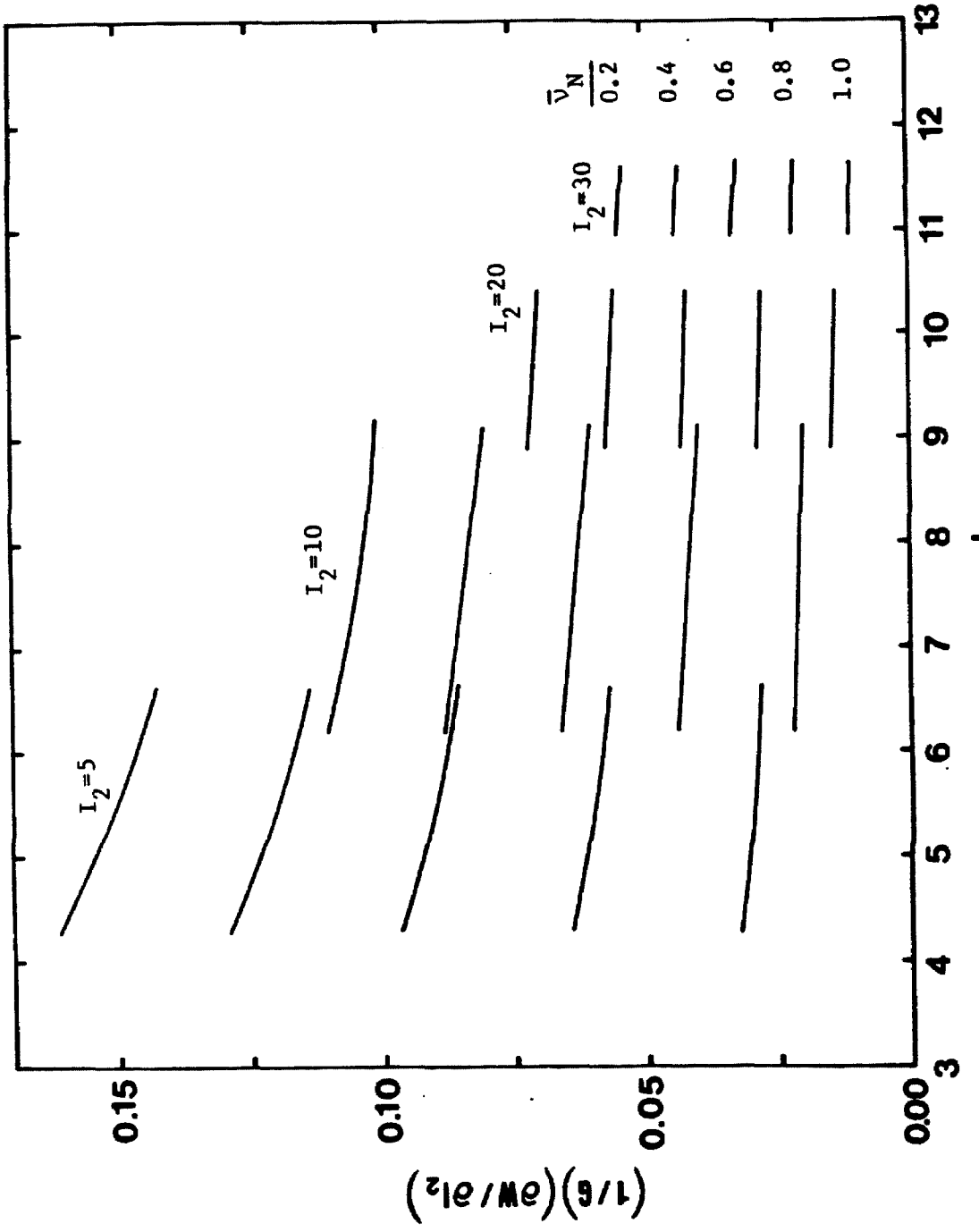

Figure 5: Predicted behavior of the derivative of the strain energy density function, W.

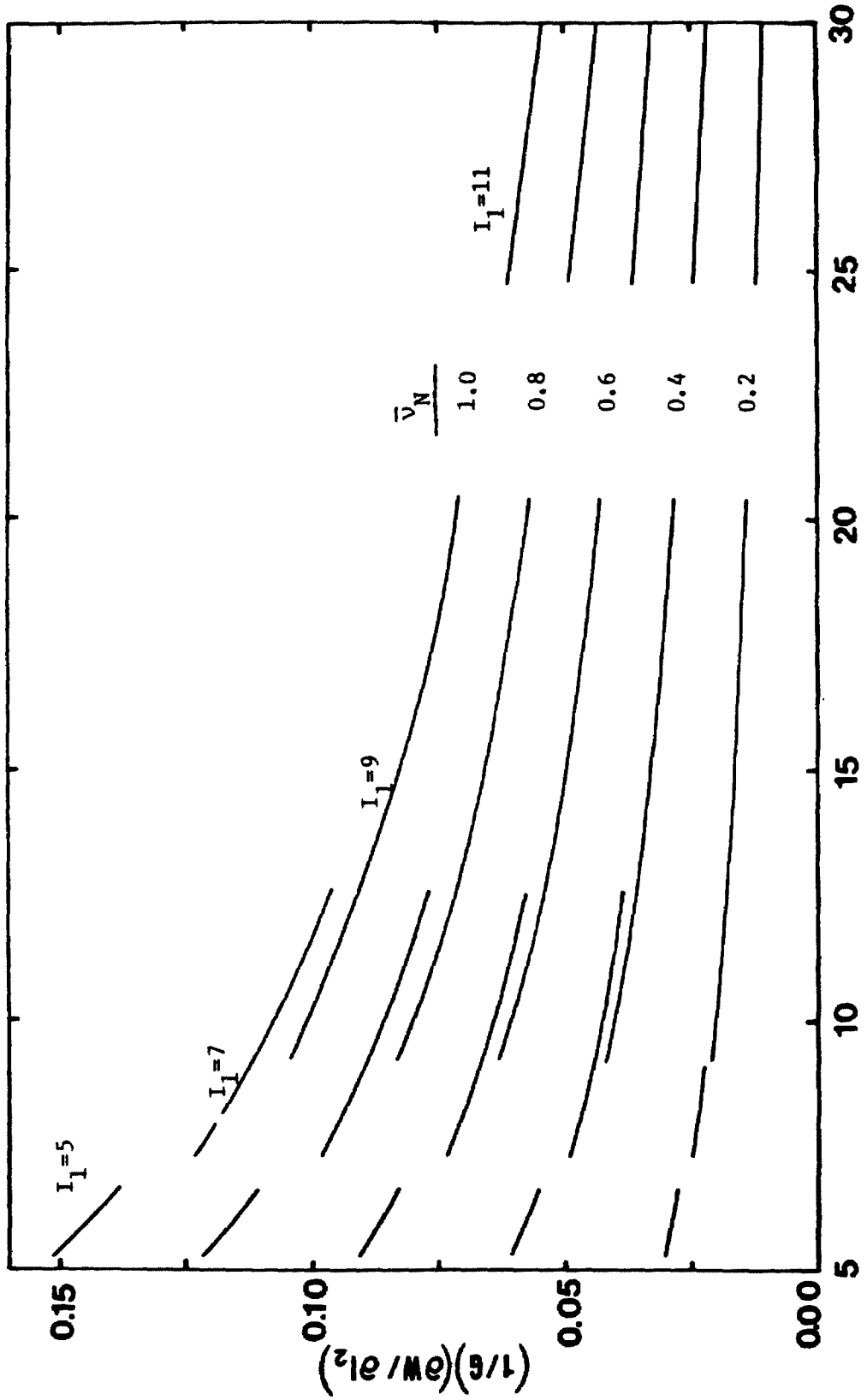

Figure 6: Predicted behavior of the derivative of the strain energy density function, W.

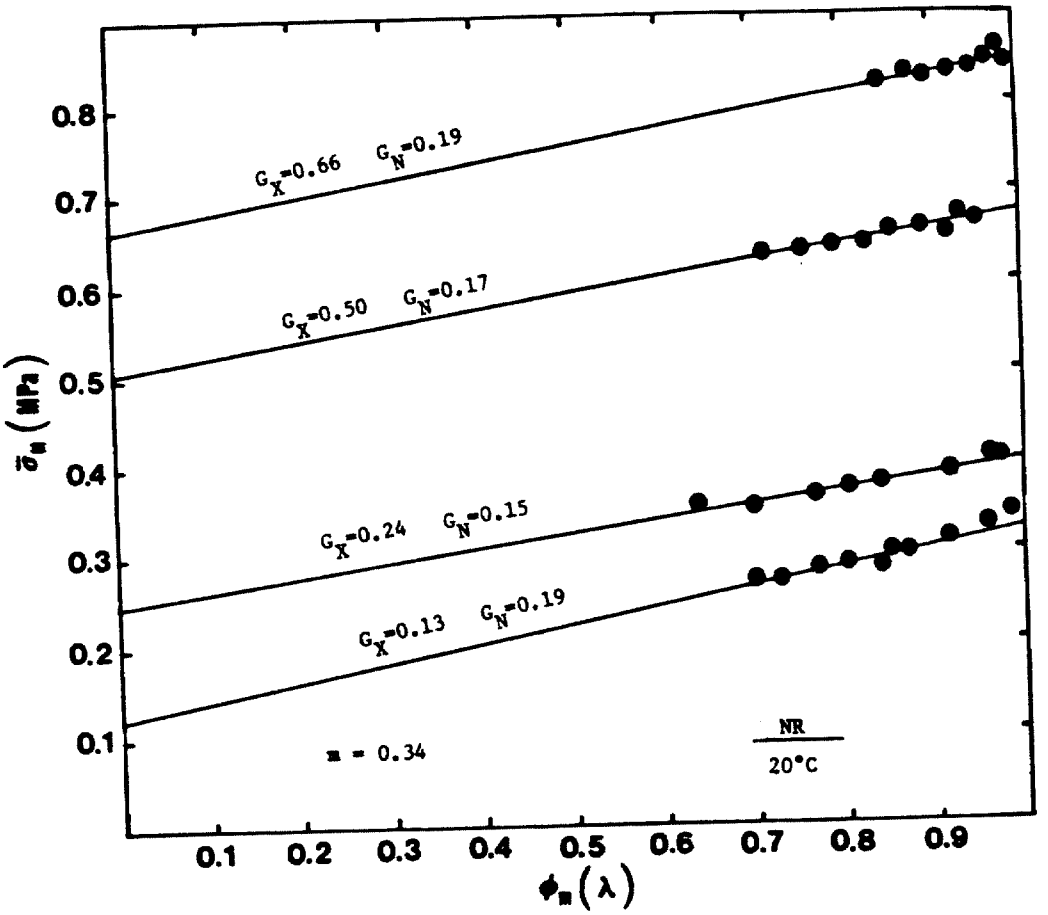

Figure 7: Equilibrium data on NR networks with varying crosslink densities compared with the predictions of the 2NW potential.

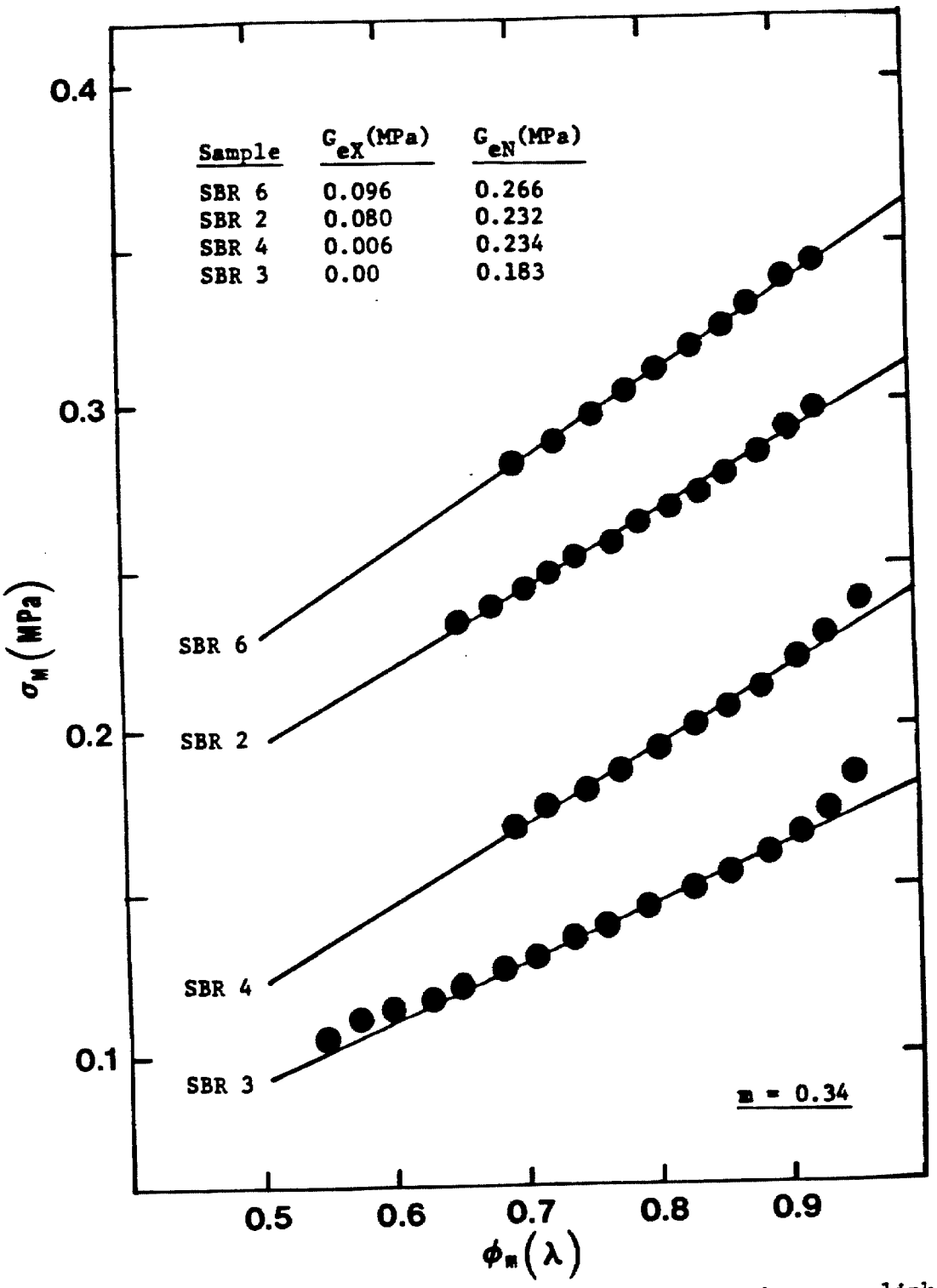

Figure 8: Equilibrium data on SBR networks with varying crosslink densities compared with the predictions of the 2NW potential.

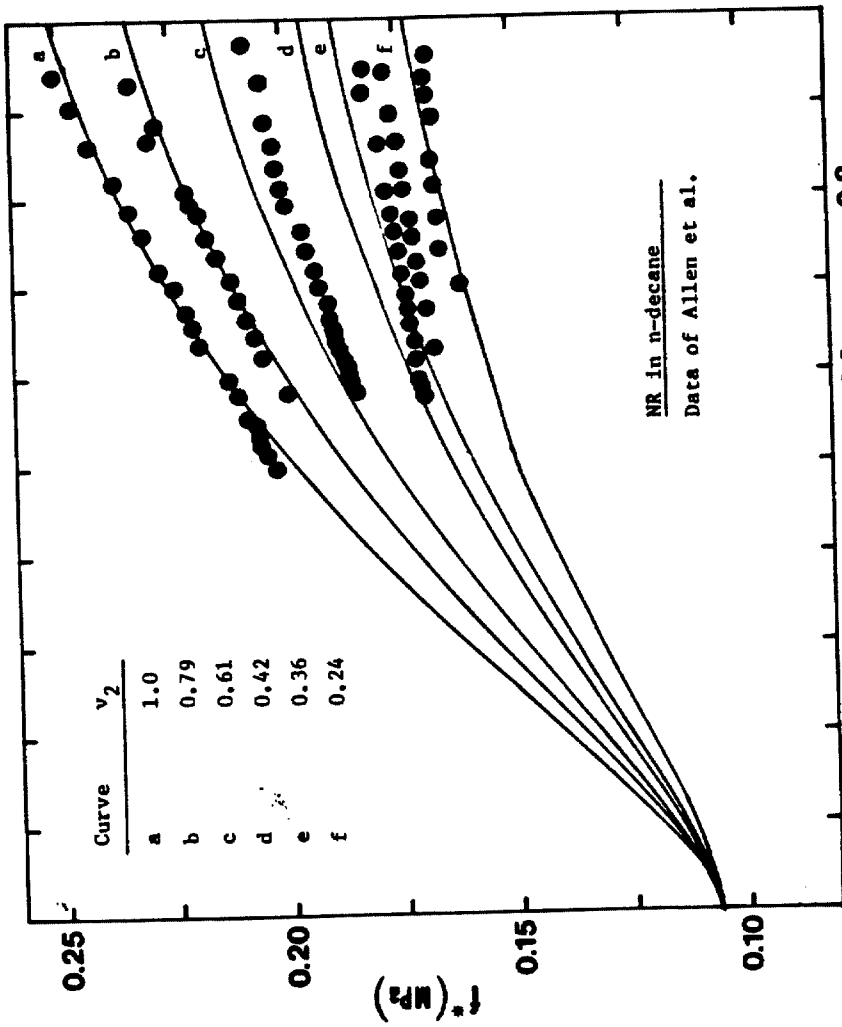

Figure 9: Stress strain behavior of a swollen network, compared to the predictions ofthe 2NW potential.

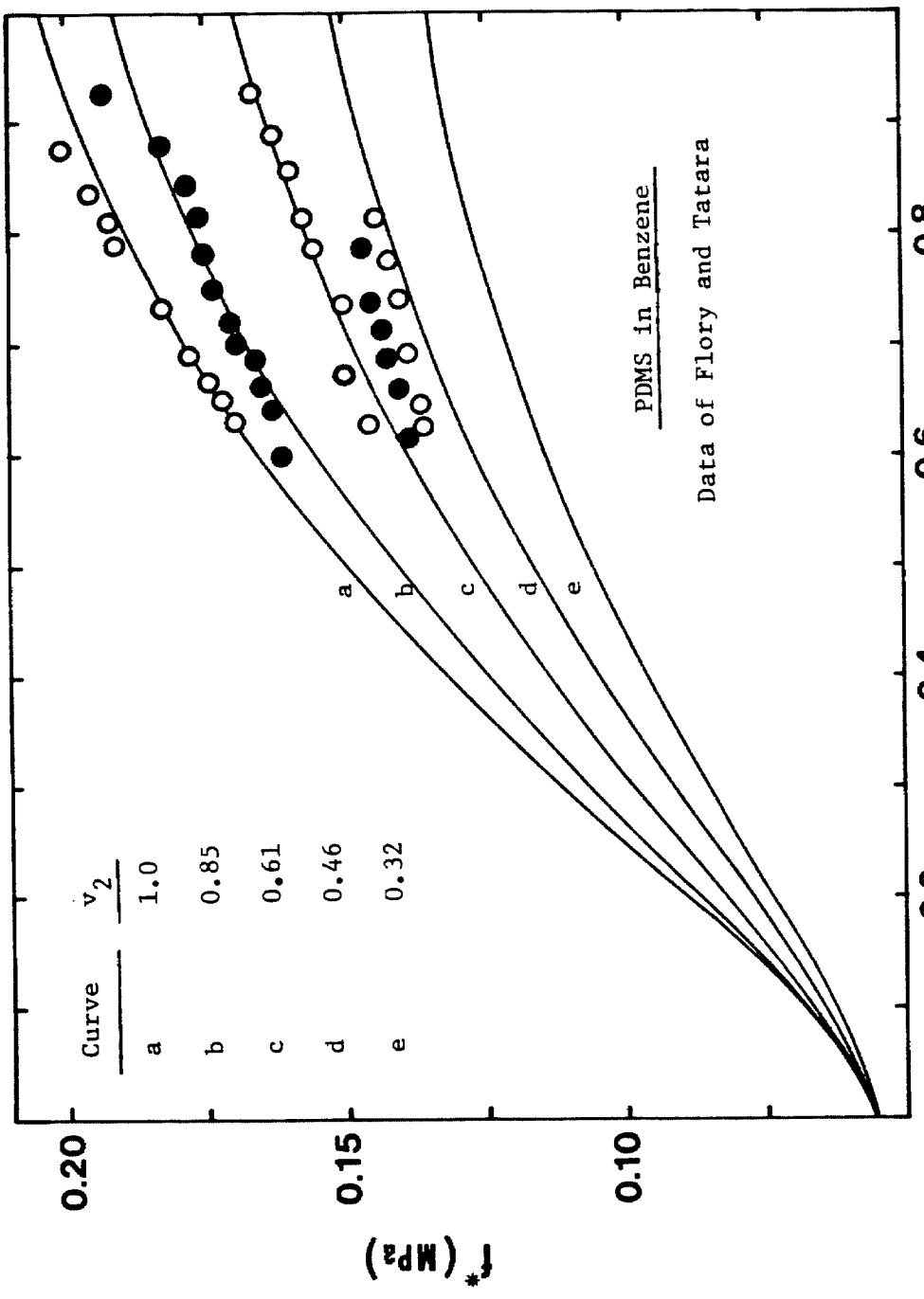

Figure 10: Stress strain behavior of a swollen network, compared to the predictions of the 2NW potential.

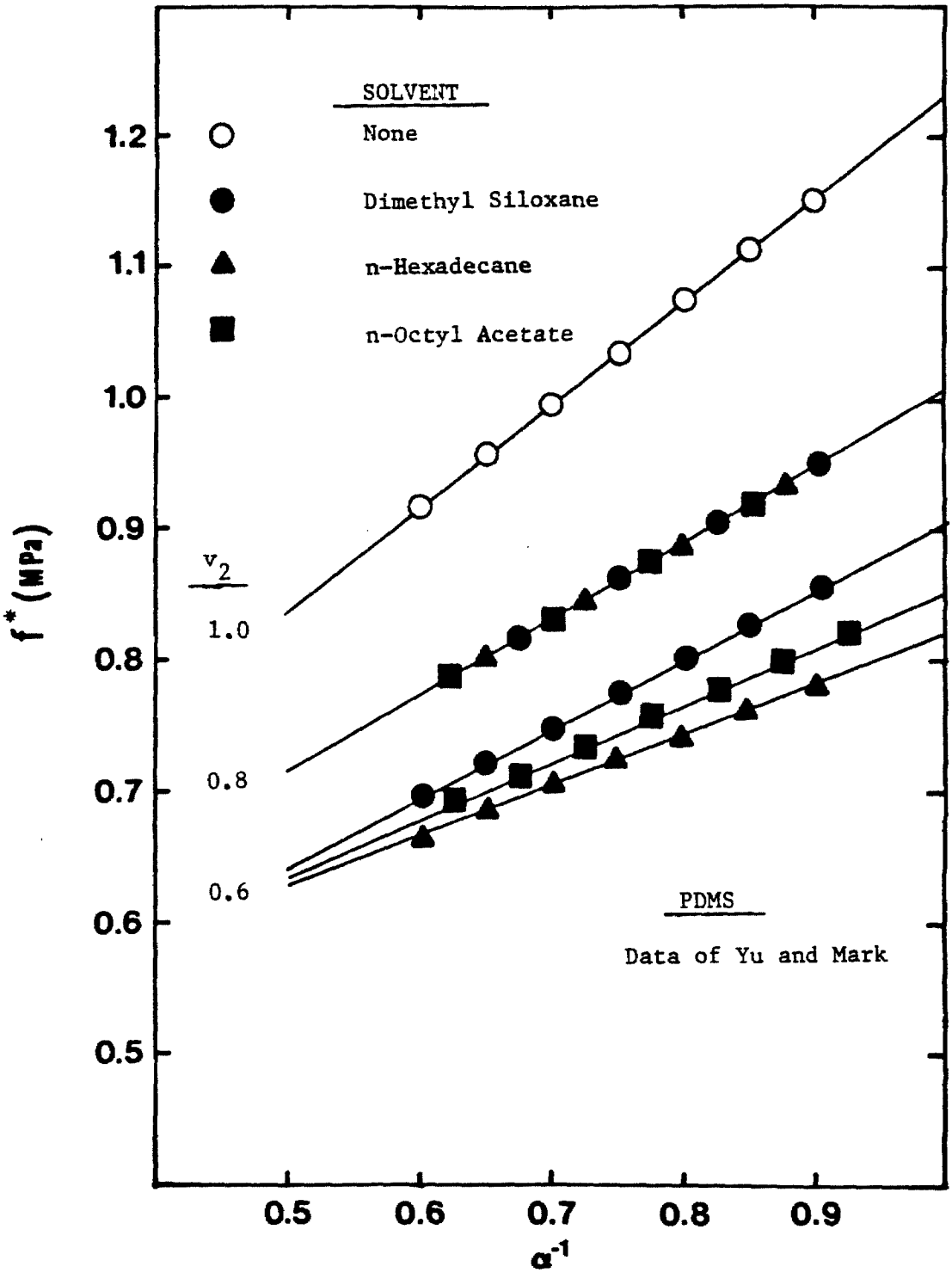

Figure 11: Stress strain behavior of a PDMS network swollen in different solvents.

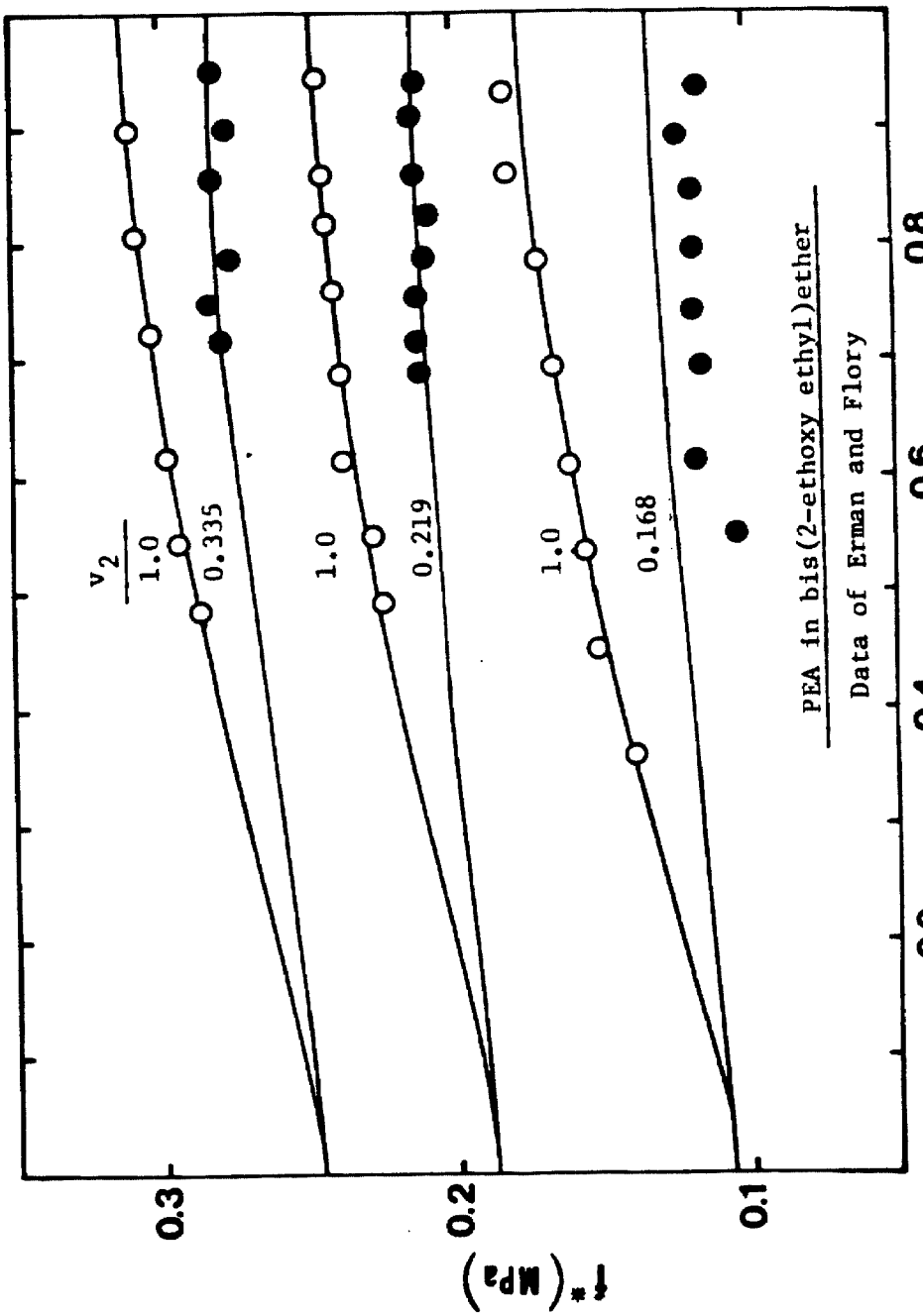

Figure 12: Stress strain behavior of PEA networks crosslinked to different degrees swollen to equilibrium. Solid lines are the predictions of the 2NW potential.

II. DETERMINATION OF THE PARAMETERS OF THE TWO-NETWORK POTENTIAL FROM MEASUREMENTS IN SMALL DEFORMATIONS

Introduction

In two previous communications[1,2], we proposed an elastic potential of the form

$$W = \frac{G_\chi}{2}(\lambda_1^2 + \lambda_2^2 + \lambda_3^2 - 3) + \frac{2G_N}{m^2}(\lambda_1^m + \lambda_2^m + \lambda_3^m - 3) \quad . \tag{1}$$

This potential was shown to be highly successful in describing arbitrary deformations (general biaxial tension) of rubberlike materials, if the deformations are moderately large, i.e., if they are restricted to the region below the upswing in a plot of the stress vs. the largest principal stretch ratio.

The potential contains three material parameters. Of these, the strain parameter m was originally left to be determined by experiment. Elsewhere,[2] however, we presented arguments which led to the adoption of a "universal" value of 0.34 for m. Of the remaining two parameters, G_χ and G_N, the first represents the modulus ascribed to the presence of chemical crosslinks in the network. The second expresses the contribution arising from topological constraints. The two moduli can be obtained from stress-strain experiments in simple tension for which eq 1 yields

$$\sigma_M = G_\chi + G_N \varphi_m(\lambda) \tag{2}$$

where

$$\sigma_M = \frac{\bar{\sigma}_1 - \bar{\sigma}_2}{\lambda_1^2 - \lambda_1^{-1}} \tag{3}$$

and

$$\varphi_m(\lambda) = \frac{2(\lambda_1^m - \lambda_1^{-m/2})}{m(\lambda_1^2 - \lambda_1^{-2})} \qquad m = 0.34. \tag{4}$$

In these equations λ is the stretch ratio and $\bar{\sigma}$ is the true stress in the direction of the stretch. The two moduli are linked by the additivity relation

$$G_X + G_N = G \tag{5}$$

in which G is the shear modulus of the material. If any two of the moduli G, G_X, and G_N are known, the third can be obtained using eq 5.

We now examine the possibility of determining the parameters of the elastic potential for moderately large deformations of rubberlike materials from measurements in small (theoretically infinitesimal) deformations. Stress relaxation measurements in such deformations on the crosslinked polymer yield the (equilibrium) shear modulus, G. We have found that G_N is proportional to the plateau modulus, G_N^0, of a high molecular weight precursor of the network, i.e., that

$$G_N = \xi G_N^0 \quad . \tag{6}$$

G_N^0 can be obtained from stress relaxation measurements in small deformations on the uncrosslinked polymer. Thus, if eq 6 is valid, and ξ is known, G_X and G_N can both be obtained from measurements in small deformations.

Results

We have tested the hypothesis contained in eq 6 on several materials for which the necessary information could be found in the literature. These materials were butyl rubber (IIR), natural rubber (NR), styrene-butadiene rubber (SBR), crosslinked cis-1,4-polybutadiene (PBD), poly(ethyl acrylate) (PEA), and poly(dimethyl siloxane) (PDMS). The values of G_N^0 for these polymers were obtained from $J_N^0 = 1/G_N^0$ as given by Ferry[3], except for PEA which was taken

from Janacek[4] et al. The values are listed in Table 1, together with estimates of $\overline{G}_N$ which were secured in the following manner. For each material, values of G_X and G_N were obtained for several crosslink densities. If our hypothesis is correct, then G_N is independent of the latter. Hence the values of G_N were averaged. These averages are shown in Table 1 as $\overline{G}_N$, together with their standard deviations (s.d.). For SBR we obtained G_X and G_N from eq 2 using our own data. For the other materials we used published values of the constants $2C_1$ and $2C_2$ of the Mooney-Rivlin equation

$$\sigma_M = 2C_1 + 2C_2/\lambda \quad . \tag{7}$$

References are listed in Table 1. From reference 6, we selected only those sets which represent variations in crosslink density.

Table I

$\overline{G}_N$ and G_N^0 for Different Rubbers

Rubber	$\overline{G}_N$ (MPa)	s.d.	N	G_N^0 (MPa)	Ref
PEA	0.0612	0.0165	5	0.160	5
PDMS	0.0764	0.0241	11	0.119	6
IIR	0.108	0.0143	3	0.288	7
NR	0.185	0.0513	37	0.575	6,8
SBR	0.244	0.0191	3	0.776	1
PBD	0.438	0.135	11	1.148	6,9

To obtain G_X and G_N we first calculated pairs of values of σ_M and $1/\lambda$ in the interval $0.5 < 1/\lambda < 0.8$ at increments of $\Delta(1/\lambda) = 0.05$, using eq 7. We then used those pairs to obtain G_X and G_N from eq 2. A plot of σ_M calculated from eq 7 is not linear in $\varphi_m(\lambda)$. However, in the interval $0.5<1/\lambda<0.8$ the departure from linearity is indistinguishable within the usual experimental error. Details of the calculations are tabulated elsewhere.[10]

A plot of $\bar{G}_N$ vs. G_N^0 is shown in Figure 1. The slope of the straight line gives ξ as 0.354. The line is the line of best fit to the natural rubber data. The error bars represent limits of ± 1 standard deviation. The errors result from a number of sources such as differences in sample preparation, vagaries in the determination of the Mooney-Rivlin constants, differences in the times used to establish equilibrium, etc. Figure 1 suggests that, for the other five materials, ξ is the same as that for natural rubber within ± 1 standard deviation.

Any crosslink density dependence of G_N, if it exists, would be hidden within the error bars in Figure 1. To determine if G_N is indeed independent of crosslink density, a plot of G_N as a function of the latter would be required. Since for most materials, the crosslinking reaction is not stoichiometric, we decided to use G_χ as a measure of crosslink density instead of the amount of crosslinker. It is shown in another publication[2] that in crosslinked polymers G_χ relaxes to its equilibrium value much faster than G_N. If any long-time relaxation processes persist, i.e., it is difficult to attain elastic equilibrium, the quantity that has not relaxed to equilibrium would be G_N. Since $G=G_\chi+G_N$, the ratio G_N/G can be expected to minimize any lack of equilibrium. Also, as shown in the next section, G_N depends more than G_N/G on network imperfections such as loose chain ends and the presence of a sol fraction. We therefore attempted to reduce the scatter by employing the ratio $\bar{\nu}_N=G_N/G$, instead of G_N. The quantity $\bar{\nu}_N$ may be viewed as the mole fraction of "equivalent crosslinks" modelling the effect of topological constraints.[11] Using eqs 5 and 6 it becomes

$$\bar{\nu}_N = \frac{G_N}{G_\chi + G_N} = \frac{\xi G_N^0}{G_\chi + \xi G_N^0} \tag{8}$$

which may be rearranged to

$$\frac{1}{\bar{\nu}_N} = 1 + \xi^{-1} \frac{G_\chi}{G_N^0}$$

(9)

The latter form is convenient in assesing the effect of crosslink density, as reflected in G_X.

The plot according to eq 9 is shown in Figure 2. The solid line is the line of best fit to the natural rubber data, the slope yielding ξ=0.354. A few of the natural rubber data were omitted from the plot for clarity of presentation.

Figure 2 strongly supports the validity of eq 6. It also suggests that ξ is independent of the nature of the polymer. A closer examination of the data reveals, however, that although eq 9 is obeyed within experimental error by all polymers examined, the main premise underlying that equation, namely, $G_N=\xi G_N^0$, sometimes appears not to be valid. A plot of G_N vs. G_X for various natural rubber networks studied by Mullins et al.[12], is shown in Figure 3. The data indicate that G_N may be weakly dependent on crosslink density. We found this dependence to be due to the presence of loose chain ends in the network. As we will show in the next section, the crosslink density dependence of G_N disappears when this is accounted for.

The Loose End Correction

According to Flory[13], the number of moles per unit volume of elastically active crosslinks, ν_X, is given by

$$\nu_X = \nu_X^{chem} (1 - 2M_C/\overline{M}_n) \tag{10}$$

where ν_X^{chem} is the number of moles of chemical crosslinks per unit volume put in, M_C is the molecular weight between crosslinks, and $\overline{M}_n$ is the number average molecular weight of the polymer before crosslinking. The modulus due to the presence of chemical crosslinks is then given by

$$G_X = \frac{1}{2}\nu_X R T \tag{11}$$

The volume fraction of loose ends, v_L, is given by

$$v_L = \frac{M_C}{M_C + \overline{M}_n} \quad . \tag{12}$$

Therefore, if networks having the same ν_X^{chem} (and thus the same M_C) were prepared with differing $\overline{M}_n$, one would be able to determine the effect of loose chain ends on G_N. Mullins et al.[12] report stress-strain data on such networks.

As shown in a previous publication,[1], in a swollen network the true stress referred to the swollen, deformed area may be represented by

$$\overline{\sigma} = G_X v_2^{1/3} (\lambda^2 - \lambda^{-1}) + \frac{2G_N}{m} v_2^{(-m+3)/3} (\lambda^m - \lambda^{-m/2}) \tag{13}$$

where v_2 is the volume fraction of the polymer. For v_2 close to unity, the dilution effect on G_X is minimal, while G_N varies linearly with the concentration of network chains. Since at equilibrium the loose ends would act like a diluent, G_N corrected for loose ends is given by

$$G_N^{corr} = \frac{G_N}{1 - v_L} \tag{14}$$

In Figure 4, Mullins's data are plotted according to eqs 10 and 11. The straight lines represent the least squares fit to the data. The intercept yields the quantity $G_X(\overline{M}_n = \infty) = \frac{1}{2}\nu_X RT$, and the slope divided by $G_X(\overline{M}_n = \infty)$ yields $2M_C$. Using eqs 12 and 14, one can calculate the G_N values corrected for loose ends. Mullins's network designated by B was left out of our analysis because the data on this particular network were badly scattered.

G_N^{corr} vs. G_X plots are presented in Figure 5. As can be seen, there is no clear trend in the data, and G_N^{corr} appears to be indeed independent of crosslink density.

Conclusions

In this paper we have examined the validity of eq 6, which suggests that the modulus characterizing the topological constraints is independent of crosslink density, and that all the information which differentiates the topological environment of a network can be obtained from the uncrosslinked polymer. One important implication of the validity of eq 6 concerns the concept of trapped entanglements. If the nature of G_N were related to trapped entanglements, its crosslink density dependence would be more pronounced. Our analysis implies that the nature of G_N is related to a decrease in the configurations available to the network chains as compared to their phantom counterparts. This is implied by the fact that the topological environment of the uncrosslinked polymer is carried over to the crosslinked counterpart.

Although in form the preceding theory appears to be similar to the theory of Langley,[14] it is in fact quite different. The latter theory has been discussed at length by Queslel and Mark[15]. In the Langley theory, one has no way of separating the effect of topological constraints from the phantom network, because the strain dependence of the constraint network is unspecified. Therefore, the conclusions one would draw from the Langley theory are dependent on the assumption made about the relation of the chemical composition of the network to the modulus due to chemical crosslinks. In our theory, no such assumption is necessary, because we obtain both moduli from experimental data.

We would like to point out that the conclusions we have drawn are not expected to be valid near the gel point. We have also based all of our conclusions on data on randomly crosslinked, tetrafunctional networks. Major differences are not expected for end-linked networks. The value of ξ would probably depend on network functionality. Most of the available data on networks that are not tetrafunctional are on PDMS. Unfortunately, PDMS has a very low G_N^0 so that the

values of G_N would be relatively small. This fact precluded the study of functionality dependence of ξ.

References

1. Chapter I of this thesis

2. Chapter III of this thesis

3. J.D. Ferry, *Viscoelastic Properties of Polymers*, John Wiley and Sons, New York, N.Y. (1980), 374

4. J. Janacek, J. Hrouz, *J. Polym. Sci., Polym. Symp.*, **53** (1975), 203

5. J.E. Mark, M. Kato, J.H. Ko, *J. Polym. Sci., Polym. Symp.*, **54** (1976), 217

6. J.E. Mark, *Rubber Chem. Tech.*, **48** (1975), 495

7. M. Kato, J.E. Mark, *Rubber Chem. Tech.*, **49** (1976), 85

8. L. Mullins, *J. App. Polym. Sci.*, **2** (1959), 257

9. B.M.E. Van der Hoff, E.J. Buckler, *J. Macromol. Sci. (A)*, 1 (1967), 747

10. Appendix IV of this thesis

11. N.W. Tschoegl, *Polymer*, **20** (1979), 1365

12. L. Mullins, *J. App. Polym. Sci. (a)*, **2** (1959), 1

13. P.J. Flory, *Principles oof Polymer Chemistry*, Cornell Univ. Press, Ithaca, N.Y. (1953), 463

14. R.N. Langley, *Macromolecules*, 1 (1968), 348

15. J.P. Queslel, J.E. Mark, Submitted to *Adv. Polym. Sci.*

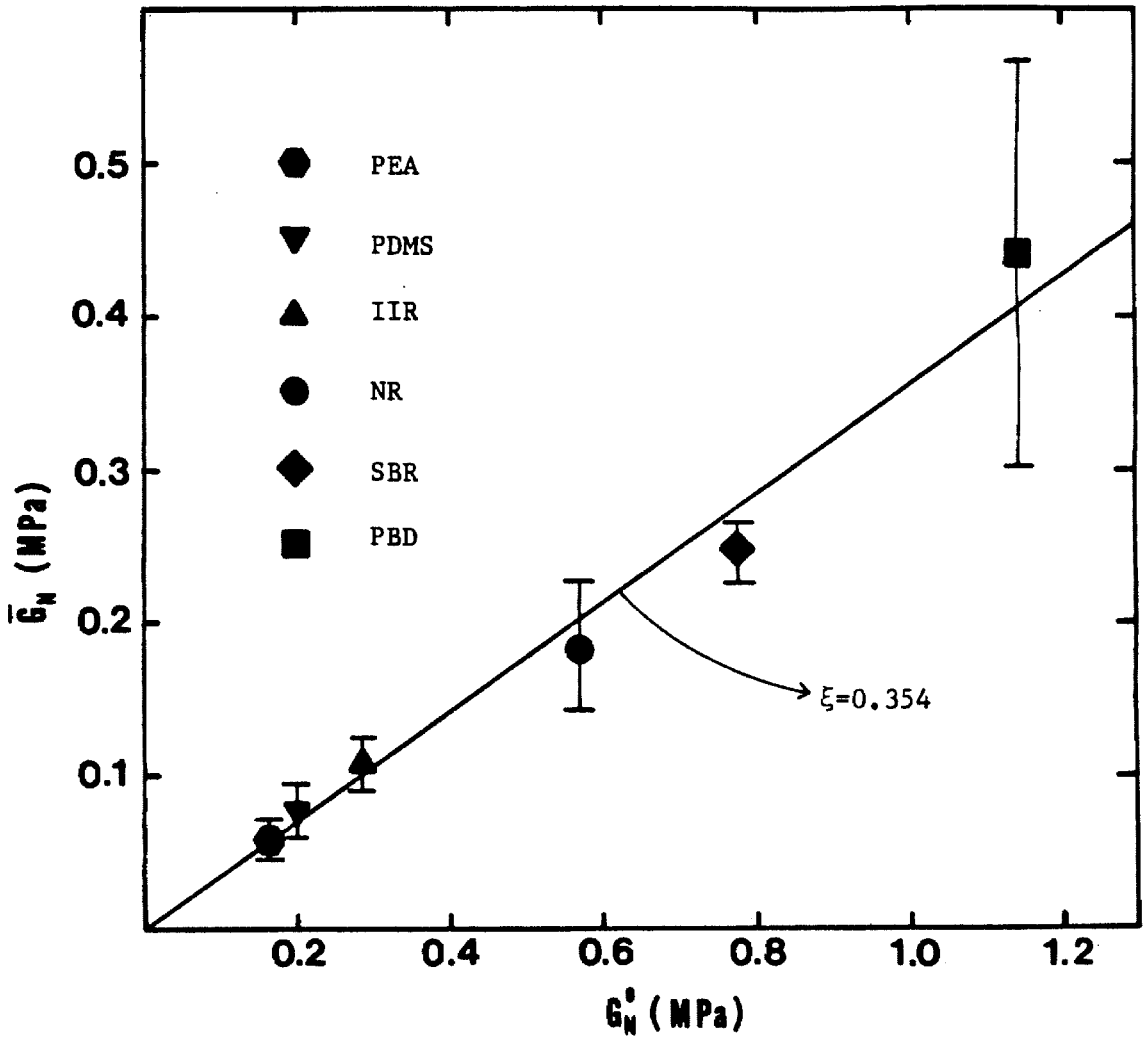

Figure 1: $\bar{G}_N$ as a function of G_N^0 for different rubbers.

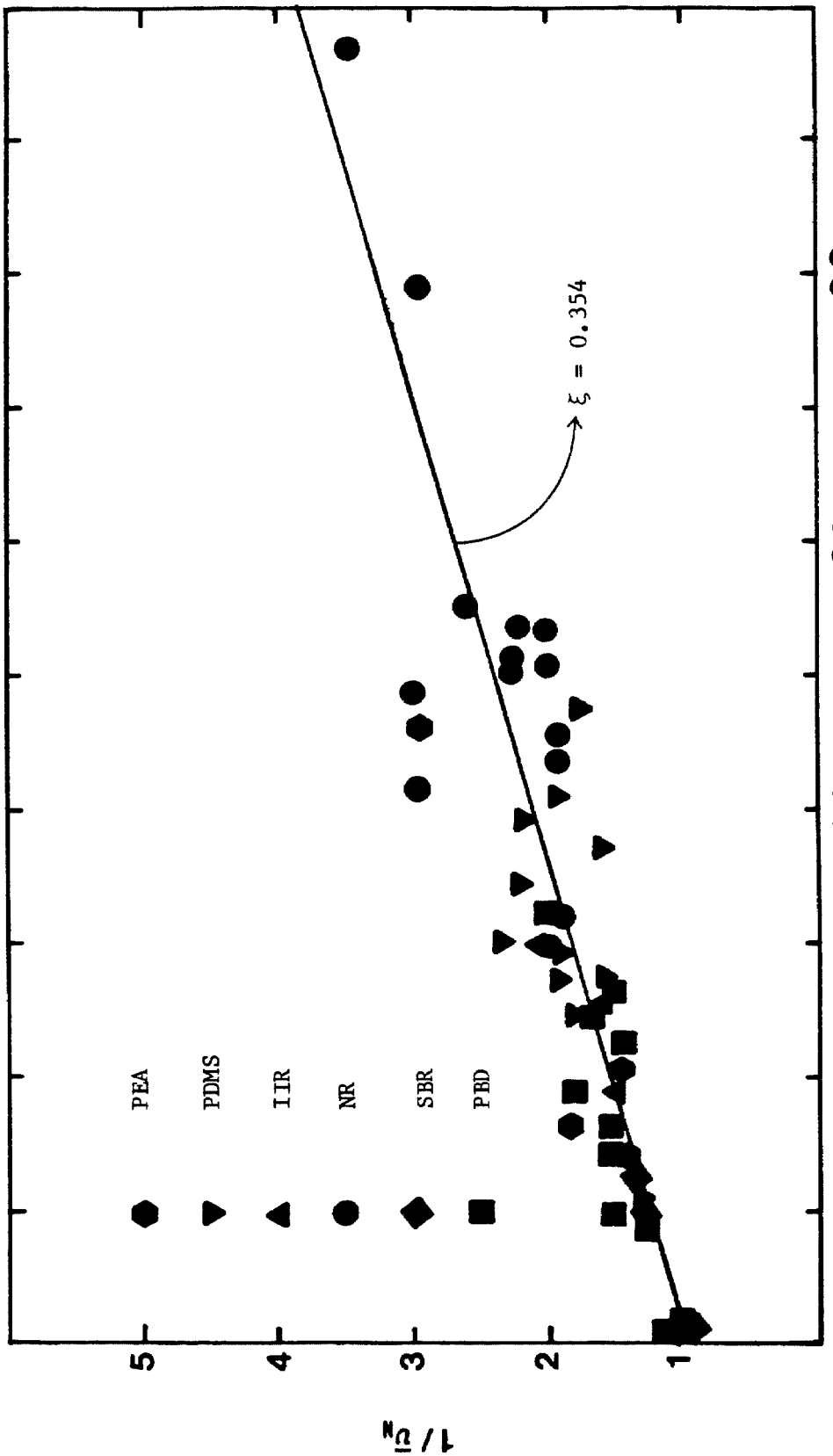

Figure 2: Mole fraction of crosslinks as a function of crosslink density, for different rubbers.

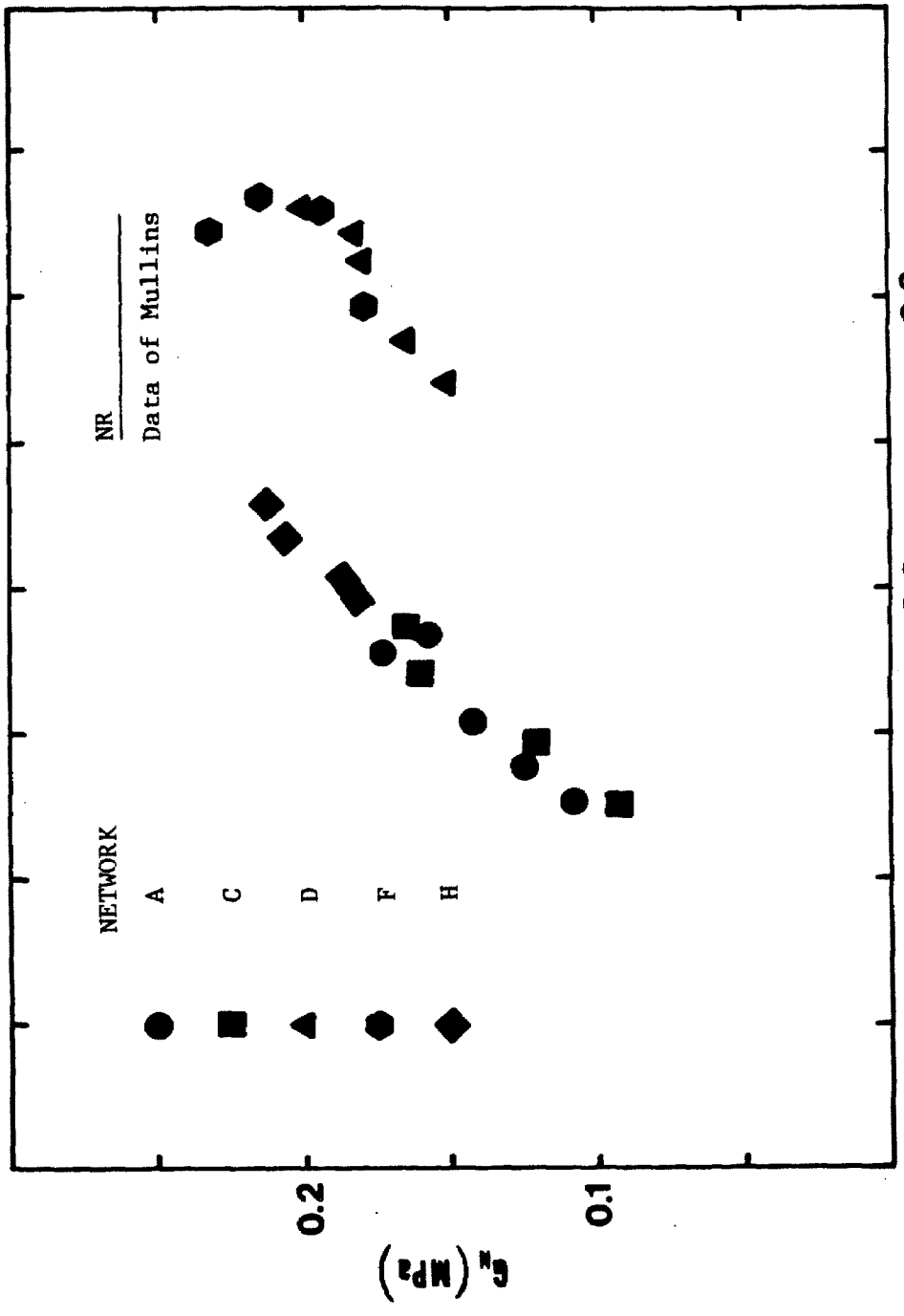

Figure 3: Data of Mullins showing G_N as a function of crosslink density.

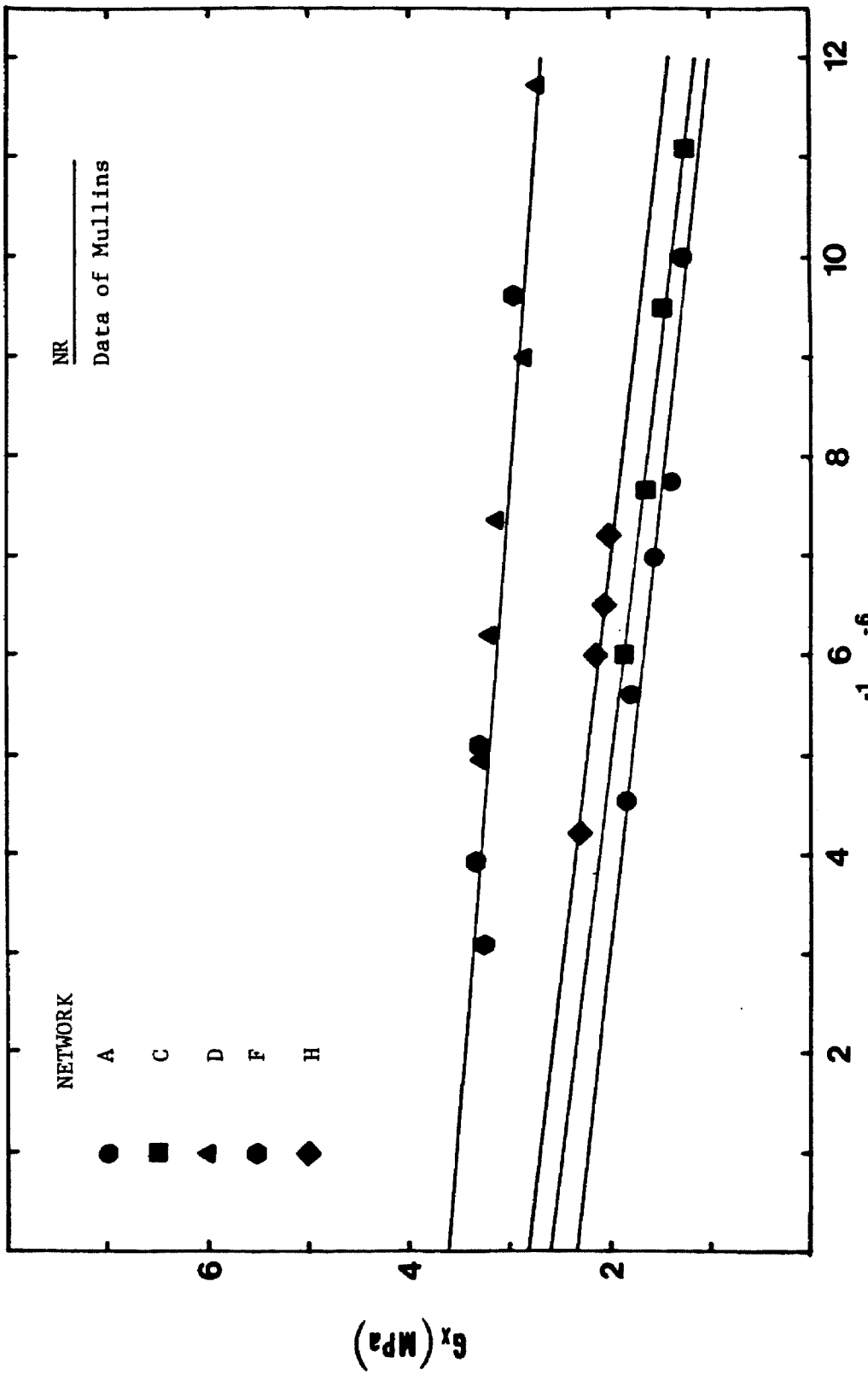

Figure 4: Dependence of G_x on the molecular weight of the precursor.

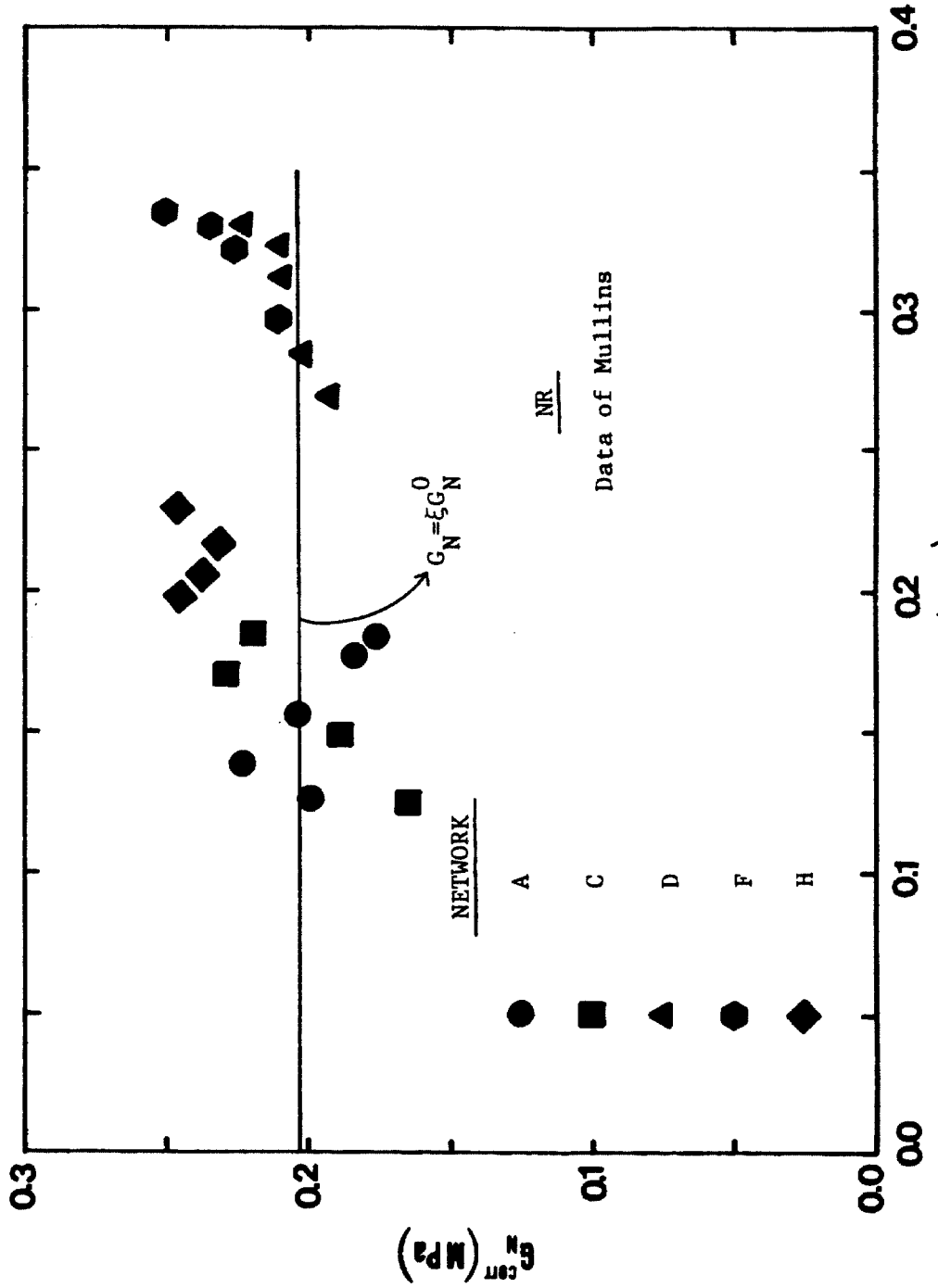

Figure 5: Data of Mullins corrected for lose ends.

III. MOLECULAR DESCRIPTION OF STRESS RELAXATION IN POLYMER NETWORKS

Introduction

In a previous publication[1] we described a two-network potential for moderately large deformations of rubberlike materials at mechanical equilibrium. Using published data, we showed[1] that the potential is constitutive in the narrower sense, i.e., it is capable of describing equilibrium deformations in different stress fields with the same set of material parameters. The potential was derived from simple considerations. In the present paper we develop a theory for the time dependent behavior of crosslinked networks, again in moderately large deformations. Our approach is based on the ideas developed by Doi[2] and, for ease of reference, we usemuch of the same notation.

We first formulate the theory and then proceed to a discussion of it using published data as well as our own obtained on styrene-butadiene rubber (SBR).

Theory

We use the mean-field approximation to formulate a molecular picture of the dynamics of crosslinked polymers. We consider the properties of a single chain embedded in a continuum formed by its neighbors. The interaction of the chain with its neighbors are modelled as interactions with this continuum. In this way, we reduce a multi-chain problem to that of a single chain. We also assume that the molecular motions of the chains result solely in changes in configurational entropy, i.e. there are no enthalpic interactions between them. These two assumptions are implicit in most theories describing the equilibrium and time-dependent properties of both crosslinked and uncrosslinked polymers in the rubbery region.

Consider a network chain terminated in chemical junction points at both of its ends. At any instant in time, the chain is confined to a certain configuration

by its neighbors. When deformed, it must move in the field so defined. To describe the effects of its neighbors on the chain, we place N slip links along its length as shown in Figure 1. Let the chain segment between two slip links be modelled by N_e Rouse (bead-and-spring) units with mean-square separation b^2. Let ζ denote the friction coefficient of the Rouse units. Let the total number of Rouse units between two crosslink points be denoted by N_0, and let a be the distance between two slip links. The complete sequence of Rouse units is called the primitive chain. It has the same end-to-end distance as the real chain which wraps around the primitive chain. Let its contour length (called the primitive path length) be denoted by L. With the definitions given above, we have

$$N = N_0 / N_e \tag{1}$$

and

$$L = aN = N_0 b^2 / a \tag{2}$$

The slip links have been introduced merely as a mathematical convenience in modelling the effect of the surrounding chains. We do not necessarily imply physical entanglements, although our model could not differentiate between entanglements and other types of topological interactions which restrict the configurations of the chain in space.

To allow us to describe the dynamics of the chain mathematically, let $\mathbf{r}_n(t)$ be the position of the nth Rouse unit at time t, and let $\mathbf{R}_n(s_n(t);t)$ be the vector defining the curvature of the primitive chain at point n, where $s_n(t)$ denotes the arc length at the same point measured from the first (n=0) segment. To represent the wriggling motion of the chain along its primitive path, denote $\mathbf{r}_n(t)$ as

$$\mathbf{r}_n(t) = \mathbf{R}_n(s_n(t);t) + \mathbf{d}_n(t) \tag{3}$$

where $\mathbf{d}_n(t)$ is a vector normal to $\mathbf{R}_n(s_n(t);t)$ at $s_n(t)$. Then, $s_n(t)$ and $\mathbf{d}_n(t)$

represent the wriggling motion in the longitudinal and transverse directions, respectively. The relaxation of $\mathbf{d}_n(t)$ corresponds to the relaxation of the Rouse units between two slip links. The relaxation of $s_n(t)$ describes the relaxation of the primitive chain between two crosslink points.

Stress Relaxation

It will be assumed that when a macroscopic deformation is applied to the polymer network as a step function of time, all junction points and slip links first move affinely with the deformation. They can then move further during the two relaxation processes just discussed.

(a) Relaxation of $\mathbf{d}_n(t)$

The relaxation of $\mathbf{d}_n(t)$ corresponds to the transverse wriggling motion of the chain. The mathematics of this process for an uncrosslinked polymer has been described in detail by Doi.[2] In the time scale of this motion, the crosslinked polymer relaxes in exactly the same way as the uncrosslinked polymer, since the length a of the relaxing unit is much smaller than the the length between two crosslinks ($N_0 b$). Therefore, the true stress resulting from the wriggling motion is the same as that given by Doi, and we have

$$\bar{\sigma}_{\alpha\beta}(t) = 3c\,(N_0/N_e)k_BT[1 + \sum_{p=1}^{\infty} exp\,(-tp^2/\tau_A)] < (\mathbf{F}\cdot\mathbf{u})_\alpha\,(\mathbf{F}\cdot\mathbf{u})_\beta>_{\mathbf{u}} - P\delta_{\alpha\beta} \qquad (4)$$

where $\tau_A = \dfrac{\zeta b^2}{6\pi^2 k_B T} N_E^2$ is the largest relaxation time associated with the relaxation of $\mathbf{d}_n(t)$, k_B and T have their usual significance, c is the number of network chains per unit volume, $\mathbf{F}$ is the deformation gradient tensor, and $\mathbf{u}$ is a unit vector with random orientation, defined by

$$\mathbf{u} = (\cos\vartheta\,,\ \sin\vartheta\cos\varphi\,,\ \sin\vartheta\sin\varphi\,) \qquad (5)$$

The average over $\mathbf{u}$ is defined by

$$<....>_u = \frac{1}{4\pi} \int_0^{2\pi} \int_0^{\pi} (....) \sin\vartheta d\vartheta \, d\varphi \tag{6}$$

(b) Relaxation of $s_n(t)$

Again following Doi, we assume that the relaxation of $s_n(t)$, corresponding to the longitudinal wriggling motion of the chain, can be described by the equation for the free Rouse chain.[2] We have

$$\zeta \frac{\partial s_n(t)}{\partial t} = (3k_BT/b^2) \frac{\partial^2 s_n(t)}{\partial n^2} + f_n(t) \tag{7}$$

where $f_n(t)$ is a random force assumed to be Gaussian, characterized by the moments

$$<f_n(t)>_u = 0 \qquad \text{and} \qquad <f_n(t)f_m(t')>_u = 2\zeta k_BT\delta(n-m)\delta(t-t') \tag{8}$$

Equation 7 is the continuous form of the diffusion equation for the Rouse chain.[3] The Cauchy stress tensor is then given by

$$\bar{\sigma}_{\alpha\beta}(t) = (3ck_BT/b^2) \int_0^{N_0} <\frac{\partial r_{n\alpha}(t)}{\partial n} \frac{\partial r_{n\beta}(t)}{\partial n}>_u dn - P\delta_{\alpha\beta} \tag{9}$$

where P is the hydrostatic pressure required by the underlying assumption of incompressibility. The approach taken here differs from the original theory of Rouse in two important points. In the Rouse theory the boundary conditions at the chain ends are $\partial s_n(t)/\partial n = 0$ at $n = 0, N_0$. As discussed by Doi and Edwards[4], a fictitious tensile force F_{eq} must be assumed to act at the chain ends. If this force were absent, the polymer chain would soon break free of the slip links and assume configurations that would allow it to interpenetrate with the surrounding chains. For an uncrosslinked polymer the average magnitude of this force is

$$F_{eq} = \frac{3k_BT}{a} = (3k_BT/b^2) <\frac{\partial s_n(t)}{\partial n}>_u \qquad n = 0, N_0 \tag{10}$$

It follows from eq 10 that

$$<\frac{\partial s_n(t)}{\partial n}>_u = \frac{b^2}{a} = \bar{l} \qquad n=0,N_0 \tag{11}$$

which implies that the primitive path length of the chain is equal to its equilibrium length, $L = \bar{l}N_0$, after $s_n(t)$ has relaxed. In other words, the chain eventually shrinks back to its undistorted length. In the case of a crosslinked polymer, the chain cannot shrink to its undistorted length because the chemical junction points will restrict its movement. The amount it can shrink will be assumed to be proportional to the macroscopic deformation. Therefore, the boundary conditions, eq 11, must be replaced by

$$<\frac{\partial s_n(t)}{\partial n}>_u = z <| \mathbf{F}\cdot\mathbf{u} |>_u \bar{l} \qquad n=0,N_0 \tag{12}$$

where z is a proportionality constant. Equation 7 and the boundary conditions given by eq 12 describe the dynamics of the chain between two chemical junction points with the stress given by eq 9 or (see Appendix 3), equivalently by,

$$\bar{\sigma}_{\alpha\beta}(t) = (3ck_BT/b^2) \int_0^{N_0} (<l_n(t)>_u)^2 <v_{n\alpha}(t)\, v_{n\beta}(t)>_u dn - P\delta_{\alpha\beta} \tag{13}$$

where

$$l_n(t) = \frac{\partial s_n(t)}{\partial n} \tag{14}$$

and

$$\mathbf{v}_n = \frac{\partial \mathbf{R}_n(s_n(t);t)}{\partial s_n(t)} \tag{15}$$

To evaluate the integral in eq 13, one needs to rewrite eqs 7 and 12 in terms of $<l_n(t)>_u$. Note that, by definition,

$$\frac{\partial l_n(t)}{\partial t} = \frac{\partial}{\partial t}\frac{\partial s_n(t)}{\partial n} = \frac{\partial}{\partial n}\frac{\partial s_n(t)}{\partial t} \tag{16}$$

Substituting eq 7 into eq 16 and taking the average, eq 7 becomes

$$\zeta \frac{\partial}{\partial t} \langle l_n(t) \rangle_{\mathbf{u}} = (3k_B T / b^2) \frac{\partial^2}{\partial n^2} \langle l_n(t) \rangle_{\mathbf{u}} \tag{17}$$

with the boundary conditions

$$\langle l_n(t) \rangle_{\mathbf{u}} = z \langle | \mathbf{F} \cdot \mathbf{u} | \rangle_{\mathbf{u}} \bar{l} \qquad n=0, N_0 \tag{18}$$

and the initial condition

$$\langle l_n(0) \rangle_{\mathbf{u}} = \bar{l} \langle | \mathbf{F} \cdot \mathbf{u} | \rangle_{\mathbf{u}} = \bar{l} \alpha(\mathbf{F}) \tag{19}$$

Equation 19 is the mathematical equivalent of the statement that the slip links and the chain segments between them deform affinely with the macroscopic deformation imposed at $t=0$. Equation 17, subject to eqs 18 and 19, can be solved by the standard method of separation of variables. The result is

$$\langle l_n(t) \rangle_{\mathbf{u}} = \bar{l} \alpha(\mathbf{F}) (1-z) \sum_{p\ odd}^{\infty} \frac{4}{p\pi} \sin \frac{p\pi n}{N_0} \exp \frac{-p^2 t}{\tau_B} + z\bar{l}\alpha(\mathbf{F}) \tag{20}$$

where the largest relaxation time, τ_B, is given by

$$\tau_B = \frac{\zeta b^2}{3\pi^2 k_B T} N_0^2 \tag{21}$$

This is twice the longest Rouse relaxation time. Note that eqs 17 or 7 can be solved only for the average of $s_n(t)$. This results in the loss of the effects of the random Gaussian force on the stress. Because the fluctuations of $s_n(t)$ are consequently not taken into account, eq 13 is true to a first approximation only. It is relatively easy to account for fluctuations in eq 13 but $s_n(t)$, rather than its average, can be calculated only as $t \to \infty$. Therefore we can assess the effects of the random force on stress only at equilibrium. This problem is addressed and discussed in detail in Appendix 3. It results that the expression for the stress given by eq 13 lacks a second term whose time dependence is not known. We therefore add it to eq 13 in its equilibrium form. This yields

$$\bar{\sigma}_{\alpha\beta}(t) = (3ck_BT/b^2) \int_0^{N_0} (\langle l_n(t)\rangle_u)^2 \langle v_{n\alpha} v_{n\beta}\rangle_u \, dn$$

$$+ G_{eN}\langle v_{n\alpha} v_{n\beta}\rangle_u - P\delta_{\alpha\beta} \tag{22}$$

Using eq 20 we obtain

$$\bar{\sigma}_{\alpha\beta}(t) = G_X(t)B_{\alpha\beta} + G_{eN}Q_{\alpha\beta} - P\delta_{\alpha\beta} \tag{23}$$

where

$$G_X(t) = (cN_0k_BT/N_e)\, z^2\, f(t) = G_{eX}\, f(t) \tag{24}$$

in which

$$f(t) = \sum_{p\ odd}^{\infty} \frac{8}{p^2\pi^2}\left[1 + \frac{1-z}{z}\exp -\frac{p^2t}{\tau_B}\right] \tag{25}$$

$$Q_{\alpha\beta} = \langle v_{n\alpha}v_{n\beta}\rangle_u = \left\langle \frac{(\mathbf{F}\cdot\mathbf{u})_\alpha\,(\mathbf{F}\cdot\mathbf{u})_\beta}{|\mathbf{F}\cdot\mathbf{u}|^2}\right\rangle_u \tag{26}$$

and

$$B_{\alpha\beta} = 3Q_{\alpha\beta}\alpha^2(\mathbf{F}) = 3\,\langle(\mathbf{F}\cdot\mathbf{u})_\alpha\,(\mathbf{F}\cdot\mathbf{u})_\beta\rangle_u \tag{27}$$

In obtaining $Q_{\alpha\beta}$ from eq 22, we have made use of Doi and Edwards's independent alignment assumption, and the fact that $\langle v_{n\alpha} v_{n\beta}\rangle_u$ has not yet relaxed and hence is constant. The eigenvalues of **B**, the Finger deformation tensor, are $B_\alpha = \lambda_\alpha^2$. Hence, the first term in eq 23 can be evaluated. The second term, however, can only be obtained analytically in case of a uniaxial deformation. For uniaxial tension, eq 23 becomes

$$\bar{\sigma}(t) = \bar{\sigma}_{11}(t) - \bar{\sigma}_{22}(t) = G_X(t)\,(B_{11}-B_{22}) + G_{eN}(Q_{11}-Q_{22}) \tag{28}$$

where

$$B_{11}-B_{22} = \lambda^2 - 1/\lambda \tag{29}$$

and

$$Q_{11}-Q_{22} = \frac{15}{2}\left[\frac{\lambda^3}{\lambda^3-1}\left[1 - \frac{\tan^{-1}\sqrt{\lambda^3-1}}{\sqrt{\lambda^3-1}}\right] - \frac{1}{3}\right] \tag{30}$$

The expression for $Q_{11}-Q_{22}$ has been adjusted by a numerical constant of 5/3 to yield a modulus of 1 as $\lambda \to 1$.

We now adduce evidence that eq 23 results from a potential that appears to be constitutive in the narrower sense[1]. We then generalize it to different strain histories. As $t \to \infty$, eq 23 yields

$$\bar{\sigma}_{\alpha\beta} = G_{eX} B_{\alpha\beta} + G_{eN} Q_{\alpha\beta} - P\delta_{\alpha\beta} \tag{31}$$

and in uniaxial tension

$$\sigma_M = G_{eX} + G_{eN}\varphi_D(\lambda) \tag{32}$$

where

$$\sigma_M = \frac{\bar{\sigma}_{11} - \bar{\sigma}_{22}}{\lambda^2 - \lambda^{-1}} \tag{33}$$

and

$$\varphi_D(\lambda) = \frac{Q_{11} - Q_{22}}{\lambda^2 - \lambda^{-1}} \tag{34}$$

In eq 34, the expression for $Q_{11} - Q_{22}$ is given by eq 30. A plot of equilibrium uniaxial tension data according to eq 32 yields a straight line with slope G_{eN} and intercept G_{eX}.

We plotted the equilibrium simple tension data[5] of Kawabata et al. according to eq 32 to obtain the two moduli. We then used those values together with the appropriate expressions for $B_{\alpha\beta}$ and $Q_{\alpha\beta}$ to predict their data for pure shear and equibiaxial tension. The predictions of our theory for equibiaxial tension were obtained using its predictions for compression, since the two deformations are equivalent for an incompressible material. The expression for $Q_{11}-Q_{22}$ in uniaxial compression can be evaluated as

$$Q_{11}-Q_{22}=\frac{15}{2}\left[\frac{\lambda^3}{1-\lambda^3}\left(\frac{\tanh^{-1}\sqrt{1-\lambda^3}}{\sqrt{1-\lambda^3}}-1\right)-\frac{1}{3}\right] \tag{35}$$

The averages involved in evaluating $Q_{\alpha\beta}$ in the case of pure shear were obtained by numerical integration of eq 26 using eq 6.

In Figure 2, we have plotted the predictions of eq 31 together with the experimental data of Kawabata et al. In the figure, the ordinate shows the normal stress differences obtained from the data, and the abscissa shows the predictions of the theory. The agreement between the experiments and the theory is excellent, and suggests that eq 31 results from a constitutive potential.

An Approximate Strain Function

To avoid the need for numerical integration, we suggest a simple expedient. Let the eigenvalues of **Q** be given by

$$Q_\alpha=\lambda_\alpha\frac{\partial w}{\partial\lambda_\alpha}\qquad\alpha=1,2,3 \tag{36}$$

where

$$w=(2/m^2)\,(\lambda_1^m+\lambda_2^m+\lambda_3^m-3) \tag{37}$$

is the normalized form (W/G) of the BST potential[1] with n replaced by m. A fit of

$$Q_{11}-Q_{22}=(2/m)\,(\lambda^m-\lambda^{-m/2}) \tag{38}$$

to eq 30 over the range $1\le\lambda\le2.5$ by a nonlinear least squares procedure yields $m=0.34$. Combining eq 37 with the (normalized) neohookean potential

$$w=(1/2)\,(\lambda_1^2+\lambda_2^2+\lambda_3^2-3) \tag{39}$$

yields the 2NW potential

$$W=(G_{eX}/2)\,(\lambda_1^2+\lambda_2^2+\lambda_3^2-3)+(2G_{eN}/m^2)\,(\lambda_1^m+\lambda_2^m+\lambda_3^m-3) \tag{40}$$

which we have shown elsewhere[1] to be constitutive for deformations in elastic equilibrium in a certain range of deformation. In uniaxial tension, the range is $1 \leq \lambda \leq 2.5$. This is the range over which the upswing in the σ vs λ curve is not observed. We have called such deformations ***moderately large***. The expedient we are suggesting is, therefore, applicable only for moderately large deformations.

Currie et al. have given[6] an expression for the potential from which the tensor **Q** can be obtained. It does not satisfy the Valanis-Landel[1] hypothesis. In other words, the potential w_D which, upon differentiation, would yield **Q** is not of the form

$$w_D = w_1(\lambda_1) + w_1(\lambda_2) + w_1(\lambda_3) \tag{41}$$

The expedient we suggest does satisfy this hypothesis. It must therefore be considered to be a purely mathematical one, and must be justified by comparing the mathematical predictions for the stress in both cases.

We demonstrate the close agreement between the two predictions in the case of uniaxial tension, pure shear, and equibiaxial tension. In uniaxial tension, the two stresses agree to better than 1% over the range $1 < \lambda < 2.5$. The corresponding range would be $1 < \lambda < 1.5$ for equibiaxial tension and $1 < \lambda < 2.2$ for pure shear. The maximum stretch ratios, 1.5 and 2.2, were calculated from the iso-w_D lines[6] on a plot of I_1 vs. I_2, where I_1 is the first, and I_2 is the second invariant of the Finger deformation tensor. When the neohookean potential is used for w, these values do not change significantly.

The agreement is demonstrated in Figure 3. The parameter $\bar{\nu}_N$ is the ratio G_{eN}/G. For most rubbers encountered in practical applications, $\bar{\nu}_N$ falls in the range[7] $0.3 < \bar{\nu}_N < 0.7$ The largest deviation observed in Figure 3 is 10% for $\bar{\nu}_N$=0.7 in equibiaxial tension. The expedient we have suggested appears, therefore, to be satisfactory for most crosslinked networks.

Since the two expressions agree to within 1% in uniaxial tension, we will discuss the time dependent data in uniaxial tension in terms of eq 40. Equation 23 has been derived for the stress response to a deformation applied as a step function of time. Extension to arbitrary time histories is straightforward. Using eq 38, eq 23 gives

$$\bar{\sigma}(t) = G_X(t)\,(\lambda^2 - \lambda^{-1}) + (2G_{eN}/m)\,(\lambda^m - \lambda^{-m/2}) \tag{42}$$

in uniaxial tension. Figure 4 shows $f(t)$ given by eq 25 as a function of $\log t$ for two different values of the relaxation time τ_B. It clearly shifts linearly with τ_B along the logarithmic time axis. Consequently, eq 42 can be generalized to other strain histories in uniaxial tension by

$$\bar{\sigma}(t) = \int_0^t G_X(t-u)\,\frac{d}{du}[\lambda^2(u) - \lambda^{-1}(u)]\,du + (2G_{eN}/m)\,(\lambda^m - \lambda^{-m/2}) \tag{43}$$

Equation 43 is the time dependent form of the 2NW potential applied to uniaxial deformations in arbitrary strain histories.

Although our theory does not predict the time dependence of G_N, we make the assumption that it also satisfies the Boltzmann superposition principle. Therefore we replace eq 43 by

$$\bar{\sigma}(t) = \int_0^t G_X(t-u)\,\frac{d}{du}[\lambda^2(u) - \lambda^{-1}(u)]\,du$$

$$+ (2/m)\int_0^t G_N(t-u)\,\frac{d}{du}[\lambda(u)^m - \lambda(u)^{-m/2}]\,du \tag{44}$$

This is the most general equation describing the time dependent behavior of rubber networks in moderately large, uniaxial deformations in the framework of our theory.

Experimental Procedure

To investigate the time-dependent properties of polymer networks experimentally, uniaxial tension measurements were made on a styrene-butadiene rubber sample designated as SBR 6. Its equilibrium stress-strain curve has been reported elsewhere.[1] The sample and specimen preparation methods are summarized in Appendix 2. The experiments were performed on a Floor Model Instron Tensile Tester equipped with an environmental chamber cooled with liquid nitrogen. The data were taken at -37.5^0C. The temperature was monitored continually during the experiment by a thermocouple. The maximum deviation observed was 0.2^0C.

To test the validity of the equations we obtained in the theoretical section, we needed stress relaxation data recorded at different elongations. To obtain these, we would have had to conduct stress relaxation experiments at a given elongation, let the specimen relax for about 30 hours at room temperature, and repeat the procedure at another elongation. We were able to reproduce a given temperature in our environmental chamber only within two degrees. Hence, data taken under these conditions would require time-temperature superposition. Since, it is not clear whether this is permissible in large deformations, we devised a different procedure. We extended a specimen to a specified elongation, let it relax for about 30 minutes, and then increased the deformation as required. This method eliminates the problems associated with time-temperature superposition but requires special processing of the data which will now be discussed.

Stress relaxation measurements were made as a step function of time. For a number of uniaxial steps superposed on one another, the time- dependent elongation ratio is given by

$$\lambda_i(u) = 1+\sum_{j=1}^{i}(\lambda_j - \lambda_{j-1})\, h(u-t_j) \tag{45}$$

where $h(u-t_j)$ is the unit step function applied at $u=t_j$, λ_j is the jth elongation ratio referred to the rest state, t_j the time at which the jth deformation is applied, $\lambda_0=1$ and $t_1=0$. With these definitions eq 45 implies

$$\lambda_i^n(u) = 1 + \sum_{j=1}^{i}(\lambda_j^n - \lambda_{j-1}^n)\, h(u-t_j) \tag{46}$$

where n will take the values $2, m, -1, -m/2$ as required. When substituted into eq 44, eq 46 yields

$$\bar{\sigma}_i(t) = \sum_{j=1}^{i}\int_0^t G_K(t-u)\,[(\lambda_j^2-\lambda_{j-1}^2) - (\lambda_j^{-1}-\lambda_{j-1}^{-1})]\,\delta(u-t_j)\,du$$

$$+ (2/m)\sum_{j=1}^{i}\int_0^t G_N(t-u)\,[(\lambda_j^m-\lambda_{j-1}^m) - (\lambda_j^{-m/2}-\lambda_{j-1}^{-m/2})]\,\delta(u-t_j)\,du \tag{47}$$

where $\delta(u-t_j)$ is the delta function acting at $u=t_j$. Performing the integration and obtaining $\bar{\sigma}_i(t)-\bar{\sigma}_{i-1}(t)$ from eq 47 we find

$$\bar{\sigma}_i(t) - \bar{\sigma}_{i-1}(t) = G_K(t-t_i)\,[(\lambda_i^2-\lambda_{i-1}^2) - (\lambda_i^{-1}-\lambda_{i-1}^{-1})]$$

$$+ (2/m)G_N(t-t_i)\,[(\lambda_i^m-\lambda_{i-1}^m) - (\lambda_i^{-m/2}-\lambda_{i-1}^{-m/2})] \tag{48}$$

This furnishes the stress in the ith experiment carried out at elongation λ_i, from which the residual stress left over from the preceding experiment at the elongation λ_{i-1} has been subtracted. The response to a series of step elongations is shown in Figure 5. The residual stress is, of course, not known since it has not been recorded. If we could predict it, $\bar{\sigma}_i(t)-\bar{\sigma}_{i-1}(t)$ where λ_i has been applied at t_i, would be completely equivalent to $\bar{\sigma}(t)$ However, we cannot do this at this stage. Instead, if the interval t_i-t_{i-1} is large enough so that the residual relaxation is negligible, we can write with excellent approximation,

$$\bar{\sigma}_i(t_i+t_i^*) - \bar{\sigma}_{i-1}(t_i+t_i^*) = \bar{\sigma}_i(t_i+t_i^*) - \bar{\sigma}_{i-1}(t_i) \tag{49}$$

where

$$t_i^* = t - t_i \qquad 0 \le t_i^* \le (t_{i+1}-t_i) \tag{50}$$

The t_i^*s can, in general, be selected at will. We make them all equal, however, to insure that the stress in each experiment represents the same state of relaxation, i.e. that it is isochronal. Substituting

$$t^* = t_i^* = t_{i-1}^* = ... = t_1^* \tag{51}$$

into eq 50 and the result into eq 49, we obtain

$$\sigma_{Mi}(t^*) = \frac{\bar{\sigma}_i(t_i+t^*) - \bar{\sigma}_{i-1}(t_i)}{(\lambda_i^2-\lambda_{i-1}^2) - (\lambda_i^{-1}-\lambda_{i-1}^{-1})} = G_N(t^*)\psi(\lambda_i) + G_X(t^*) \tag{52}$$

where

$$\psi(\lambda_i) = \frac{2[(\lambda_i^m-\lambda_{i-1}^m) - (\lambda_i^{-m/2}-\lambda_{i-1}^{-m/2})]}{m[(\lambda_i^2-\lambda_{i-1}^2) - (\lambda_i^{-1}-\lambda_{i-1}^{-1})]} \tag{53}$$

and m=0.34. The symbol $\sigma_{Mi}(t^*)$ is the equivalent of the Mooney stress at the isochronal time t^* in the ith experiment. Equation 52 implies that a plot of $\sigma_{Mi}(t^*)$ vs $\psi(\lambda_i)$ yields a straight line with slope $G_N(t^*)$ and intercept $G_X(t^*)$. Data plotted according to eq 52 are shown in Figure 6 for three different isochronal times t^*. The linearity of the plots indicates that our procedure for data reduction is adequate. The plots were constructed by taking isochronal cuts from Figure 7 which represents $\sigma_i(t-t_i;\lambda_i)$ as a function of t in logarithmic coordinates. The symbol $\sigma_i(t-t_i;\lambda_i)$ refers to the nominal stress at the indicated time and elongation.

Figure 8 compares the time dependence of $G_X(t)$ obtained from these experiments with the time dependence predicted by our theory. The prediction requires knowledge of z^2 and τ_B. The parameter z^2 was obtained from eq 24 which gives

$$z^2 = \frac{G_{eX}}{ck_BTN_0/N_e} \tag{54}$$

But

$$ck_BTN_0/N_e = \rho RT/M_e^x \tag{55}$$

where ρ and R have their usual meaning, and M_e^x is the molecular mass of a segment between slip links in the crosslinked network. In a previous publication,[7] we have shown that

$$G_{eN} = \xi G_N^0 \tag{56}$$

where the value of ξ has been estimated as 0.354 for a tetrafunctional undiluted network. G_N^0 is the plateau modulus of the uncrosslinked polymer which has a value of 0.776 MPa for SBR.[8] Equation 56 together with eq 27 of Appendix 3 imply

$$\rho RT/M_e^x = \xi G_N^0 \tag{57}$$

which, using eq 54, allows us to estimate z^2.

The value of $\log \tau_B = 1.70$ was obtained by shifting the theoretical curve onto the experimental points. Equation 21 can be scaled to yield

$$\tau_B = \frac{(\zeta_0 Z)\,(a_0 Z^{1/2})^2}{3\pi^2 k_B T} \tag{58}$$

in terms of monomeric parameters. In eq 58 ζ_0 is the monomeric friction coefficient, Z is the degree of polymerization, and a_0 is the monomer length. If one calculates Z from the equilibrium value of $G_X(t)$ as $G_{eX} = \rho RT/2M_C$, and uses the published values[8] for ζ_0 and a_0, one obtains τ_B=1.78, in excellent agreement with the experimental value.

Figure 9 shows the experimental time dependence of $G_N(t)$. Although from our theory we predict its existence and its strain dependence, we cannot predict its time dependence. Knowledge of the linear relaxation modulus of the polymer

is required before one can predict its nonlinear time-dependent properties.

As a further test of our theory, we examine its predictions when it is applied to different strain histories. We consider two strain histories, namely constant rate of strain, and trapezoidal excitation. The experimental data were taken from the work of Bloch, Chang, and Tschoegl.[9]

Constant Rate of Strain

For a deformation in uniaxial tension at a constant rate of strain $\dot{\varepsilon}$, the time-dependent extension ratio is given by

$$\lambda(u) = 1 + \dot{\varepsilon} u \tag{59}$$

Substituting this into eq 44 we obtain

$$\bar{\sigma}(t;\dot{\varepsilon}) = 2\dot{\varepsilon} \int_0^t G_\chi(t-u)\,[(1+\dot{\varepsilon}u) + 0.5(1+\dot{\varepsilon}u)^{-2}]du$$

$$+ 2\dot{\varepsilon} \int_0^t G_N(t-u)\,[(1+\dot{\varepsilon}u)^{m-1} + 0.5(1+\dot{\varepsilon}u)^{-(m+2)/2}]du \tag{60}$$

where $\dot{\varepsilon}$ has been shown as a parameter in the symbol for the stress to distinguish the deformation from stress relaxation.

From the near equilibrium stress relaxation data at different levels of elongation reported in reference 9, we obtained the parameters required for our theory as follows. We took an isochronal cut at 10 minutes, and plotted $\bar{\sigma}(t^*)$ as a function of λ. We then used eq 52 with i=1, to obtain $G_\chi(t^*)$ and $G_N(t^*)$, where t^*=10 minutes. We found $G_\chi(t^*)$=0.102 MPa and $G_N(t^*)$=0.193 MPa. SBR allowed to relax at room temperature for 10 minutes is close to elastic equilibrium. Thus, we obtained $\log\tau_B$=–5.63 min. and z^2=0.371 from $G_\chi(t^*)$, using eqs 54 and 58. The sum of the two moduli $G=G_\chi+G_N$ is different from the estimate of the linear shear modulus, given by Bloch et al. This is due to an error in their data

reduction scheme,[10] and associated with converting from engineering units to SI units. Our estimate of G fits their data using their theory.

Bloch et al. approximate the linear shear modulus of their sample using the equation

$$G(t) = G_e + \frac{G}{1+(t/\tau)^k} \tag{61}$$

with G_e=0.249 MPa, G=1.356 MPa, τ=6.8x10^{-7} min, and k=0.1848. Once again the values reported here differ from those of reference 9, by a constant factor. In terms of our theory we have

$$G_e = G_{eX} + G_{eN} \tag{62}$$

with G_{eX}=0.102 MPa and G_{eN}=0.1470 MPa, and we approximate $G_N(t)$ by

$$G_N(t) = G_{eN} + \frac{G}{1+(t/\tau)^k)} \tag{63}$$

Note that we have taken $G_X(t)$ equal to its equilibrium value. As seen from Figure 4, relaxation of $G_X(t)$ is complete when $\log t$ is greater than $\log \tau_B$+1. Experimentally, in relaxation at a constant rate of strain, the relaxation time of order $(1/\dot{\varepsilon})$ is the most heavily weighted one. The highest strain rate used in reference 9, 4.56 min^{-1}, correponds to a time of 0.22 min. That is several decades longer than τ_B, and therefore the relaxation of $G_X(t)$ is not observable in the experiments. We make the same assumption in eq 60 also, and set $G_X(t-u)=G_{eX}$. Using eq 63 for $G_N(t)$, we integrated eq 60 for the given strain rates. The trapezoidal rule, with 500 subintervals, was used for the second term. No appreciable difference was observed in the results when the number of subintervals was increased to 1000. Figure 10 shows the experimental results of Bloch, Tschoegl and Chang together with our predictions. The agreement is very good.

Trapezoidal Excitation

We now consider the following deformation. Impose a constant rate of strain $\dot{\varepsilon}_1$ from $t=0$ to $t=t_1$. Let the sample relax at that elongation until $t=t_2$, and impose another constant rate of strain $-\dot{\varepsilon}_2$ in the opposite direction. The excitation function thus has the shape of a trapezoid. The time-dependent elongation ratio is now given by

$$\lambda(u) = 1 + \dot{\varepsilon}_1 u\, h(u) - \dot{\varepsilon}_1 (u-t_1) h(u-t_1) - \dot{\varepsilon}_2 (u-t_2) h(u-t_2) \tag{64}$$

Substituting eq 64 into eq 45, we obtain

$$\overline{\sigma}(t) = \overline{\sigma}(t;\dot{\varepsilon}_1) \qquad 0 \le t \le t_1 \tag{65}$$

where $\overline{\sigma}(t;\dot{\varepsilon}_1)$ is given by eq 60, and

$$\overline{\sigma}(t) = \overline{\sigma}(t;t_1,\dot{\varepsilon}_1) = G_{eX}\,[\lambda^2(t_1) - \lambda^{-1}(t_1)]$$

$$+ 2\dot{\varepsilon}_1 \int_0^{t_1} G_N(t-u)\,[(1+\dot{\varepsilon}u)^{m-1} + 0.5(1+\dot{\varepsilon}u)^{-(m+2)/2}]du \qquad t_1 < t \le t_2 \tag{66}$$

$$\overline{\sigma}(t) = \overline{\sigma}(t;t_1,\dot{\varepsilon}_1) + G_{eX}\,[\lambda^2(t) - \lambda^{-1}(t) - \lambda^2(t_1) + \lambda^{-1}(t_1)]$$

$$+ 2\dot{\varepsilon}_2 \int_{t_2}^{t} G_N(t-u)\,[(\lambda_P(u))^{m-1} + 0.5(\lambda_P(u))^{-(m+2)/2}]du \qquad t_2 < t \tag{67}$$

In eqs 65 through 67 $\overline{\sigma}(t;\dot{\varepsilon}_1)$ is given by eq 66 and

$$\lambda_P(u) = 1 + \dot{\varepsilon}_1 t_1 - \dot{\varepsilon}_2 (u - t_2) \tag{68}$$

To obtain the stress resulting from this deformation, we used eqs 61 through 63 in eqs 65 through 69. Figure 11 shows the data of Bloch et al. and our predictions as stress plotted as a function of time in logarithmic coordinates. The value of $\dot{\varepsilon}_2$ we used for our predictions is 1/10 of the strain rate they report, a difference attributed to typographical error.[10] Since the plot in Figure

11 is logarithmic, it is not very sensitive to differences between experiment and theory. Therefore, we calculated the elongation ratio and the stress from the strain rate and plotted the results in Figure 12 together with the data of Bloch et al. The agreement between our theory and the experimental data is again excellent even in this more sensitive plot.

Conclusions

We have developed a molecular theory which describes the time-dependent properties of rubber networks. The theory predicts a two term potential which determines the stress-strain properties of the network. The first term of the potential has a modulus G_{eX} associated with it at equilibrium. This term arises from the change in the average path length of the primitive path. The predicted stress-strain behavior is neohookean for this term. An expression for its time dependence is also obtained. The second term of the potential, which has a modulus G_{eN} associated with it, arises from segment length fluctuations. It has a complicated strain dependence which requires numerical integration in all but uniaxial deformations. We have shown, however, that the simple BST potential furnishes an adequate approximation.

The resemblence of the obtained form and the interpretation of its parameters bears a striking resemblence to the equilibrium theory of Flory and Erman,[11] although the route we have chosen is quite different from theirs.

Our molecular picture for crosslinked networks is based on the ideas introduced by Doi.[2] Thus, we would like to compare our predictions with Doi's predictions for an uncrosslinked polymer. In the uncrosslinked polymer, the relaxation process corresponding to the relaxation of $s_n(t)$ is not observed in infinitesimal deformations. It becomes activated at large strains, and manifests itself in a hump in a plot of $\log \sigma(t)$ vs. $\log t$. Furthermore, time-shift invariance

is not preserved when this relaxation process is activated. All of these predictions are in accordance with the stress relaxation data of Nordermeer and Ferry.[12]

An examination of eqs 23 through 31 reveals that in a crosslinked network,the restrictions that are imposed by the chemical junction points on the movement of the chains results in a picture that is qualitatively different. First, our theory predicts a plot of $\log \sigma(t)$ vs. $\log t$ which is monotone nonincreasing for a deformation applied as a step function of time. Also as $\lambda \to 1$, we obtain $\sigma(t) = 3\,G(t)\,\varepsilon$ in uniaxial tension, where $G(t) = G_X(t) + G_N(t)$. Consequently, one can use the information obtained in linear stress-relaxation experiments to predict nonlinear, time-dependent behavior. Second, when the polymer is uncrosslinked, the chains can escape from their constraints and attain random orientation after the relaxation of $s_n(t)$ reaches equilibrium.Such a reptation motion is impossible in a crosslinked network, because of the presence of the chemical crosslinks.

The effects of segment length fluctuations are not considered by Doi in the nonlinear deformation region. Graessley[13] points out that such fluctuations would compete with the reptation motion. This is not a problem for a mathematical description of the crosslinked network. Thus, the nonlinear stress-strain behavior of crosslinked networks is predicted to be less complicated than the behavior of the uncrosslinked polymer.

We consider it to be the outstanding feature of our theory that it allows one to use the information gleaned from stress-relaxation experiments in infinitesimal deformations to predict nonlinear, time-dependent stress-strain behaviorin moderately large deformations.

References

1. Chapter I of this thesis

2. M. Doi, *J. Polym. Sci., Polym. Phys. Ed.*, **18** (1980) 1005

3. M. Doi, private communication

4. M. Doi, S.F. Edwards, *J. Chem. Soc. Faraday Trans. 2*, **74** (1978) 1802

5. S. Kawabata, M. Matsuda, K. Tei, H. Kawai, *Macromolecules*, **14** (1981), 154

6. P.K. Currie, *J. Non Newtonian Fluid Mech.*, 11 (1982), 53

7. Chapter II of this thesis

8. J.D. Ferry, *Viscoelastic Properties of Polymers*, John Wiley, New York, N.Y., (1980) 374

9. R. Bloch, W.V. Chang, N.W. Tschoegl, *J. Rheol.*, 1 (1978) 22

10. R. Bloch, private communication

11. P.J. Flory, B. Erman, *Macromolecules* **15** (1982) 800

12. J.W.M. Nordermeer, J.D. Ferry, *J. Polym. Sci. Polym. Phys. Ed.* **14** (1976) 509

13. W.W. Graessley, *Adv. in Polym. Sci.*, **47** (1982) 67

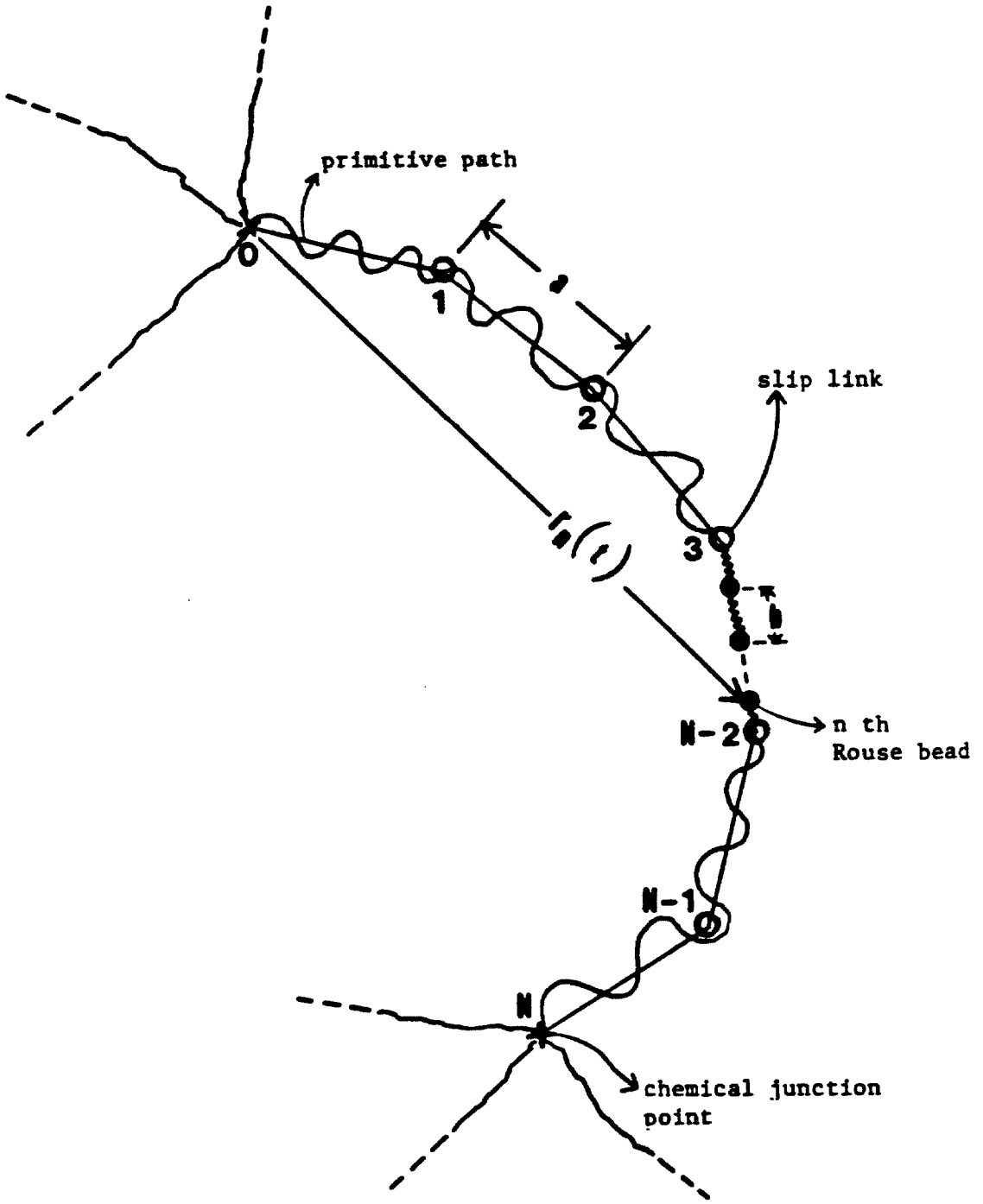

Figure 1: Schematic of the model of the polymer chain.

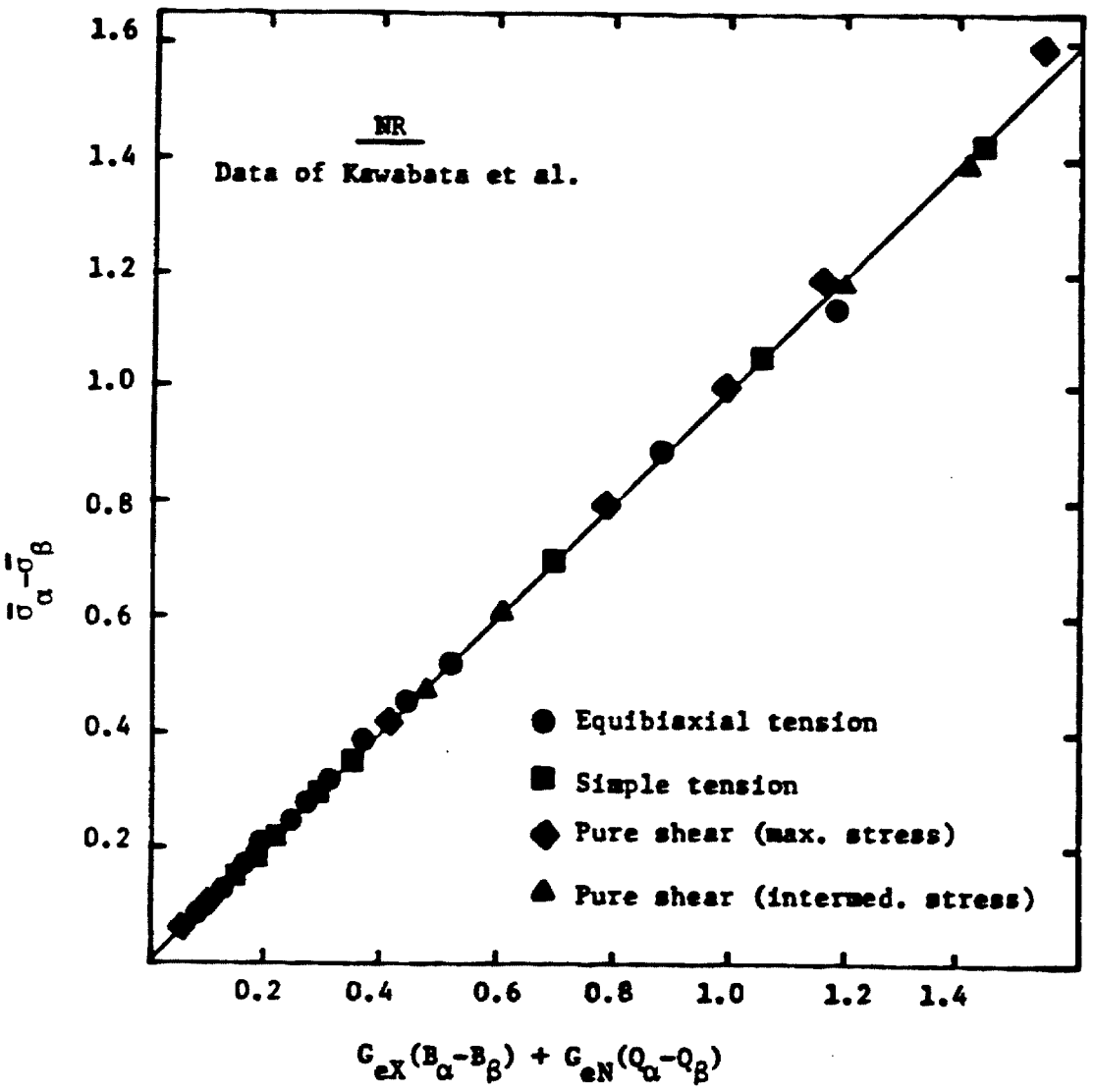

Figure 2: Time dependent theory compared to data.

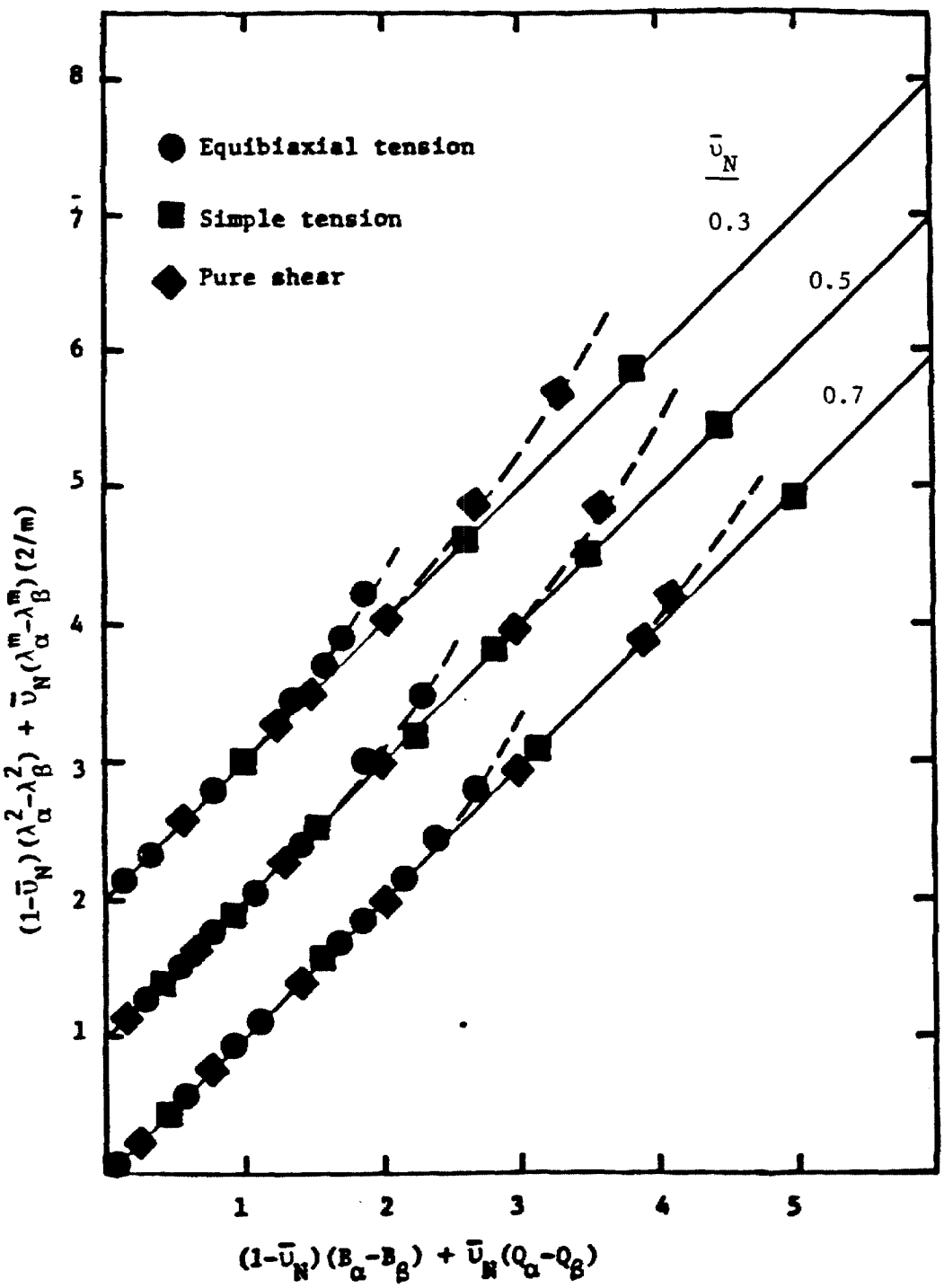

Figure 3: Comparison of the full tensorial form of the strain function with the BST potential.

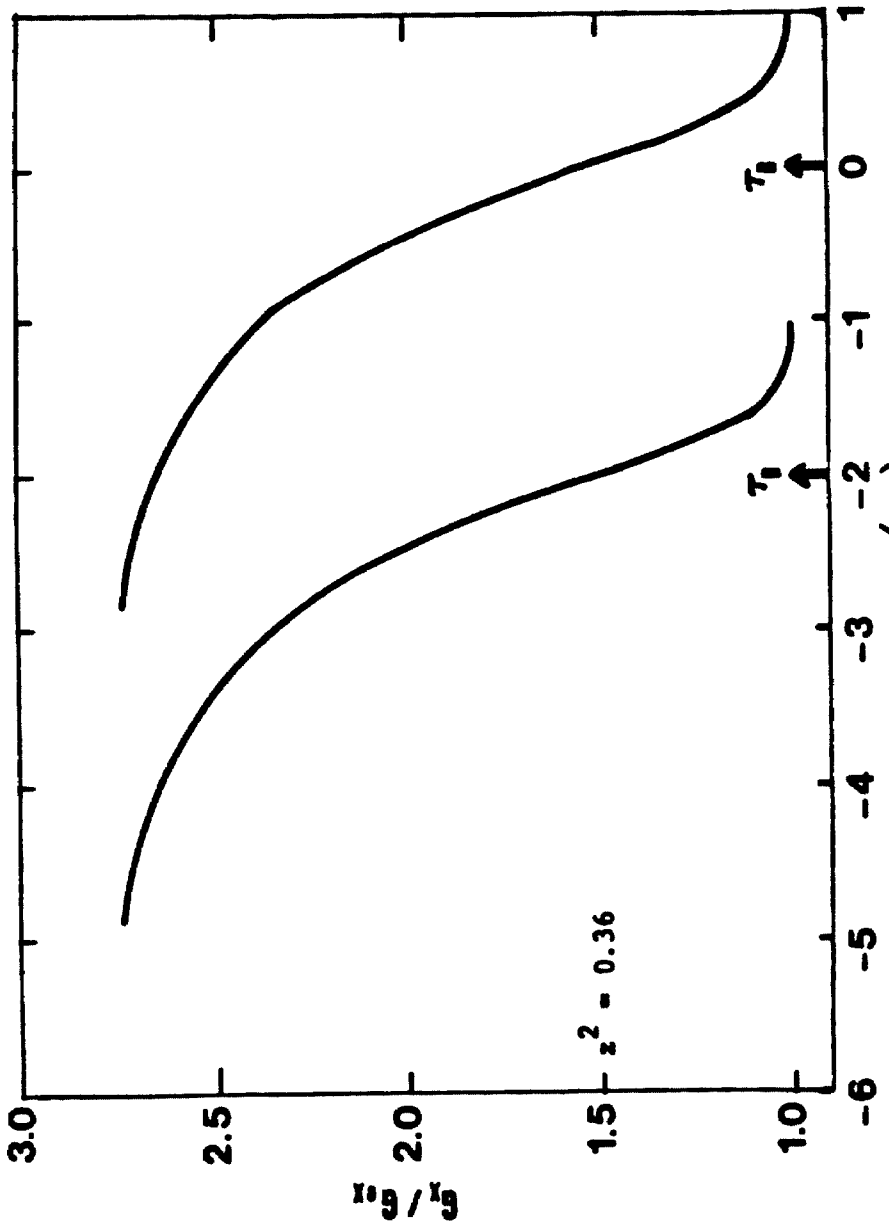

Figure 4: The predicted time dependence of G_X as a function of reduced time.

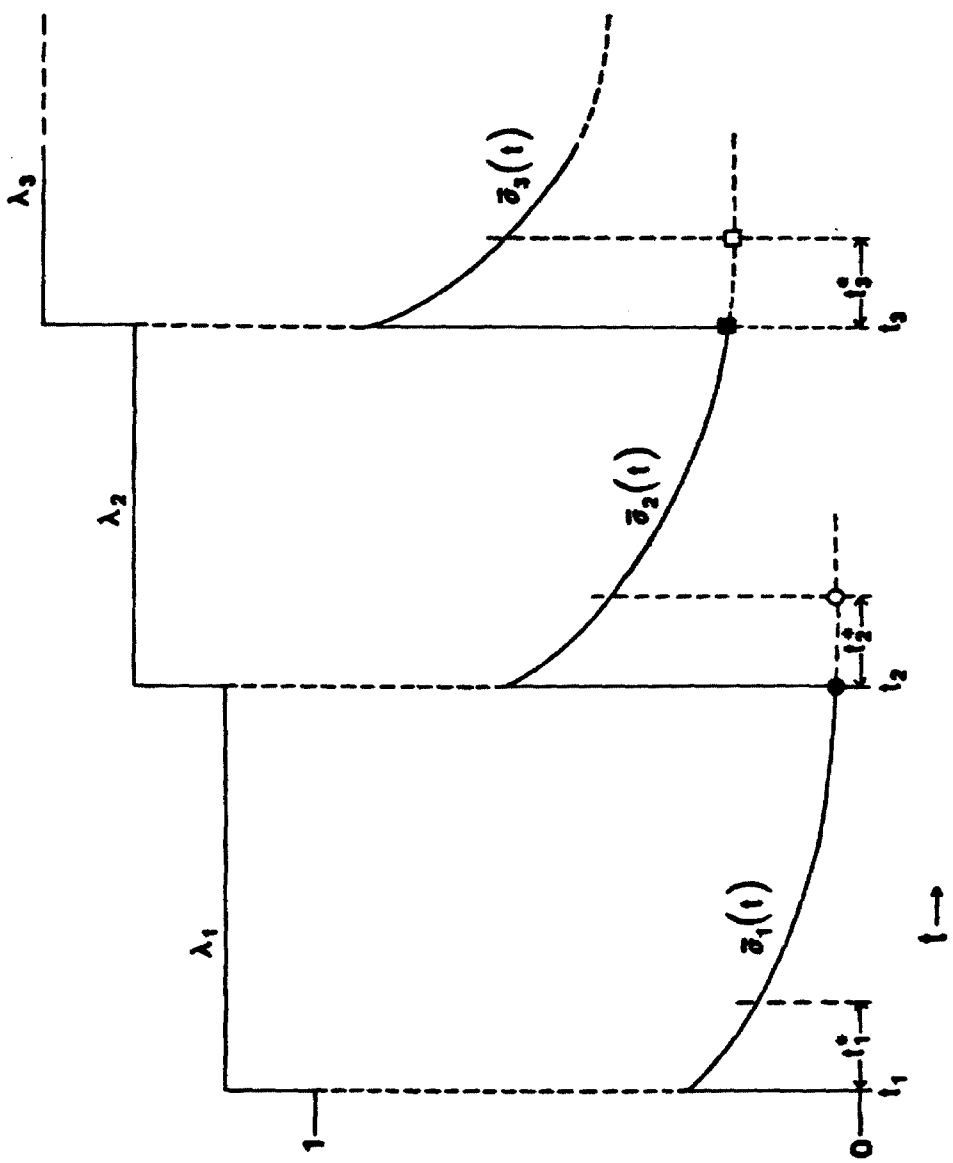

Figure 5: A schematic of the experimental procedure used to obtain stress relaxation data at different elongations.

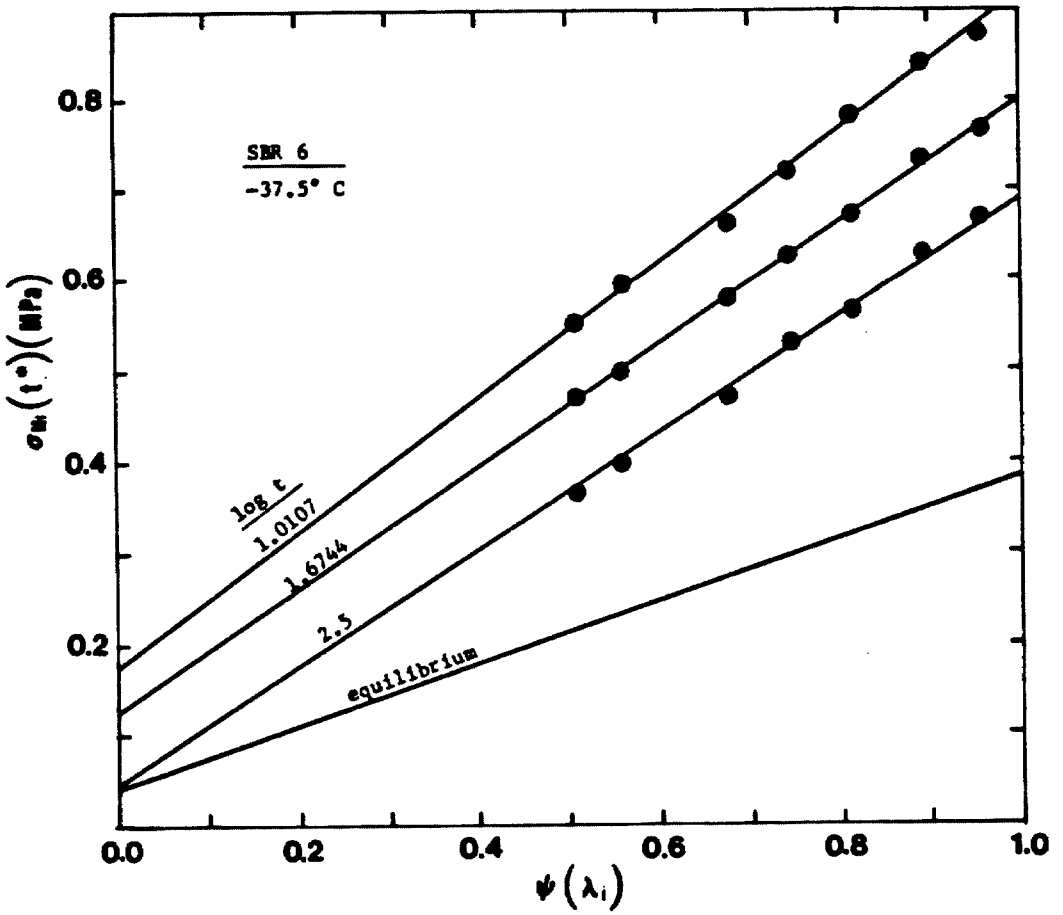

Figure 6: Isochronal cuts from stress relaxation data on appropriate coordinates to obtain the time dependence of G_X and G_N.

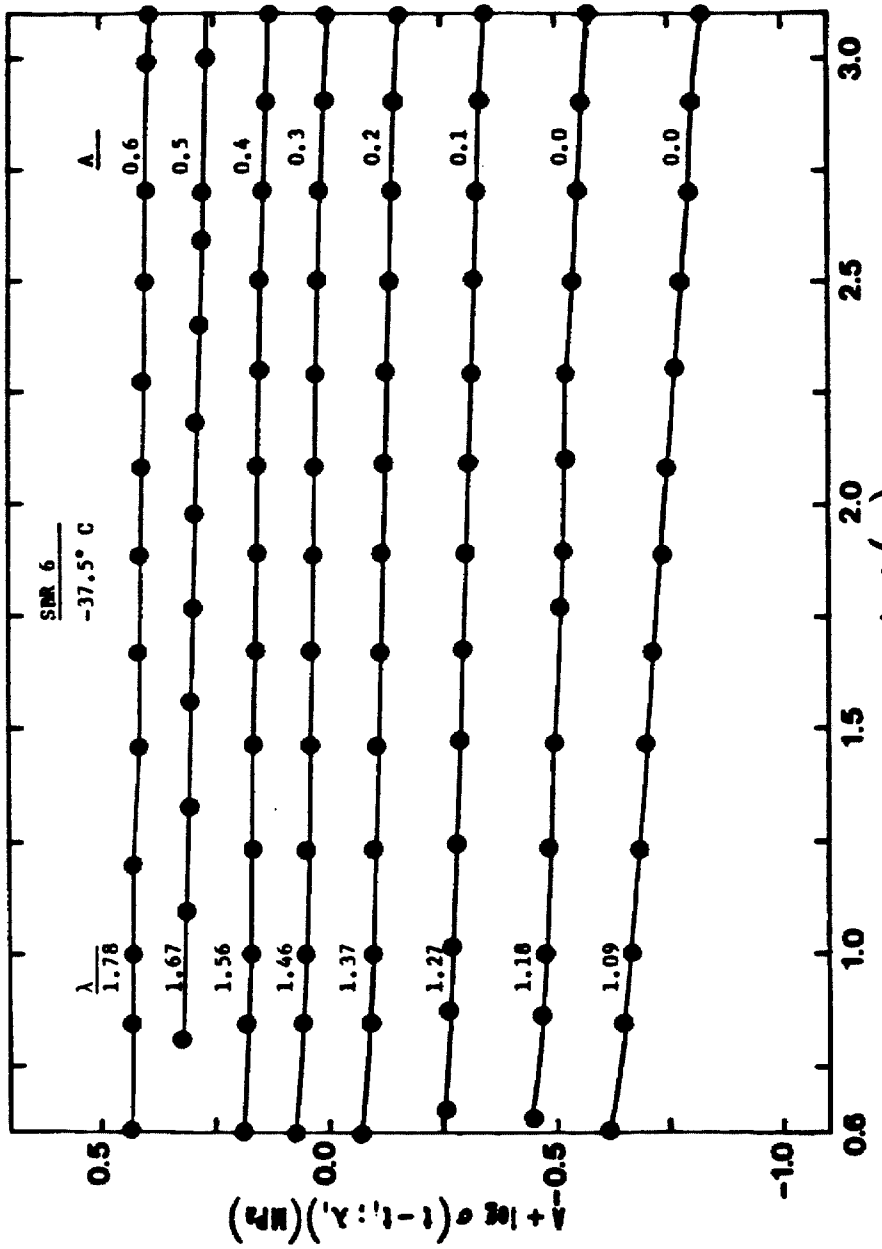

Figure 7: Stress relaxation data at different elongations.

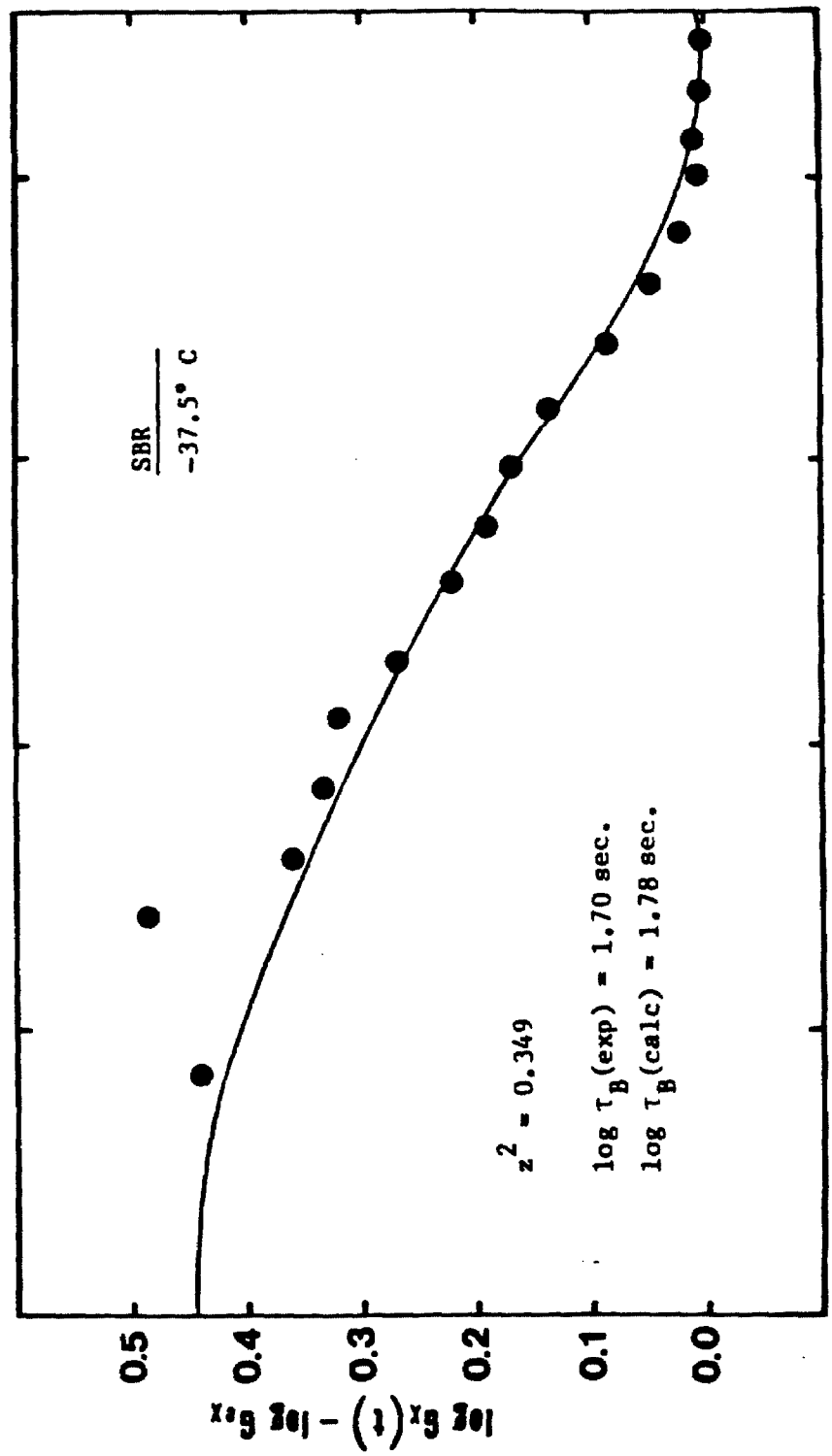

Figure 8: Experimental time dependence of G_x compared to the predicted one.

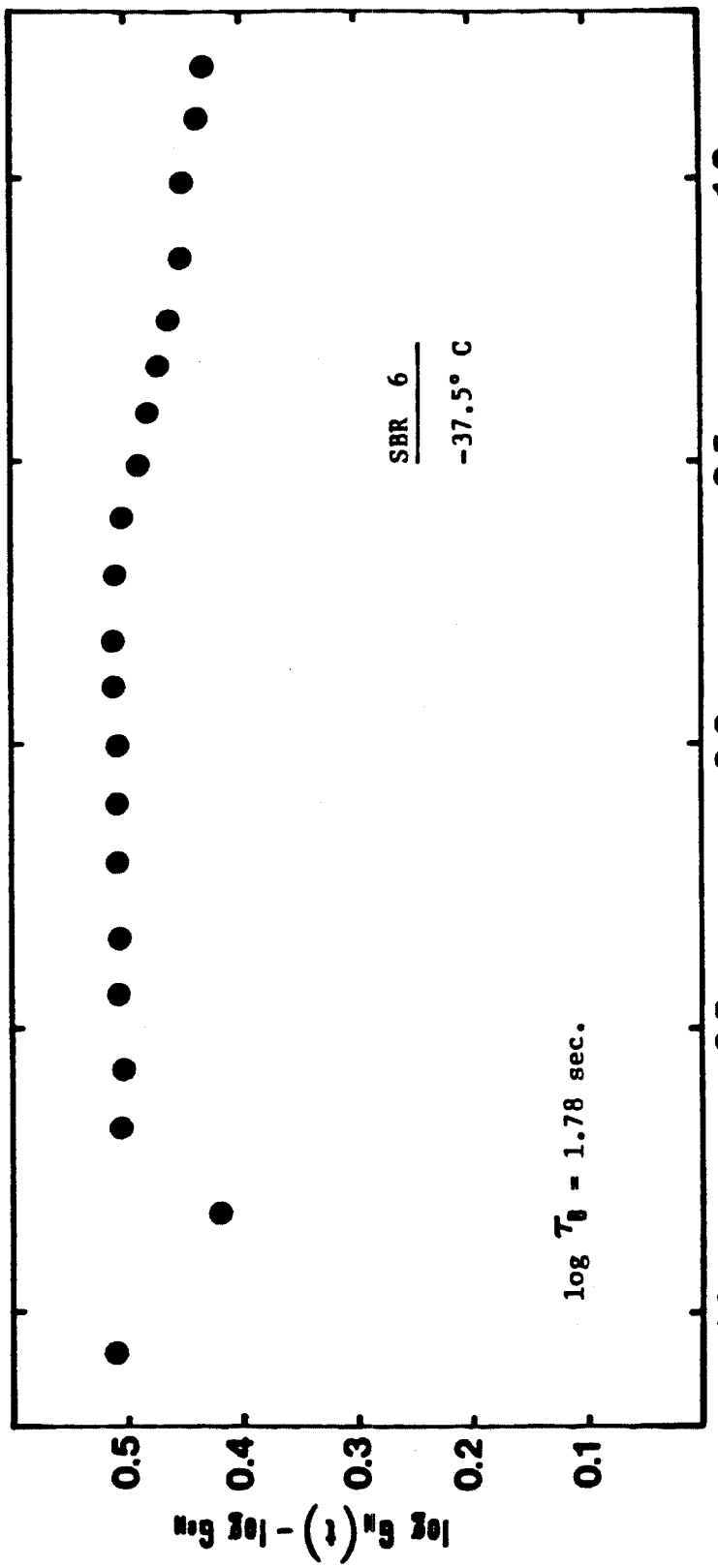

Figure 9: Experimental time dependence of G_N.

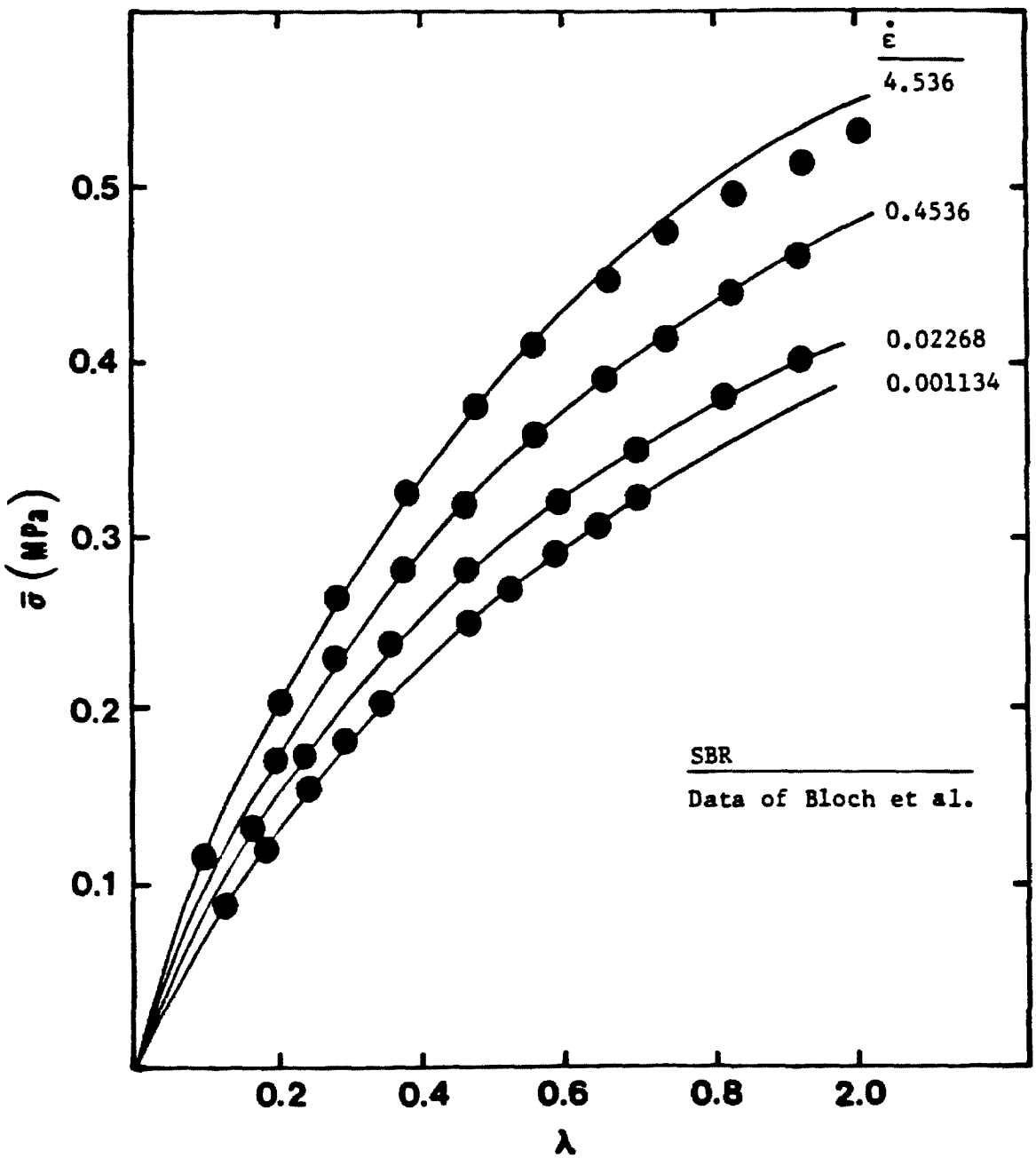

Figure 10: Constant rate of strain experiments at different strain rates compared to the theoretical predictions.

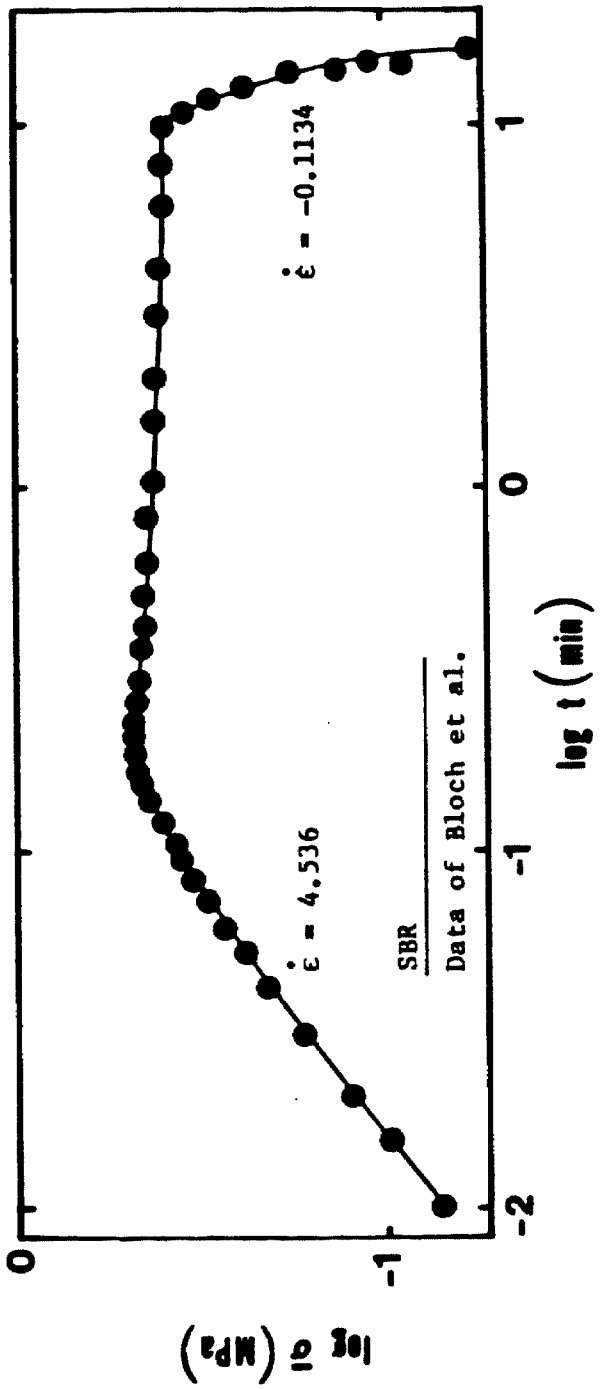

Figure 11: Response of SBR to a trapezoidal function of strain.

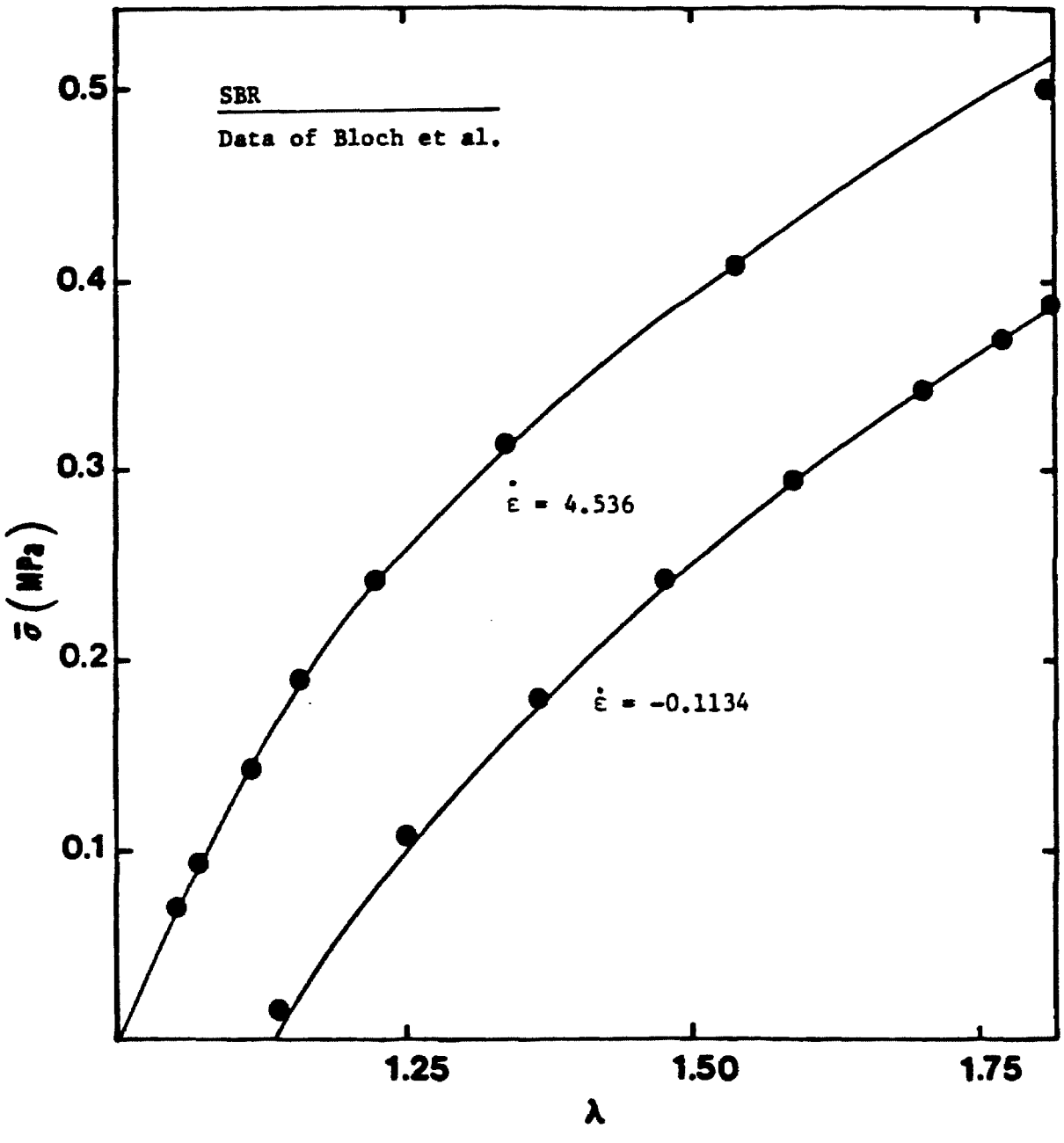

Figure 12: Response of SBR to a trapezoidal function of strain.

Appendix I

This appendix gives a mathematical description of admissible deformations, and the related deformation gradient tensors. A schematic defining the various vectors and tensors mentioned here, is supplied in Figure A-1.

Let the material points of a continuum occupy a region B before deformation. The position of a material point P in this region can be specified by a vector **P** with the cartesian coordinates X_1, X_2, X_3. Let B be mapped into region b, and P into p, as a result of the deformation. Denote the position vector of point p with **p**, and let it have the cartesian coordinates x_1, x_2, x_3. Mathematically, using indicial notation, this mapping can be described as

$$x_k = y_k(X_1,X_2,X_3) \qquad k = 1,2,3 \tag{A-1}$$

or the inverse mapping by

$$X_K = Y_K(x_1,x_2,x_3) \qquad K = 1,2,3 \tag{A-2}$$

The deformation is admissible if the mapping is one-to-one with a nonvanishing Jacobian. Y_K and y_k are then inverses of each other. Note that the conditions of admissibility express the fact that matter is *indistructible;* i.e. no region with a finite volume is mapped into one with infinite or zero volume, and that it is *impenetrable;* i.e. the deformation carries curves into curves,surfaces into surfaces, and a region into another region.

Equations A- 1 and A-2 imply

$$dx_k = y_{k,K}\, dX_K \quad , \quad dX_K = Y_{K,k}\, dx_k \tag{A-3}$$

where a comma indicates partial differentiation.

If one now defines the differential position vectors in both systems, one obtains

$$d\mathbf{p} = dx_k\,\mathbf{i}_k \quad , \quad d\mathbf{P} = dX_K\,\mathbf{I}_K \tag{A-4}$$

and

$$(ds)^2 = d\mathbf{p}\cdot d\mathbf{p} = \delta_{kl}\,dx_k\,dx_l = dx_k\,dx_k \tag{A-5}$$

$$(dS)^2 = d\mathbf{P}\cdot d\mathbf{P} = \delta_{KL}\,dX_K\,dX_L = dX_K\,dX_K \tag{A-6}$$

where ds and dS are the line elements in the two systems, and $\mathbf{i}_k$ and $\mathbf{I}_K$ are the unit vectors of the coordinate systems. Substituting eq A-3 into eq A-4 one obtains

$$d\mathbf{p} = \mathbf{c}_k\,dx_k \quad , \quad d\mathbf{P} = \mathbf{C}_K\,dX_K \tag{A-7}$$

where

$$\mathbf{c}_k = Y_{K,k}\,\mathbf{I}_K \quad , \quad \mathbf{C}_K = y_{k,K}\,\mathbf{i}_k \tag{A-8}$$

Substituting eq A-7 into eqs A-5 and A-6, one obtains

$$(ds)^2 = C_{KL}\,dX_K\,dX_L \quad , \quad (dS)^2 = c_{kl}\,dx_k\,dx_l \tag{A-9}$$

where

$$c_{kl} = \mathbf{c}_k\mathbf{c}_l \quad , \quad C_{KL} = \mathbf{C}_K\mathbf{C}_L \tag{A-9}$$

and c_{kl} and C_{KL} are the Cauchy and the Green deformation tensors. Their inverses are the Finger and the Piola deformation tensors respectively.

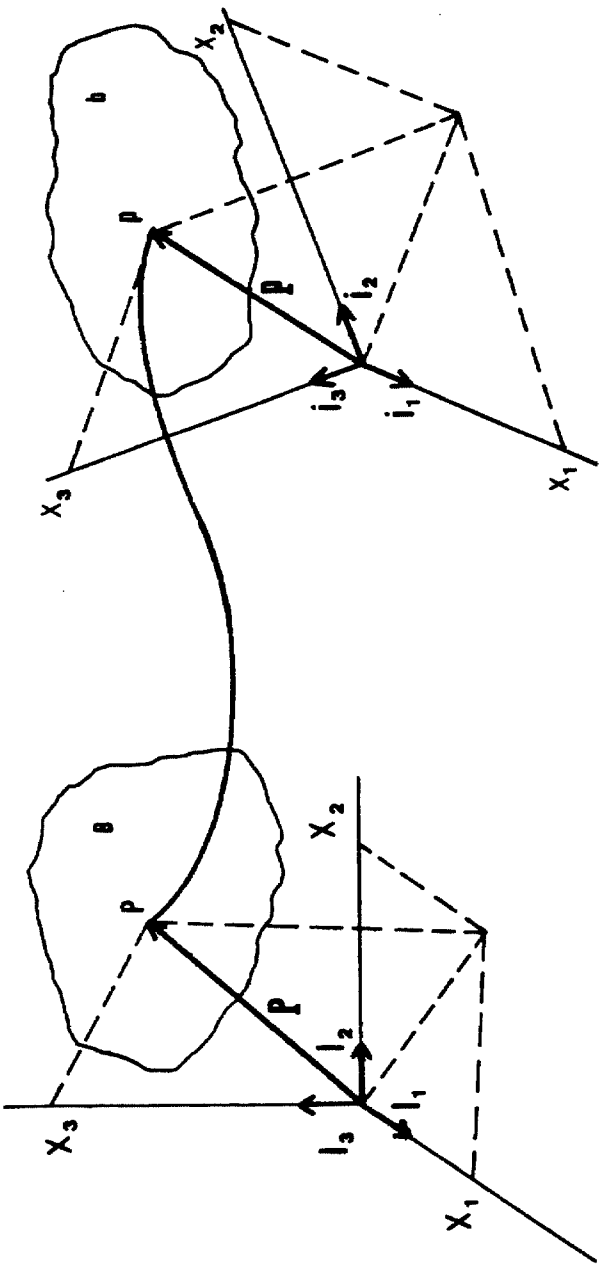

Figure A-1: An admissible deformation that carries region B into region b and point P into point p.

Appendix II

This appendix summarizes the sample and specimen preparation methods. The styrene-butadiene rubber networks had the following composition:

SBR 1502	100 parts
antioxidant	1 part
crosslinker	variable

The following amounts of crosslinker were added:

SAMPLE	CROSSLINKER (phr)
SBR 6	1.02
SBR 2	0.67
SBR 4	0.5
SBR 3	0.3

N-phenyl-2-napthyl amine was used as antioxidant.The crosslinker was Hercules Inc. Di-Cup 40, which is dicumyl peroxide supported on calcium carbonate. The weight fraction of dicumyl peroxide was 40%. This crosslinker was used instead of straight dicumyl peroxide to facilitate dispersion.

The ingredients were milled on a two-roll laboratory mill cooled with water. The SBR 1502 was milled for 15 minutes until an even spread was obtained on the rolls. The antioxidant was then added and the sheet was milled for an additional 20 minutes. During this process, the roll separation was reduced and again increased, and the sheet was folded several times both lengthwise and widthwise to obtain better dispersion. The Di-Cup 40 was added, and the sheet was milled for 10 more minutes, following the same procedure as in the case of the antioxidant. Finally, the sheet was allowed to recover at room temperature for at least 48 hours.

After the recovery was complete, the required amount of material was placed in a 15.2 by 15.2 by 0.2 cm. mold and cured at 157^{0}C and 175 MPa for 45 minutes. The press, the mold and the rubber were then cooled to room temperature overnight. This molding procedure was necessary to avoid the formation of bubbles in the sheet.

The natural rubber (NR) was obtained through the generosity of the Goodyear Tire and Rubber Company in the form of cis-polyisoprene (NATSYN 2200). The samples were prepared for us by the courtesy of Phillips Petroleum Company. The networks were prepared by adding the required amount of dicumyl peroxide to the rubber. The sheets were then molded at 150^{0}C for two hours. No antioxidant was added. The amount of dicumyl peroxide used for the various samples are listed below:

SAMPLE	CROSSLINKER (phr)
B	3.44
C	2.31
D	1.13
E	0.77

Specimen Preparation

The same specimen preparation technique was used for both natural rubber and for SBR. Strips were cut from the molded sheets by a knife-edged mill blade. The sheets were bonded to the surface of a polyethylene sheet, using double-sided adhesive tape to facilitate the cutting. The strips had dimensions of 12 x 0.5 x 0.2 cm. Phosphor-bronze U-tabs were first bonded to the specimen ends with epoxy resin. After the resin had set, the tabs were removed and were then reglued using Zip-Grip 10. This procedure was necessary, because the Zip-Grip did not form strong enough bonds between the U-tabs and the strips

without the epoxy. To minimize end effects, the tab ends were made to extend over the specimen for no more than 2 mm. Before testing, the specimens were allowed to relax at room temperature.

Measurement of Mechanical Properties

A Floor Model Instron Tensile Tester was used in our stress relaxation experiments. The temperature was controlled through a Missimer's Environmental Chamber. Liquid nitrogen was used if cooling was needed.

The force measuring system of the Instron uses load cells with an accuracy of + 0.25%.The output of the load cells was observed to be nonlinear and they were therefore calibrated with several weights before and after an experiment. A typical calibration curve is shown in Figure A-2. In the figure, the symbols show the calibration points for the three scales of the load measuring system. The solid line is the curve fitted to the experimental points.

In some instances the crosshead would creep, i.e. after the initial deformation, during stress relaxation, the crosshead would move up, changing the initial elongation. For this reason, the elongation was measured before and after every stress relaxation experiment. Data sets during which the elongation changed were discarded.

The forces were recorded on a Hewlett-Packard recorder connected to the load weighing system.

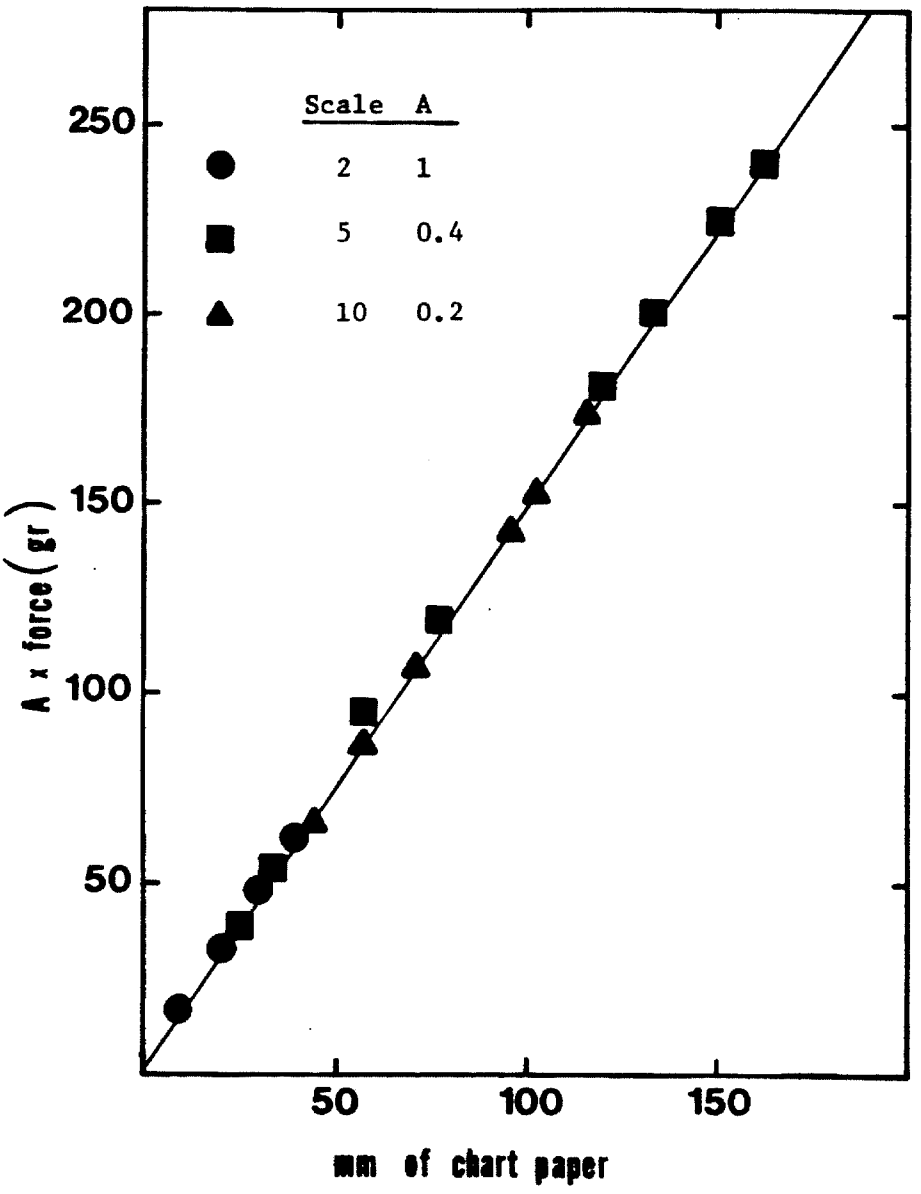

Figure A-2: A typical calibration curve.

Appendix III

In this Appendix we derive the contribution of path length fluctuations to stress at equilibrium. For completeness, parts of reference 2 have been reproduced. Our eqs A-1 through A-5 correspond to eqs 6.1, 6.2, 6.3, 6.5, 6.6 of reference 2. Our eq A-7 corresponds to eq 6.19, our eqs A-8 and A-10 correspond to eqs 6.20 and 6.21, respectively.

Consider a Rouse chain consisting of $N_s + 1$ Rouse segments, $\mathbf{r}_0, \mathbf{r}_1, \ldots\ldots, \mathbf{r}_{N_s}$ with its ends $n = 0$ and $n = N_s$ fixed in space at the origin and at $\mathbf{R}$, respectively. Calculate the stress defined by

$$\bar{\sigma}_{\alpha\beta}(t) = (3ck_BT/b^2) \int_0^{N_0} \left\langle \frac{\partial r_{n\alpha}(t)}{\partial n} \frac{\partial r_{n\beta}(t)}{\partial n} \right\rangle_u dn - P\delta_{\alpha\beta} \qquad \text{(A-1)}$$

subject to the initial conditions

$$\mathbf{r}_n(0) = \mathbf{F}\cdot\mathbf{r}_n^0 \quad , \quad \mathbf{R} = \mathbf{F}\cdot\mathbf{R}^0 \qquad \text{(A-2)}$$

where the superscript 0 denotes the quantities before deformation. The equation describing the motion of $\mathbf{r}_n$ is

$$\zeta \frac{\partial \mathbf{r}_n(t)}{\partial t} = (3k_BT/b^2) \frac{\partial^2 \mathbf{r}_n(t)}{\partial n^2} + \mathbf{f}_n(t) \qquad \text{(A-3)}$$

Since $\mathbf{r}_n(t) = 0$ at $n=0$, and $\mathbf{r}_n(t) = \mathbf{R}$ at $n=N_s$, we introduce the normal coordinate $\mathbf{x}_p$ as

$$\mathbf{r}_n(t) = \frac{n}{N_s}\mathbf{R} + \left(\frac{2}{N_s}\right)^{1/2} \sum_p \mathbf{x}_p(t) \sin\left(\frac{p\pi n}{N_s}\right) \qquad \text{(A-4)}$$

where the time dependence of $\mathbf{x}_p$ is exponential and decays to zero as $t \to \infty$. Using eq A-4 in eq A-1 the integration can be carried out and yields

$$\bar{\sigma}_{\alpha\beta}(t) = (3ck_BT/b^2)[\ \langle R_\alpha R_\beta \rangle_u / N_s$$

$$+\sum_{p}(p\pi/N_e)^2 <x_{p\alpha}(t)\, x_{p\beta}(t)>_u] - P\delta_{\alpha\beta} \qquad \text{(A-5)}$$

This describes the relaxation process characterized by τ_A. At its completion the second term on the right hand side has decayed to zero. Therefore, the stress due to a length of chain between slip links is

$$\bar{\sigma}_{\alpha\beta} = \frac{3ck_BT}{N_e b^2} <R_\alpha R_\beta>_u \qquad \text{(A-6)}$$

Next we show that for $t>\tau_A$ the stress is given by eq 13 of the text. Note that a chain between two crosslink points has N slip-links, $\mathbf{R}_0,\mathbf{R}_1,.....,\mathbf{R}_N$ denoting their positions. Then it follows from eq A-6 that the stress due to the complete chain is

$$\bar{\sigma}_{\alpha\beta} = \frac{3ck_BT}{N_e b^2} \sum_{k=1}^{N} <(\, R_{k\alpha}-R_{(k-1)\alpha})(\, R_{k\beta}-R_{(k-1)\beta})>_u \qquad \text{(A-7)}$$

since $\mathbf{R}$ now is $\mathbf{R_k}-\mathbf{R_{k-1}}$. We set

$$<(\, R_{k\alpha}-R_{(k-1)\alpha})(\, R_{k\beta}-R_{(k-1)\beta})>_u = <v_{n\alpha}v_{n\beta}>_u N_e^2 <l_n(t)>_u^2 \qquad \text{(A-8)}$$

for $N_e(k-1)\le n\le N_e k$ because $v_{n\alpha}v_{n\beta}$ gives the direction of $(R_k-R_{k-1})_\alpha(R_k-R_{k-1})_\beta$ and $N_e<l_n(t)>_u$ is the *average* length of $(\mathbf{R_k}-\mathbf{R_{k-1}})$. Therefore

$$<(\, R_{k\alpha}-R_{(k-1)\alpha})(\, R_{k\beta}-R_{(k-1)\beta})>_u = N_e \int_{N_e(k-1)}^{N_e k} <v_{n\alpha}v_{n\beta}>_u \qquad \text{(A-9)}$$

since $\mathbf{v_n}$ and l_n are independent of n provided $N_e(k-1)\le n\le N_e k$. Substituting eq A-9 into eq A-7 we obtain

$$\bar{\sigma}_{\alpha\beta} = \frac{3ck_BT}{b^2} \int_0^{N_0} <v_{n\alpha}v_{n\beta}>_u <l_n(t)>_u^2 \, dn \qquad \text{(A-10)}$$

which is the stress due to the change in the average path length. This is eq 13 of the text.

As discussed in the text, we cannot write the boundary conditions and the initial condition in terms of s_n. We can only estimate the magnitude of fluctuations on the stress at equilibrium. To calculate the contribution of the fluctuations to the stress, we need to consider the boundary conditions at the chain ends at equilibrium. By eq 7 of the text, the motion of $s_n(t)$ is described by

$$\zeta \frac{\partial s_n}{\partial t} = (3k_B T / b^2) \frac{\partial^2 s_n}{\partial n^2} + f_n(t) \tag{A-11}$$

The boundary conditions at equilibrium result from the requirement that the chain ends be fixed at the crosslink points. Thus, we write the boundary conditions as

$$s_{n(t)}|_{n=0} = 0 \quad , \quad s_{n(t)}|_{n=N_0} = N_0 z \bar{l} \alpha(\mathbf{F}) \tag{A-12}$$

In eq A-12 the random force satisfies

$$\langle f_n(t) \rangle_u = 0 \qquad \text{and} \qquad \langle f_n(t) f_m(t') \rangle_u = 2\zeta k_B T \delta(n-m)\delta(t-t') \tag{A-13}$$

The following form satisfies eq A-12

$$s_n(t) = nz\bar{l}\alpha(\mathbf{F}) + (2/N_0)^{1/2} \sum_p x_p(t) \sin(p\pi n / N_0) \tag{A-14}$$

Substituting eq A-14 into eq A-12, we obtain

$$\frac{dx_p(t)}{dt} = -\lambda_p x_p(t) + f_p(t) \tag{A-15}$$

where

$$\lambda_p = \frac{3k_B T}{b^2 \zeta} \frac{p^2 \pi^2}{N_0^2} \tag{A-16}$$

and $f_p(t)$ is defined by

$$f_p(t) = (2/N_0)^{1/2} (1/\zeta) \int_0^{N_0} \sin \frac{p\pi n}{N_0} f_n(t)\, dn \tag{A-17}$$

Using eq A-13 it can be shown that the average of f_p is zero and

$$\langle f_p(t_1)\, f_p(t_2)\rangle_u = \frac{2N_0 k_B T}{\zeta}\,\delta(t_1 - t_2) \tag{A-18}$$

Equation A-15 can be solved to yield

$$x_p(t) = x_p(0)\exp(-\lambda_p t) + \int_0^t \exp[-\lambda_p(t-t_1)]\, f_p(t_1)dt_1 \tag{A-19}$$

which when used in eq A-14, gives

$$s_n(t) = nz\bar{l}\alpha(\mathbf{F}) + (2/N_0)^{1/2}\sum_p \sin\frac{p\pi n}{N_0}\exp(-\lambda_p t)\,[x_p(0)$$

$$+ \int_0^t \exp(\lambda_p t_1)\, f_n(t)\, dt_1\ ] \tag{A-20}$$

From eq A-20 the contribution of fluctuations to the arc length at equilibrium can be calculated as

$$\langle (s_n(t) - \langle s_n(t)\rangle_u)^2\rangle_u = \frac{N_0^2 b^2}{3}\sum_p \frac{2}{p^2\pi^2}\sin^2\frac{p\pi n}{N_0} \tag{A-21}$$

The square of the primitive path length of the chain is given by

$$L^2 = \bar{L}^2 + \langle (L-\bar{L})^2\rangle_u \tag{A-22}$$

where $\bar{L}$ is the average of L, and

$$\langle (L-\bar{L})^2\rangle_u = \frac{\int_0^{N_0}\langle (s_n(t) - \langle s_n(t)\rangle)^2\rangle_u\, dn}{\int_0^{N_0} n dn} = \frac{N_0 b^2}{3} \tag{A-23}$$

Per chain segment between two slip links, the square of the path length is

$$l_F^2 = 1/N\ (\langle (L-\bar{L})^2\rangle_u) \tag{A-24}$$

where the subscript F has been used to denote fluctuations. Thus the curvature of the chain due to fluctuations results as

$$\langle (R_{k\alpha}-R_{(k-1)\alpha})(R_{k\beta}-R_{(k-1)\beta})\rangle_{\mathbf{n}}^{F} = \langle v_{n\alpha}v_{n\beta}\rangle_{\mathbf{u}} l_F^2 \qquad \text{(A-25)}$$

where now the superscript F on the components of **R** denote fluctuations. In eq (A-25), $\langle v_{n\alpha}v_{n\beta}\rangle$ is the direction, and l_F^2 is the square of the length due to fluctuations, of **R**. Substituting eq A-24 and A-25 into eq A-7 gives

$$\bar{\sigma}_{\alpha\beta}^{F} = ck_B T N_0 / N_e \ \langle v_{n\alpha}v_{n\beta}\rangle_{\mathbf{u}} \qquad \text{(A-26)}$$

which is the contribution to stress at equilibrium due to fluctuations. We set

$$G_{eN} = ck_B T N_0 / N_e = \rho RT / M_e^{x} \qquad \text{(A-27)}$$

to obtain eq 22 of the text.

Appendix IV

This appendix lists the values of C_1 and C_2 from which G_X and G_N were obtained, in section 2. The references are given in Table 1 of section 2. Table entries are grouped in fives for ease of reference

Table 1

Poly(Ethyl Acrylate)-(PEA)

$2C_1$ (MPa)	$2C_2$ (MPa)	G_X (MPa)	G_N (MPa)
0.0814	0.0335	0.074	0.038
0.0462	0.0585	0.033	0.067
0.0357	0.0578	0.022	0.066
0.0365	0.0463	0.0260	0.053
0.0181	0.0718	0.001	0.082

Table 2

Butyl Rubber-(IIR)

$2C_1$ (MPa)	$2C_2$ (MPa)	G_X (MPa)	G_N (MPa)
0.0772	0.100	0.054	0.114
0.0995	0.112	0.073	0.128
0.104	0.728	0.087	0.83

Table 3

Poly(Dimethyl Siloxane)-(PDMS)

$2C_1$ (MPa)	$2C_2$ (MPa)	G_X (MPa)	G_N (MPa)
0.061	0.054	0.048	0.061
0.065	0.051	0.054	0.058
0.069	0.039	0.060	0.045
0.074	0.083	0.054	0.095
0.080	0.049	0.068	0.056
0.098	0.105	0.078	0.120
0.100	0.078	0.082	0.089
0.120	0.109	0.095	0.124
0.036	0.062	0.022	0.071
0.071	0.057	0.058	0.065
0.079	0.049	0.068	0.056

Table 4

Natural Rubber-(NR)

$2C_1$ (MPa)	$2C_2$ (MPa)	G_X (MPa)	G_N (MPa)
0.196	0.196	0.150	0.224
0.230	0.196	0.184	0.224
0.280	0.202	0.233	0.230
0.340	0.206	0.292	0.235
0.344	0.206	0.296	0.235
0.498	0.204	0.450	0.233
0.604	0.280	0.557	0.228
0.031	0.088	0.011	0.101
0.048	0.123	0.020	0.140
0.066	0.127	0.037	0.145
0.076	0.128	0.046	0.146
0.092	0.133	0.061	0.152
0.107	0.129	0.077	0.147
0.129	0.145	0.095	0.165
0.150	0.152	0.115	0.173
0.088	0.139	0.056	0.159
0.149	0.137	0.117	0.156
0.188	0.157	0.151	0.179
0.196	0.147	0.162	0.168
0.196	0.196	0.150	0.224
0.122	0.112	0.096	0.128
0.140	0.136	0.108	0.155

0.198	0.142	0.165	0.162
0.286	0.158	0.249	0.180
0.300	0.166	0.261	0.189
0.358	0.176	0.317	0.201
0.304	0.119	0.276	0.136
0.340	0.110	0.314	0.125
0.230	0.196	0.184	0.224
0.188	0.157	0.151	0.179
0.147	0.112	0.121	0.128
0.265	0.108	0.240	0.123

Table 5

cis-1,4-Poly-Butadiene Rubber-(PBD)

$2C_1$ (MPa)	$2C_2$ (MPa)	G_X (MPa)	G_N (MPa)
0.14	0.42	0.042	0.479
0.15	0.18	0.108	0.205
0.16	0.30	0.090	0.342
0.18	0.93	0.056	0.624
0.30	0.34	0.221	0.388
0.33	0.53	0.206	0.604
0.38	0.54	0.254	0.616
0.41	0.45	0.305	0.513
0.085	0.206	0.037	0.235
0.241	0.343	0.161	0.391
0.364	0.376	0.296	0.429
0.192	0.298	0.123	0.340